Micro Combined Heat and Power Management for a Residential System

University of Cape Town

Prepared by:

Anesu Tichagwa

Supervised by:

Paul Barendse

Prepared for:

Department of Electrical Engineering

University of Cape Town

A thesis submitted in fulfilment of the requirements for the degree of

Masters of Science (MSc) in Electrical Engineering, at the University of Cape Town

29 September 2013

Declaration

I declare that this is my own work. Information and research gathered and used has been properly referenced.

This thesis is being submitted for the degree of Masters of Science in Engineering at the University of Cape Town.

This thesis has not been submitted for any other degree or examination in another university.

Anesu Tichagwa ……..

Date ……..

ACKNOWLEDGEMENTS

I wish to extend my gratitude to:

- My supervisor, Dr. P. S. Barendse, and co-supervisor, Dr. A. Khan, for providing me with the opportunity to pursue my Masters Degree and for the constant support, honest opinions and guidance throughout this research period.
- HySA for sponsoring my research project.
- Mr. C. Wozniak for always assisting during the practical aspect of my work.
- All members of the AMES group, especially to Mr. P. Liu, Mr. J. De la Bat, Mr. C. De Beer and Ms. D. Reddy, who I have spent most time with during these two years.
- Mr. P. Titus for assistance in the lab.
- My friends and family for the love and support.
- My father for always providing me a good example to follow.
- My mother for always allowing me to follow my dreams.
- God for the natural gifts He has given me and continual guidance.

ABSTRACT

Fuel cell technology has reached commercialisation of fuel cells in application areas such as residential power systems, automobile engines and driving of industrial manufacturing processes. This thesis gives an overview of the current state of fuel cell-based technology research and development, introduces a µCHP system sizing strategy and proposes methods of improving on the implementation of residential fuel cell-based µCHP technology.

The three methods of controlling residential µCHP systems discussed in this thesis project are heat-led, electricity-led and cost-minimizing control. Simulations of a typical HTPEMFC-based residential µCHP unit are conducted using these control strategies. A model of a residential µCHP system is formulated upon which these simulated tests are conducted. From these simulations equations to model the costs of running a fuel-cell based µCHP system are proposed.

Having developed equations to quantify the running costs of the proposed µCHP system a method for determining the ideal size of a µCHP system is developed. A sizing technique based on industrial CHP sizing practices is developed in which the running costs and capital costs of the residential µCHP system are utilised to determine the optimal size of the system. Residential thermal and electrical load profile data of a typical Danish household are used.

Having simulated the system a practical implementation of the power electronics interface between the fuel cell and household grid is done. Two topologies are proposed for the power electronics interface a three-stage topology and a two-stage topology. The efficiencies of the overall systems of both topologies are determined. The system is connected to the grid so the output of each system is phase-shifted and DC injection, harmonic distortion, voltage range and frequency range are determined for both systems to determine compliance with grid standards. Deviations between simulated results and experimental results are recorded and discussed and relevant conclusions are drawn from these.

Keywords: proton exchange membrane fuel cell, PEMFC, combined heat and power, CHP system, power management, micro-CHP.

TABLE OF CONTENTS page

List of Figures page

List of Tables

NOMENCLATURE

PEM	proton exchange membrane
PEMFC	proton exchange membrane fuel cell
HTPEMFC	high temperature proton exchange membrane fuel cell
LTPEMFC	low temperature proton exchange membrane fuel cell
CHP	combined heat and power
AFC	alkaline fuel cell
PAFC	phosphoric acid fuel cell
SOFC	solid oxide fuel cell
DMFC	direct methanol fuel cell
MCFC	molten carbonate fuel cell
HySA	Hydrogen South Africa
CO	carbon monoxide
R	Universal gas constant, $8.314 \frac{J}{mol\ K}$
F	Faraday's constant, $96\ 485 \frac{C}{mol\ e^-}$
ΔH	change in Enthalpy
ΔG	change in Gibbs free energy
ΔS	change in Entropy
UK	United kingdom
DK	Denmark
PBI	polybenzimidazole
SHP	separate heat and power
H_2	hydrogen
O_2	oxygen
$	United States Dollar
η	efficiency

Chapter 1

1. Introduction

1.1. Background

As global demand for energy increases so does the need for progress in renewable energy technology research and development. There is increasing pressure on industries to reduce carbon footprints whilst still increasing energy output. Research into technologies with minimal carbon-dioxide emissions is thus being supported but government funding and legislature in countries around the world. Renewable energy sources are looked to as a solution to this global energy demand increase and examples of these are photovoltaic cells (solar energy), wind energy and fuel cells. The focus of this paper will be on fuel-cell based technology in the Combined Heat and Power (CHP) field. Fuel cells are emerging as suitable replacements for engine-based technologies in the residential μCHP system application area due to their low heat-to-power ratio, high electrical efficiency, low carbon footprint and untapped research and development potential. Research has already resulted in the improvement of fuel cell dynamics, increased availability of hydrogen, fuel cell efficiency and fuel cell manufacturing costs and as this trend continues the fuel cell may completely replace established energy generating technologies such as combustion-based engines in the near future which necessitates further research in this field. This thesis validates existing literature on the subject and practically applies HTPEMFC theory in literature in response to a Hydrogen South Africa (HySA) initiative.

1.2. Purpose of Investigation

As the demand for energy increases, so does the need for alternative schemes to meet this demand. The hydrogen economy is pivotal to the future energy mix. In residential applications, it is predicted that μCHP systems would prove to be a viable solution to the more efficient use

of energy. This work serves to explore the potential of fuel cell based micro CHP applications. An average household in Denmark is selected for the case study since it has a natural gas feed and it is progressive in the uptake of alternative schemes.

A μCHP system model is devised in order to conduct simulations of the proposed residential μCHP system since three different μCHP control strategies are available and there are a number of scenarios in which each can be preferable to the others. The model is used to develop a sizing method to determine the size of a residence given project load profile and tariff data. It is necessary to size the system appropriately because too large a system will result in energy wastage and too small a system will result in not the energy requirements of the household not being met.

An interface between the HTPEMFC and the household is designed and constructed since the voltage output of the fuel cell is varies non-linearly and may damage household appliances if not controlled. In addition to providing voltage control, the interface will isolate the fuel cell and connect the residential μCHP system to the national electricity grid in order to import and export electrical energy. Connection to the grid must adhere to the grid connection standards of the country in which the μCHP system is being implemented.

1.3. Objectives of this Thesis

The main objectives of the research are as follows:

- Conduct a literature scan of fuel cell based CHP systems.
- Develop a residential μCHP model that can be used to simulate these systems.
- Use the μCHP model to determine costs associated with implementing fuel cell-based μCHP systems for various control strategies.
- Determine a sizing methodology for fuel cell-based residential μCHP systems.
- Design, build and test two topologies for load interfacing between the fuel cell and the household. One topology enabling the option of including a standard battery as a storage element, the other making use of less circuit elements.

- Construction of the two designed power electronic interfaces for comparison of their performance.

1.4. Scope of Work

Though a number of Distributed Generation (DG) methods are discussed in this thesis, fuel cells are the form of DG which will be investigated. HTPEMFCs are the type of fuel cell to be focused on in the simulations of this thesis and the Combined Heat and Power application of fuel cells is researched. MacroCHP systems are discussed but all simulations and practical work of the thesis are at µCHP scale with MacroCHP theory being applied to µCHP systems where applicable.

The practical implementation of the µCHP system modeled in chapter 3 is limited to the interfacing of the electrical output of the fuel cell first to a resistive load and then to the grid. Thermal output of the HTPMEFC is simulated in the sizing strategy of chapter 4 but not implemented practically due to lack of availability of sufficient resources to construct the complete thermodynamic cycle.

1.5. Outline of Thesis

Chapter 1: Identifies the purpose of the investigation, followed by the objectives, scope of work and the plan of development. Justification for the simulations of chapter 4, design approach of chapter 5 and practical tests of chapter 6 is given in this chapter.

Chapter 2: Presents a literature survey of current fuel cell technology and CHP systems. The theory required to understand the modelling of chapter 3, calculations of chapter 4 and power electronic theory of chapters 5 and 6 is discussed. Sources of further discussion are referenced should more detail be required.

Chapter 3: Presents a model of a residential µCHP System. This is the model on which the simulations of chapter 4 and design of chapter 5 is based. This model can be expanded to accommodate a larger fuel cell rating should this be required by changing the Balance of Plant ratings of this chapter.

Chapter 4: Presents a μCHP system sizing methodology. The model of chapter 3 is used to simulate a residential μCHP system. Different μCHP control strategies are used in order to show the impact these and other factors have on μCHP system size.

Chapter 5: Discusses the design of the power electronic interface built during this thesis project. Two topologies are designed: A two stage interface and a three-stage interface. Calculations, component selection and control issues are discussed in this chapter.

Chapter 6: Discusses the power electronic interface simulation and experimental results. The results of both the two-stage interface and three-stage interface are discussed and comparisons are made between the two. The dynamics, grid code adherence and efficiency of the power electronic interfaces are tested and the results are discussed in this chapter.

Chapter 7: Conclusions are drawn based on the findings of this thesis in this chapter. These are then followed by suggestions for future research.

Chapter 2

2. Literature Review

2.1. Introduction

This chapter presents an overview of fuel cell-based Combined Heat and Power (CHP) systems. There is comprehensive literature on industrial-scale CHP systems and much of this theory is applicable to the smaller µCHP systems so reference will be made to the current practices in industry. The theory required to fully comprehend and validate the calculations, simulations and practical implementation of the hardware in the chapters that follow will also be discussed in this chapter.

2.2. Distributed Generation

Distributed Generation (DG) of Energy, discussed in detail by the authors of [1], has become more viable as a method of energy generation and is being applied more frequently by energy suppliers as a result of the need for cheaper, more efficient supplies of electrical and thermal energy for domestic purposes. DGs are typically placed at considerable distances from major power stations that generate the large supply of national electricity. Generation takes place closer to the load and a larger number of generators with lower power ratings are used. Advantages of DG, discussed in [2], as opposed to conventional power station electricity generation and distribution include:

- A decrease in losses along distribution network electric cables. These can be dissipative losses due to the resistance of the cables and aging transmission equipment.
- Increase in power quality due to decrease in poor network switching operations, voltage dips and transients.
- The ability to cater to specific power load specifications (flexibility).
- Minimising electrical energy demand during peak demand times.
- Lower investment risks because of smaller capital costs of DGs.

Examples of DGs are photovoltaic cells, combustion engines (internal and external combustion), fuel cells and wind turbines. For the purposes of this thesis emphasis will be placed on fuel cell-based DG due to the fuel cell's potential for positive environmental impact and improved performance as a result of advances in research and development. Also, as will be revealed, the fuel cell is better suited to residential applications of DG.

2.3. Fuel Cells

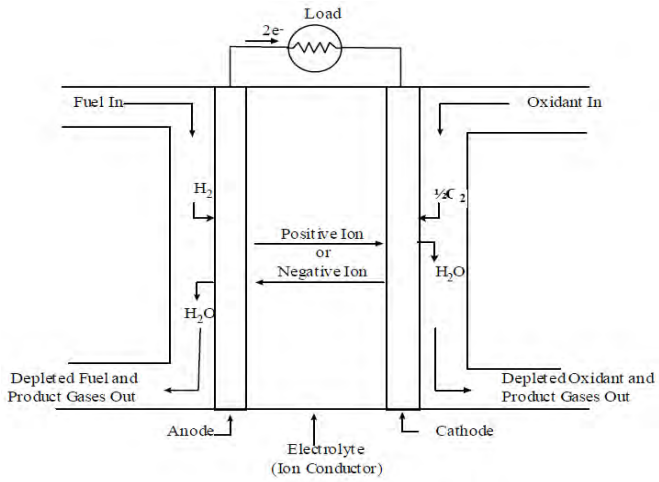

Figure 2-1: Schematic of a Fuel Cell Connected to a Resistive Load [1]

A fuel cell can be defined as an electrochemical device that facilitates conversion of chemical energy from a fuel (usually hydrogen) directly into electrical energy via the chemical reaction of equation (2.1) without combustion (burning) of the fuel [3]:

$$2H_2 + O_2 \rightarrow 2H_20 + \text{heat} \qquad (2.1)$$

Equation (2.1) is an exothermic chemical reaction which means energy is given off in the form of heat. During chemical reactions electrons are released by some reactants and received by other reactants in this process electrons are released from the H_2 gas to flow across the external circuit and 'Load' of figure 2-1 to the O_2 which results in the formation of water. This can be understood better by analysing the redox (oxidation and reduction) reactions associated with equation (2.1).

$$2H_2 \rightarrow 4H^+ + 4e^- \qquad (2.2)$$

$$O_2 + 4e^- + 4H^+ \rightarrow 2H_2O \quad (2.3)$$

By definition loss of electrons is oxidation and the gain of electrons is reduction as discussed in [4]. Therefore the hydrogen is oxidised and the oxygen is reduced in equations (2.2) and (2.3) which when combined form equation (2.1). The electrons released from this process are free to flow through an external circuit and in so doing supply electrical energy to a load.

In chemical reactions bond-making is exothermic and bond breaking is endothermic meaning energy is released when bonds are made and energy is absorbed when bonds are broken. The overall reaction of equation (2.1) is exothermic meaning the product(s), H_2O in this case, possess less energy than the H_2 and O_2 reactants. Excess energy is liberated in the form of thermal energy and electrical energy as energy cannot be created or destroyed but can only be converted from one form to another.

There are different types of fuel cells and these are classified by the type of electrolyte that is used in each. The electrolyte shown in figure 2-1 prevents the electrons released in the fuel cell chemical reaction from crossing directly from the anode to the cathode without passing through the external electrical circuit while allowing the H^+ ions to pass through. The main types of fuel cells discussed in detail by the authors of [1] are:

- Alkaline Fuel Cell (AFC)
- Proton Exchange Membrane Fuel Cells (PEMFC)
- Solid Oxide Fuel Cells (SOFC)
- Molten Carbonate Fuel Cells (MCFC)
- Phosphoric Acid Fuel Cells (PAFC)
- Direct Methanol Fuel Cells (DMFC)

The PEMFC also known as the solid polymer membrane fuel cell is easier to design because of the absence of liquid electrolyte and is less prone to corrosion. Research in the PEMFC area is being directed towards the development of longer lasting membranes and catalysts. The PEMFC can be operated at high temperature or at low temperature (both discussed in [3]) and for this thesis a high temperature PEMFC (HTPEMFC) discussed in [5].

The advantages of PEMFCs over other fuel cell technologies are:

- Low operating temperature which results in shorter start-up period.
- Greater durability because they are less susceptible to corrosion.

The advantages HTPEMFCs have over LTPEMFCs include:

- Less catalyst is required by the fuel cell's chemical reaction.
- Greater heat production from the exothermic reaction of the fuel cell which is desirable for the Combined Heat and Power application of fuel cells.
- Can make use of lower quality hydrogen such as that from a reformer because of a high tolerance for impurities.

Disadvantages of HTPEMFCs compared to LTPEMFCs:

- Longer start up period.

. PEMFCs and SOFCs are regarded as suitable for residential energy generation due to their lower operating temperature requirements and ability to operate at relatively low power. As will be observed throughout the simulations of chapter 4 low operating points are also required in a residential system when there is a low demand for energy.

2.4. Combined Heat and Power

Combined Heat and Power (CHP) Systems (defined in [6] and [7]) generate both electrical and thermal energy to meet an energy demand. Every CHP system consists of a prime mover which is the device responsible for generating the energy such as a combustion engine or a fuel cell. The balance of plant (BOP) of the CHP system refers to the components physically surrounding the prime mover that support the energy generation process.

A major characteristic that separates the different types of CHP systems is the thermodynamic cycle being employed by the system. This is the method in which heat is actually captured for useful purposes as opposed to allowing it to be dissipated as in non-CHP applications. The heat recovery method adopted in a CHP system can be a topping thermodynamic cycle, bottoming thermodynamic cycle or a combined thermodynamic cycle as discussed in [6]. The prime mover

either generates thermal energy with electrical energy being a by-product (bottoming-cycle) or generates electrical energy with thermal energy being a by-product (topping-cycle). Combined Cycle systems have a dual-cycle thermodynamic cycle as explained in [6]. In this thesis a topping-cycle system will be assumed due to the predetermined focus on the residential application of CHP as stated in chapter 1 of this thesis. Bottoming-cycle CHP systems are not suitable for residential applications due to the relatively high thermal demand of households in comparison to household electrical demand. In bottoming-cycle systems excess heat is used to generate electricity but in the residential case even when heat demand is low the amount of excess heat generated will not be enough to generate sufficient electricity to meet the residential electrical load. An industrial example of a fuel-cell based topping-cycle system will be given to illustrate the concept of a Combined Heat and Power topping thermodynamic cycle.

2.4.1. Industrial Topping-Cycle Example

Figure 2-2 is an industrial CHP Topping cycle system which will be used to discuss the concept of topping thermodynamic cycles. The scale of this CHP system is much larger than that of a fuel-cell based residential system but the balance of plant components of a residential system will be similar but with smaller dimensions and the general operating temperature of a residential system will be lower. Information in section 2.5 will assist in comparing between large MacroCHP systems such as that of figure 2-2 and μCHP systems investigated in this thesis.

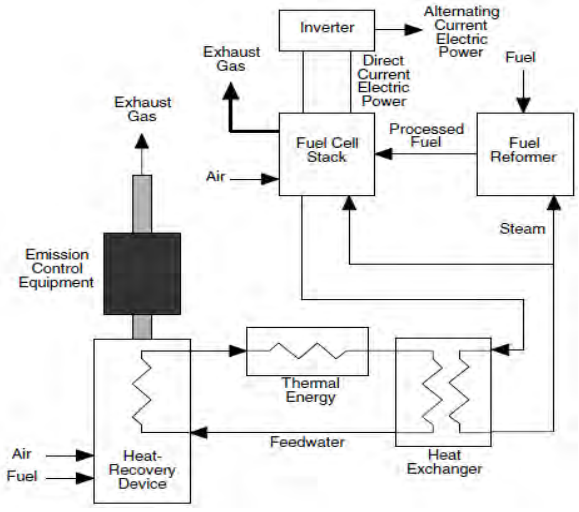

Figure 2-2: Fuel cell-based topping cycle CHP System

In the CHP system of figure 2-2 electricity is generated by the fuel cell stack and heat is given off as a by-product. The fuel reformer is used to convert natural gas to pure hydrogen which is required by the fuel cell in order to generate the electricity. The basic chemical reaction taking place in the reformer is given by equation (2.4) taken from [1]

$$CH_4 + 2H_2O \rightarrow 4H_2 + CO_2 \quad (2.4)$$

The by-product heat is absorbed by the feed-water in the heat exchanger of figure 2-2 which is then fed through the heat recovery device indicated by the 'Thermal Energy' box of figure 2-2. In a domestic system the Heat-Recovery Device would be a thermal storage tank as will be discussed in chapter 3.

The 'emission control equipment' of figure 2-2 is a system designed to filter out carbon dioxide and any polluting gases caused by reactions involving impurities in the air. The carbon dioxide in particular is from the reaction within the reformer. A model of a reformer is discussed by the authors of [8].

2.4.2. Types of Prime Mover

A prime mover, as explained in [6], can be defined as the mechanism that converts energy in the form of a fuel to electrical and thermal energy in the case of CHP systems. Prime movers differ in the amount of energy produced per unit fuel, the ratio of thermal energy to electrical energy generated (heat-to-power ratio), the range and speed which the output of the prime mover varies as well as the general installation and maintenance costs. Table 2-1 displays these and some other characteristics of commonly used industrial prime mover technologies.

Fuel cells have a lower heat-to-power ratio (discussed in section 2.8.3) than other prime mover technologies meaning that more electricity is generated by fuel cells per unit heat. This is more suitable for the residential scenario because electrical energy demand is always high but there are times throughout the course of the year when thermal demand is not as high. It is easier to add to the thermal energy generated by the fuel cell when it is insufficient than it is to store excess thermal energy that has been generated.

Often engine-based CHP systems generate excess heat in summer months because even in summer there is still a significant electrical load but less thermal demand. With a high heat to power ratio, engine-based CHP systems end up generating too much heat in summer months.

Table 2-1: Prime Movers Characteristics adapted from [6]

Prime Mover Characteristic	**Steam Turbine**	**Gas Turbine**	**Microturbine**	**Reciprocating Engine (Compression ignited)**	**Fuel Cell**
Power to Heat Ratio	0.05 to 0.2	0.5 to 2	0.4 to 0.7	0.5 to 1	1
Part Load Operation	Good	Poor	Satisfactory	Good	Good
Operating Modes	Load-tracking and continuous base-loaded operation	Base-loaded, load tracking, and peak shaving operations	Base-loaded, load tracking, and peak shaving operations	Base-loaded, load tracking, emergency, and peak shaving operations	Base-loaded and load-tracking operations
Noise	High	High	Moderate	High	Low
Installed Cost $/kW	200 to 1,000	400 to 1,800	1,300 to 2,500	900 to 1,500	2,800 to 5,500
Maintenance cost, $/kWh	up to 0.002	0.003 to 0.01	up to 0.018	0.005 to 0.015	0.007 to 0.02*a*

a Excludes stack replacement

Fuel cells are still more expensive to install than the other prime movers and is mainly due to the devices not being able to reach a stage of mass production. Fuel cells are generally not to be turned on and off repeatedly during operation due to the irreversible degradation of the fuel cell membrane and catalyst, discussed is [9]-[11], that takes place as a result of this. Fuel cells are thus not suitable for peak shaving as because prime movers used for this are switched on when demand exceeds certain thresholds and are switched off when demand is below certain thresholds. High maintenance costs of fuel cells can be attributed to the high cost of

replacement of parts which are not mass produced as well as shortage of expertise in maintaining fuel cells. Residential µCHP units follow similar trends to those shown in table 2-1 and information about the usage of fuel cells in industry can aid the implementation of fuel cells as prime movers in residential µCHP systems.

2.5. Macro CHP vs. Micro CHP

Macro CHP systems are defined by the European Commission (EC) as CHP systems with a power rating of 50kWe and above. Micro CHP systems are defined by the EC as CHP systems with a power rating below 50kWe as discussed in[12]. The operating principles of CHP systems at both these scales are similar but the application of these principles differs due to the different scales of operation. In this section a comparison will be made between these two systems, based on the work done in [13]:

2.5.1. Year Round Heating/Cooling Load

Macro CHP facilities have heating and cooling requirements that are often not seasonally dependant but are rather driven by industrial demand and are often all year round. Residential µCHP facilities may require large amounts of thermal energy during winter and considerably less during summer. This must be taken into consideration when determining energy requirements of a µCHP system and indicates that the sizing of a residential µCHP system is not purely based on maximum thermal demand.

2.5.2. System Sized to Heating Needs

Macro CHP systems in industry are sized so that no waste heat is generated. This is achieved by sizing the system according to the month of lowest thermal demand. Any extra heat required will be obtained via other methods which, in an industrial setup, will be readily available. In the case of µCHP, if such a sizing strategy is chosen an auxiliary burner will be required to meet heat demand and this may not be optimal. Also at a small scale, the option of storing this waste heat for later usage is available. If the µCHP system is grid-tied, factors such as the electrical tariff structure become more significant as the tariff fluctuates more frequently. Tariffs will be more constant in the macro CHP case because industrial energy demand is less prone to

fluctuation. Micro CHP sizing is dealt with in more detail in chapter 4 of this thesis project where a sizing strategy is outlined.

2.5.3. Recovered Heat

Micro CHP systems are often succumbing to what is known as 'summer heat dumping' whereby too much thermal energy is produced in summer. It can be difficult to store this heat which cannot be sold back to the electrical utility unlike excess electrical energy that can be sold back for a feed-in tariff. The demand for heat in Macro CHP systems is not dependant on the season and summer heat dumping is not an issue.

2.5.4. Maximizing of Capacity Factor

The capacity factor of a CHP system is defined in [13] as being the ratio of actual energy being produced over a time period to the total amount of energy that could be produced over the same time period. A control strategy that maximises this is usually required and macro CHP are almost always operational because demand for production is almost always high. In µCHP systems however it is not always beneficial to generate thermal and electrical energy as there might be no energy demand even though the option of storage is available this can result in a decrease in the overall efficiency of the µCHP system as will be discussed in chapter 4.

2.5.5. Operating Hours

As a general rule of thumb, a CHP prime mover should operate for 5,000 hours per year in order to guarantee financial feasibility this rule applies in both µCHP and macro CHP systems especially with fuel cell-based micro CHP systems that should not be switched on and off regularly in order to avoid irreversible degradation. It is only feasible to implement the CHP system if the savings on the running costs of the factory or household exceed the annual capital costs incurred by the system. This will be discussed further in chapter 4 of this thesis.

2.6. Challenges Facing Residential µCHP

As µCHP units, such as the Eneos ENE Farm discussed in [14], become commercially available the manufacturers of these systems encounter challenges that must be overcome to ensure the success of the technology. Micro CHP is not the only form of distributed generation available as

stated earlier and table 2-2 highlights some of the challenges manufacturers of μCHP units are currently facing. These challenges are likely to be faced by all individuals or organisations developing residential μCHP systems and knowledge of them can help to model simulations.

Table 2-2: Current Challenges Facing Commercially Available μCHP Units [15]

Challenge	Reason	Implications	Potential Actions
Micro-CHP is able to meet household heating needs but it may take the system longer to heat up the house	• Boilers tend to be oversized and have higher thermal output than the Micro-CHP units that replace them. • Micro-CHP systems tend to have smaller thermal ratings in order to ensure efficient performance.	• Potential customer perception that the system is not able to provide the required levels of comfort. • If units are oversized to address this, then Micro-CHP units may not perform optimally.	• Manufacturers have partially addressed this by adding auxiliary 'boost' burners. • Installers need to ensure that units are always sized correctly. • Suppliers to continue to educate customers on the characteristics of their system and how to get the best performance from it.
Some users prefer to locate Micro-CHP units in 'external' Rooms	• Micro-CHP systems have so far tended to be slightly larger and noisier than conventional heating systems.	• Case losses no longer provide useful heat to the living area. • Users potentially less likely to make optimal use of system controls if located externally.	• Manufacturers need to be aware of implications for installation/operation. • The latest Micro-CHP units are expected to be considerably quieter, which should reduce the likelihood of this occurring.

Challenge	Reason	Implications	Potential Actions
In some cases householders have found the control interface complicated	• This is thought to be due to the early stage of technology development rather than being a fundamental problem.	• Potential for customers to programme system incorrectly, leading to sub-optimal performance.	• Manufacturers are known to be enhancing their user interface designs in subsequent product versions.
Large supply companies have had difficulty in responding to some customer issues	• Call centre staff may have limited or no knowledge of Micro-CHP. The problems raised are often complex and specific to individual installations.	• Potential customer perception of poor levels of service and support in early days of the market.	• Suppliers need to build knowledge and put in place relevant support services. This is already in progress for leading suppliers. • Service offerings should ideally involve call-out support from skilled local technicians.
Some customers have not noticed any reduction in their energy bills	• This may to be due to underlying increases in energy prices being larger than any savings during the period. • Monthly estimated billing and fixed direct debit payments often mask any savings in the short term.	• Customers may perceive that Micro-CHP has not delivered on promises made by suppliers.	• Suppliers need to ensure customers are provided with relevant and up-to-date information. • Some suppliers are now providing export reward tariffs and this provides an opportunity to clearly communicate financial benefits to customers.

Challenge	Reason	Implications	Potential Actions
If customers switch energy suppliers, their new supplier may not have an equivalent Micro-CHP offering	• Customers are able to switch energy suppliers at short notice and are encouraged to do so via online service providers. • Some energy suppliers are not equipped to handle queries relating to Micro-CHP devices and do not provide export reward payments.	• Customers may find that they are unable to discuss their Micro-CHP device with their new energy supplier. (However, they should still receive technical support from the original device provider) • Customers receiving export payments may not get these from their new supplier.	• Suppliers to educate early adopters of Micro-CHP products regarding the support they can expect to receive from their device provider and energy supplier, as appropriate. • Energy suppliers to ensure adequate support available for customers as the market grows.

In addition to these challenges, the legislature of the countries in which the systems are to be developed and/or operated can determine the effectiveness of the implementation of potential/proposed actions described in table 2-2.

2.7. Standalone vs. Grid-tied µCHP Systems

Not all residences are connected to the national electricity grid and gas supply networks the connection to the grid or lack of connection influences the sizing and operating strategy of a residential µCHP system. If a µCHP system is not connected to the grid all energy requirements of the household are to be met via the µCHP system and the system will be sized to cater for the thermal and electrical demand peaks. This section compares systems connected to the electricity grid and systems not connected to the grid.

2.7.1. Standalone Residential µCHP Systems

A standalone micro CHP system will have different power and energy requirements to a grid-tied system. These systems are installed when it is not economically feasible to connect to

electrical grids or gas supply networks. All thermal and electrical power peaks on the load profile must be met entirely by the stand-alone µCHP system but with grid-tied systems, the burden of the highest electrical power peaks can be split between the Micro CHP system and the National Electricity Utility.

The characteristics of the stand-alone (SA) Micro CHP according to [16], an example of which is shown in figure 2-3, are as follows:

- SA energy systems operational capacity is matched to the demand.
- These systems are ideal for remote locations where the system is required to operate at low plant load factors.
- Storage of electricity is required for periods where there is no generation leading to extra battery and heat storage costs, or else the excess power generated has to be discarded.
- The power and energy requirements of the stand-alone µCHP system are less dependent on the operating strategy and more dependent on actual energy demand of the Micro CHP site.

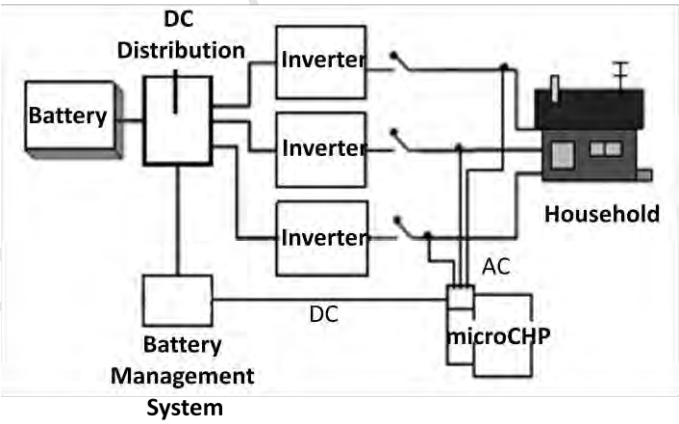

Figure 2-3: Stand-alone Residential µCHP System [17]

2.7.2. Grid-tied Residential µCHP Systems

These µCHP systems import electrical energy from the grid in addition to electricity and heat generated via the µCHP prime mover to meet household energy demands. The DC output from the prime mover is inverted to single-phase AC used to meet household electrical energy

requirements. The amount of energy generated by the prime mover at a point in time is determined by the control strategy employed by the µCHP system. Electrical energy is taken from the grid but it is also possible to sell energy back to the electricity supply authority by delivering power back to the grid. A feed-in scheme is possible and involves the selling of electricity back to the electricity supply authority for a fixed price (the feed-in tariff). These schemes are already being implemented in some countries as a way to support µCHP market growth as this is regarded as a preferred way of generating energy.

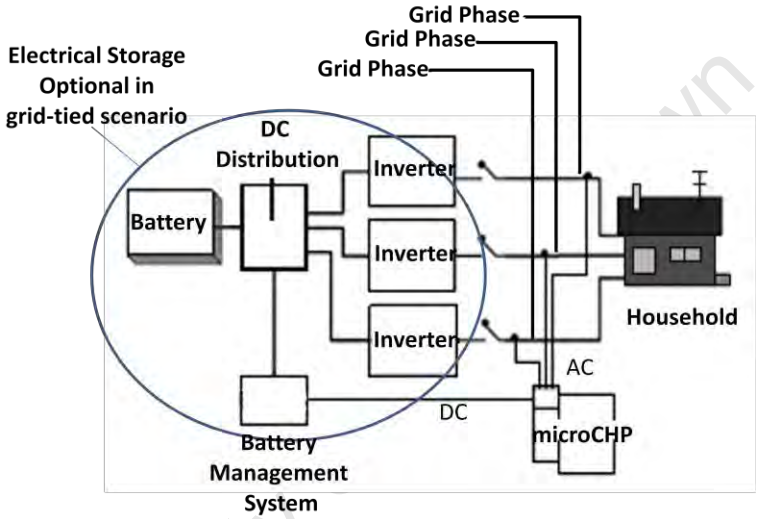

Figure 2-4: Stand-alone Residential µCHP System [17]

The characteristics of a grid-tied residential µCHP system according to [16] are:

- A grid-connected energy system is an independent decentralized power system that is connected to an electricity transmission and distribution system (referred to as the electricity grid).
- They are ideal for locations close to the grid.
- The operational capacity is determined by the supply source. The system functions only when the supply sources are available.
- Because of the supply driven operation, the system may have to ignore the local demand during times of unavailability of supply sources.
- The system could either be used to meet the local demand while surplus is fed to the grid, or otherwise, the system may exist only to feed the grid.

- The connectivity to grid enables setting up relatively large-scale systems and hence they can operate at high plant load factors improving the economic viability of the operation.
- In a grid-connected power system the grid acts like a battery with an unlimited storage capacity. So it takes care of seasonal load variations. As a result, the overall efficiency of a grid-connected system will be better than the efficiency of a stand-alone system, as there is virtually no limit to the storage capacity, the generated electricity can always be stored, and the additional generated electricity need not be ‘‘thrown away’’.
- In addition to the initial cost of the system, cost for interface of the system with grid is incurred.
- For systems operating on renewable sources like biomass, wind and solar PV, there will be a high pressure on these renewable sources, as the system usually operates at high scales and need more biomass for its operation which is discussed in [18] and [19].
- Not all energy demand has to be met by the CHP system and thus the power and energy requirements are more dependent on the operating strategy used than the actual energy demand of the µCHP site.

In this thesis emphasis will be placed on grid-tied residential µCHP systems where a gas supply network is available as the market infrastructure is already available in target countries such as Denmark.

2.8. Fuel Cell Power Conditioning

A fuel cell-based µCHP system operating at the maximum possible efficiency is desired to minimize operating costs. In order to achieve this, the electrical and thermal output of the fuel cell must be controlled to ensure that maximum usage is made of all energy generated by the fuel cell. As electrical *and* thermal energy are being generated in CHP there is an electrical efficiency and a thermal efficiency associated with the prime mover. During the operation of the fuel cell, the efficiencies (both thermal and electrical efficiency) may vary as the operating point (power output level) of the fuel cell varies. This affects the running costs of the fuel cell as the amount of electrical and thermal energy used is proportional the thermal and electrical efficiency. The electrical and thermal efficiency of the fuel cell will be discussed briefly.

2.8.1. Electrical Efficiency

The electrical efficiency of a fuel cell can be defined as the ratio of electrical energy being generated by the fuel cell's operation to the total energy being put into the system. Mathematically this can be expressed as:

$$\text{Electrical efficiency} = \frac{electrical\ \ energy\ \ output}{total\ \ energy\ \ input} \tag{2.5}$$

The electrical efficiency of the fuel cell varies as the operating point of the fuel cell varies due to changes in the energy losses associated with the fuel cell discussed in section 2.8.4. This has been accounted for by the authors of [17] who proposed equation (2.6):

$$\text{Electrical efficiency} = -ax + y \tag{2.6}$$

Where x = the fraction of the fuel cell's capacity at the operating point

y = electrical efficiency of fuel cell at 0% load

a = electrical efficiency at 100% load - y

2.8.2. Thermal efficiency

The thermal efficiency of a fuel cell can be defined as the ratio of thermal energy being generated by the fuel cell to the total energy required by the system. Mathematically this can be expressed as:

$$\text{Thermal efficiency} = \frac{thermal\ \ energy\ \ output}{total\ \ energy\ \ input} \tag{2.7}$$

The electrical efficiency of the fuel cell varies as the operating point of the fuel cell varies due to changes in the energy losses associated with the fuel cell discussed in section 2.8.4. This has been incorporated by the authors of [17] in equation (2.8):

$$\text{Thermal efficiency} = bx + y \tag{2.8}$$

Where x = the fraction of the fuel cell's capacity at the operating point

y = thermal efficiency of fuel cell at 0% load

b = thermal efficiency at 100% load - y

2.8.3. Heat-to-Power Ratio

The heat-to-power ratio of a fuel cell can be defined as the ratio of the fuel cell's thermal output to its electrical output. This can be expressed mathematically as:

$$\text{Heat-to-power Ratio} = \frac{thermal\ \ energy\ \ output}{electrical\ \ energy\ \ output} \tag{2.9}$$

The heat-to-power ratio is also equivalent to the ratio of thermal efficiency to electrical efficiency of the prime mover.

$$\text{Heat-to-power Ratio} = \frac{thermal\ \ efficiency}{electrical\ \ efficiency} \tag{2.10}$$

$$= \frac{thermal\ \ energy\ \ output}{electrica\ l\ energy\ \ output} \times \frac{energy\ \ input}{energy\ \ input}$$

$$= \frac{thermal\ \ energy\ \ output}{electrical\ \ energy}$$

This ratio increases as the current density of the fuel cell increases as shown in figure 2-5. A high heat-to-power ratio can be desirable when thermal demand exceeds electrical demand. However, as will be seen in chapter 4, residential heat demand is not constantly high so a high heat-to-power ratio will result in the need for an excessively large thermal storage tank or the loss of thermal energy during low thermal energy demand periods.

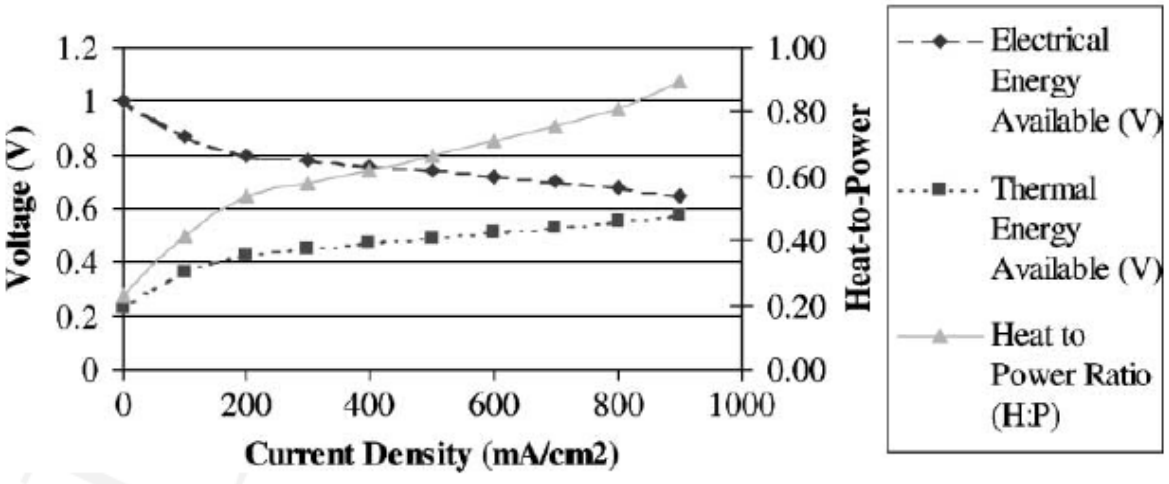

Figure 2-5: Heat-to-power ratio and polarisation curve for PEM Fuel cell [20]

In large manufacturing factories excess thermal energy can be used for other industrial processes by utilising a bottoming-cycle thermodynamic cycle discussed by the authors of [6]. Thermal demand is always high enough to warrant production of heat and in many manufacturing processes a much larger proportion of electrical energy is needed as opposed to thermal energy.

2.8.4. Fuel Cell Subsystems (BOP)

The fuel cell of figure 2-1 simply shows the anode and cathode chambers and membrane and excludes the external components that make up the fuel cell. A fuel cell stack requires a Balance of Plant (BOP) and includes all the subsystems responsible for ensuring the operation of the fuel cells in the fuel cell stack. In order to control the fuel cell stack all the subsystems of the stack need to be monitored and these can be divided into the Reactant Flow Subsystem, Heat and Temperature Subsystem, Water Management Subsystem, Power Management Subsystem and Fuel Processor subsystem as discussed in [21].

Figure 2-6 is a block diagram of a fuel cell indicating the mechanisms in place to ensure correct operation of the fuel cell (balance of plant).

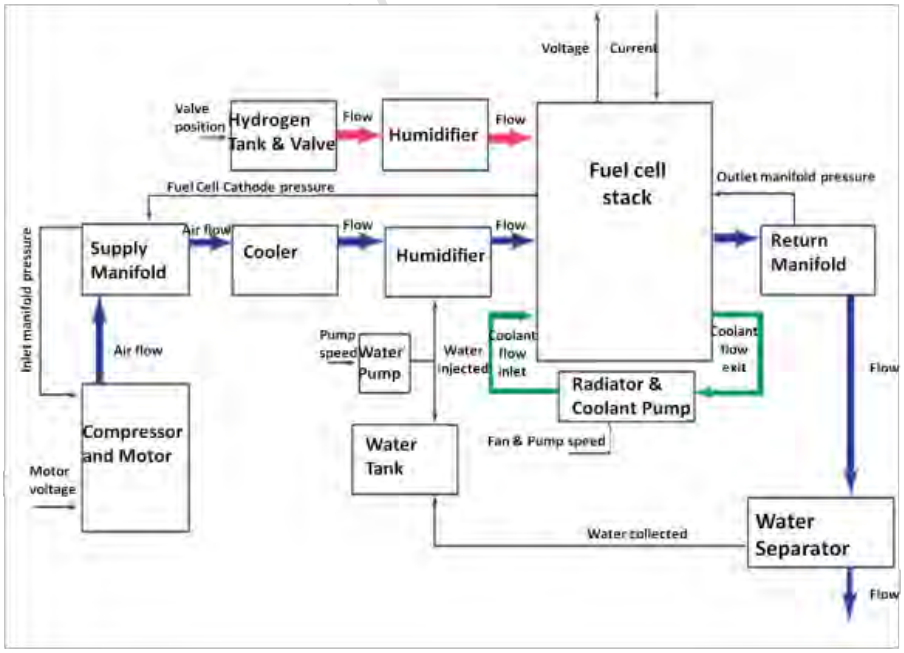

Figure 2-6: Fuel Cell System Block Diagram [22]

The Reactant Flow Subsystem consists of hydrogen supply and air supply loops shown by the arrows labelled 'flow' in figure 2-6. Hydrogen flow in the anode and air flow in the cathode are adjusted using a valve and positive pressure flow device. The control objective is to provide adequate reactant flows (maintaining the desired excess ratio) thereby minimizing auxiliary power consumption.

The Heat and Temperature Subsystem includes the fuel cell stack cooling system (labelled Radiator and Coolant Pump) and reactant temperature system. De-ionized water must be used as a coolant instead of a more effective coolant fluid since coolants with contain charged particles will interfere with the chemical reaction of the fuel cell. In the Combined Heat and Power Application of fuel cells this is not the case. The speed of the cooling fan and recirculation pump are adjusted by a bypass valve.

The task of the Water Management Subsystem, consisting of the Water Separator, the Water Tank, the Return Manifold and the Water Pump, is to hydrate the polymer membrane (for PEMFCS) and to balance water consumption/usage of the system. Dry membranes and flooded fuel cells cause high polarization losses. Lack of proper humidification control can result in a 20% to 40% drop in voltage.

The Power Management Subsystem controls the power drawn from the fuel cell stack and is the power electronic interface that will be developed in this thesis. The current drawn from the fuel cell affects the other subsystems. The control of this current can be used to indirectly control the other subsystems.

The Fuel Processor Subsystem is necessary due to the absence of pure hydrogen to run the fuel cell. Many fuel cell-based systems will use natural gas which is a naturally occurring mixture of methane and other hydrocarbon gases. In the case of using natural gas, a fuel reformer is required which was described in section 2.4.1 and involves the chemical reaction of equation (2.4).

2.8.5. Fuel Cell Operation

Figure 2-7 shows an equivalent circuit model of a fuel cell often used as a reference for control of the fuel cell:

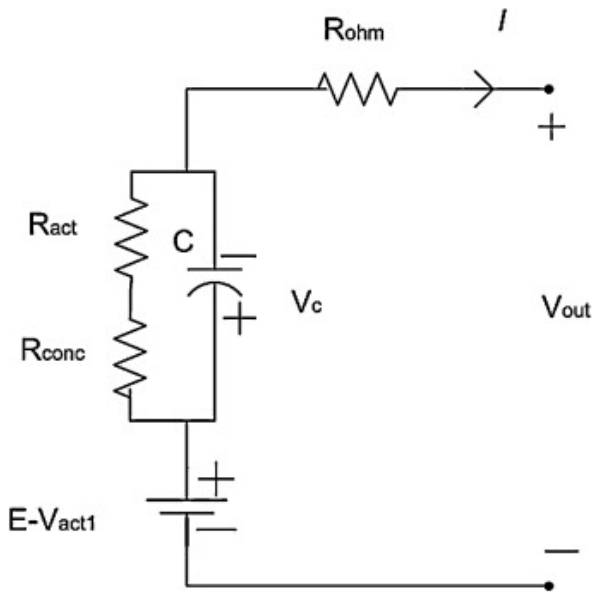

Figure 2-7: Fuel cell Equivalent Circuit [23]

The voltage across the fuel cell is dependent on the values of each of these losses. The equation to describe the voltage across the fuel cell is known as Nernst equation. Equation (2.11) shows a simplified version of Nernst equation.

$$V_{fc} = E - v_{act} - v_{ohm} - v_{conc} \quad (2.11)$$

Where:

- E = open circuit over-voltage of fuel cell
- v_{act} = activation losses
- v_{ohm} = ohmic losses
- v_{conc} = concentration losses

A detailed discussion of Nernst equation was given by the authors of [3]. By controlling the voltage output of the fuel cell each of the losses represented in equation (2.11) can be minimized. The electrical efficiency of the fuel cell is proportional to the voltage across its terminals and as this voltage drops the activation, ohmic and concentration losses increase. As

illustrated earlier the thermal efficiency increases as the electrical efficiency increases so an ideal operating point is not necessarily the one with greatest electrical efficiency.

A fuel cell is a non-linear energy generator whose dynamics are not always suitable for a particular application area (residential application in this case). The I-V characteristic of any fuel cell is given by its polarisation curve and figure 2-8 illustrates the general polarisation curve of a PEMFC.

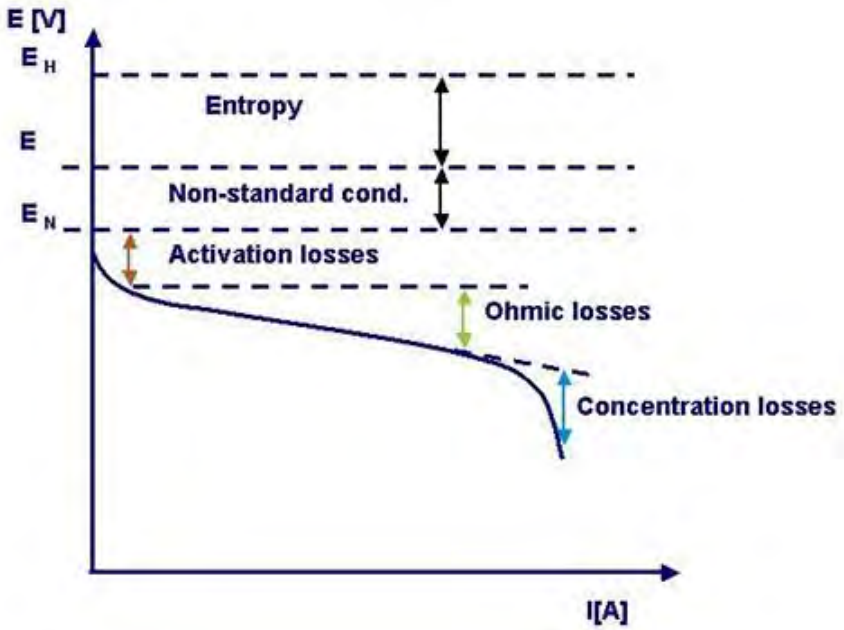

Figure 2-8: Polarisation curve for a Fuel Cell [24]

In order for the fuel cell stack to be used to supply a steady DC current the load should be shielded from fluctuations in fuel cell voltage. This is done using a power electronic interface which regulates the voltage output from the fuel cell. The power electronic interface isolates the fuel cell from the load and prevents current from flowing back into the fuel cell which would result in damages. The majority of interfaces make use of DC/DC Full-bridge Boost Converters, DC/DC converters and inverters to manage the power output of the fuel cell. The following section will give a brief overview of the topologies available for these electronic interfaces. A power electronic interface will be designed to manage the HTPEMFC as per the objectives of this thesis project. These components are going to be developed in the laboratory

so that comparison can be made between simulation of the hardware and experimental results of the laboratory-built and tested interface.

2.8.6. DC/DC Full-bridge Boost Converters

According to the authors of [7] there exist two varieties of DC/DC Full-bridge Boost Converters namely: controllable and uncontrollable rectifiers. These are used in multi-stage Power Electronic Interfacing circuits where the DC from the fuel cell has been chopped to produce AC. The ultimate goal of these interfaces is to connect to the grid discussed in section 2.9 and converters of this nature enable stepping up of the fuel cell voltage via a step-up transformer which is necessary in the household applications of µCHP. A $220V_{RMS}$ AC output is required which is higher than the 20V to 40V fuel cell output.

The uncontrollable rectifiers that are most frequently implemented are diode rectifiers. Figure 2-9 shows a single phase full diode bridge rectifier. This topology will be used in this thesis project and will be discussed in section 5.2.3. The high frequency transformer is used to step up the voltage coming from the DC/DC converter enabling a high DC voltage to be obtained from the high AC voltage input.

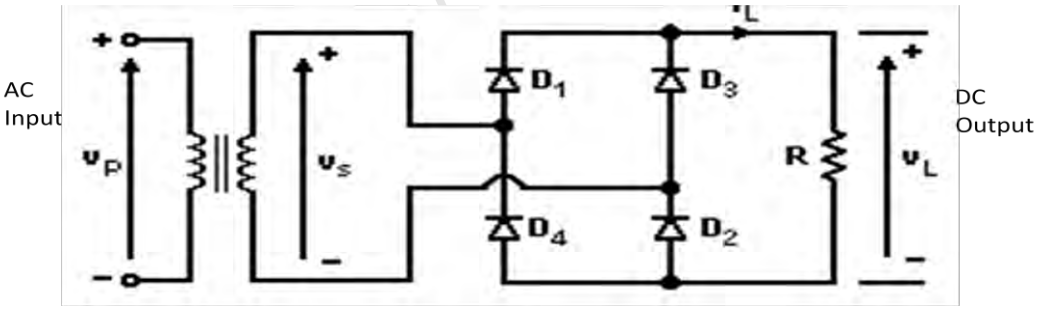

Figure 2-9: DC/DC Full Bridge Boost Converter [25]

The Full DC/DC Full Bridge Boost Converter electrically isolates the fuel cell from load current transients that may result in current flowing back into the fuel cell which would damage it and steps-up the low fuel cell voltage in order to obtain the 400V DC Bus required by the final stage of the topology (the inverter) as will be discussed later.

Controllable rectifiers are normally thyristor-based rectifiers and pulse width modulated bridge rectifiers. A thyristor-based rectifier is controlled by the firing angle of the thyristors gate signals. This is explained in detail in [7].

2.8.7. DC/DC Converters

The voltage level of a fuel cell varies throughout the lifespan of the fuel cell and gradually decreases as the fuel cell ages. The voltage across a fuel cell stack is relatively low for residential applications and varies non-linearly with current density. There is a need to regulate this voltage via a DC/DC converter. According to [7] these can be classified into isolated converters and non-isolated converters.

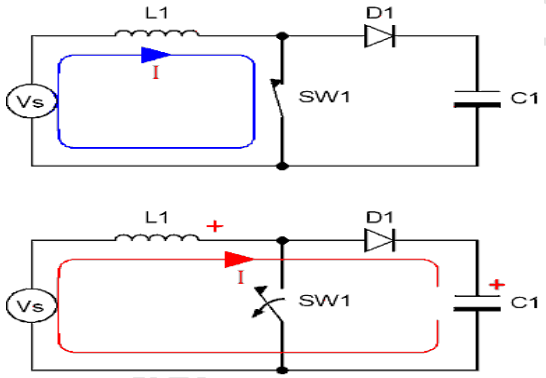

Figure 2-10: Boost converter with switch in on state and switch in off state [26]

Non-isolated converters include boost (step-up), buck (step-down), buck-boost, Cúk and full bridge converters. The boost converter shown in figure 2-9 has an output voltage higher than that of the input voltage. This will form part of an interface connecting a fuel cell to the grid as discussed in section 2.9. The relation between the input and output is given by equation (2.12):

$$Vout = \frac{Vin}{1-D} \tag{2.12}$$

Where D = Duty ratio of switch (usually a MOSFET)

By varying the value of the duty cycle D in response to the value of the voltage output of the converter, a constant voltage can be maintained at the output of the converter thereby regulating the non-linearly varying output voltage of the fuel cell.

The isolated converters types are fly-back, forward, push-pull, isolated half-bridge and isolated full bridge. The isolated converters all have an electrical isolation device between their input and outputs and this is typically a high frequency transformer. These are discussed in detail in [7] but not implemented in this project because the isolation required is provided by the DC/DC Full-bridge Boost Converter.

2.8.8. DC/AC Inverters

These constitute the final stage in a power electronic interfacing circuit converting the DC into AC to be fed into the household. The goal when implementing these converters is to connect to the grid as discussed in section 2.9. There are single phase and three phase inverters and in the case of residential μCHP systems a single phase inverter is used because the fuel cell generates energy for the household directly and household appliances use single phase electrical power. Figure 2-11 shows a single-phase inverter. Sinusoidal pulse width modulation is used to control the switching times of the switches T1 to T4 and the result is a high voltage PWM signal between terminals A and B. A sine wave is produced by filtering the pulse width modulated inverter output discussed in the following next section. The body diodes connected across the IGBTs are there to mitigate turn-off transients of the IGBTS by providing and alternate current path.

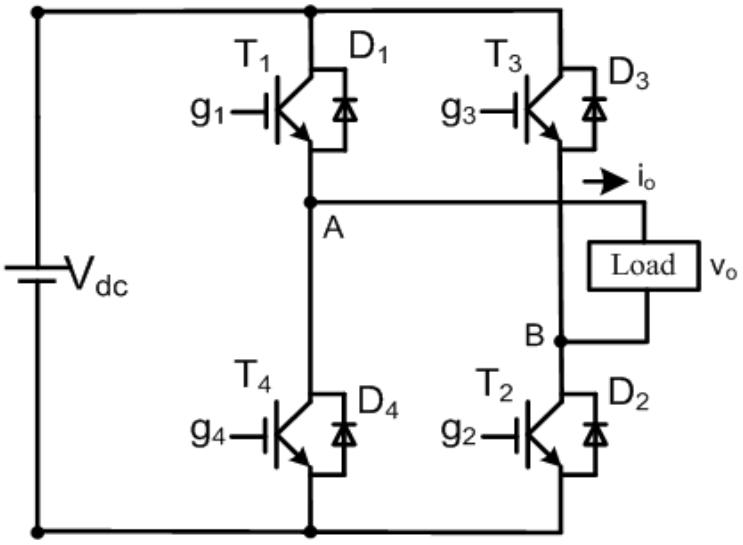

Figure 2-11: Single Phase Full Bridge Inverter [27]

2.8.9. Harmonic Mitigation

Harmonic mitigation refers to the removal of harmonics (frequency components) that are not desired in the output of a power source. Whereas the closed-loop voltage amplitude control implemented in the power electronic interfaces of this thesis deal with input side distortion, the sinusoidal PWM driven output will contain frequencies components above the desired 50Hz and a harmonic mitigation technique must be employed to reduce these. The following options exist for the removal of the harmonics:

- Line reactors: a reactance is placed in series with the load.
- DC Chokes: A reactance is placed in series with the DC bus.
- Active IGBT Rectifiers: Rectifiers that are actively controlled in the way that they conduct current as described in [28].
- Passive filters: Components with frequency-dependant reactance are used to allow some frequencies to pass not attenuated and some to be significantly attenuated.

Table 2-3: Harmonic Mitigation Methods Advantages and Disadvantages [28]

Harmonic Mitigation Method	**Advantages**	**Disadvantages**
Line reactors	Relatively cheap	Only lower harmonics by 50%
DC Chokes	Relatively cheap, smaller size	Not effective at dealing with spikes and overvoltage
Active IGBT Rectifiers	High quality sinusoidal output	Expensive
Passive filters	Simple, harmonic study not required	Bulky, must be connected in series with load causing voltage drop, an only be used with non-linear loads

Passive filters will be used in this thesis project due to their simpler implementation and lower cost than active rectifiers. Line reactors will not lower harmonic levels enough resulting in an unacceptable harmonic distortion level. DC chokes will not effectively deal with voltage spikes. No control is required in implementing passive filters and a method of accurately determining the size of an LC filter, which will be used in this thesis, is discussed in chapter 5 of this thesis.

2.9. Grid Codes and Power Flow

The system being developed in this thesis is grid-tied and as such must adhere to the same grid connection codes as distributed generators. The authors of [30] discuss these requirements in terms of connecting wind farms to the national electricity grid. This knowledge can be transferred to fuel cell based μCHP systems because wind farms are also a form of distributed generation. The following requirements must be adhered to when connecting to the grid:

1) Voltage operating range: The voltage output must not vary between maximum and minimum values stipulated in the code. Typically between 85% and 110%.
2) Frequency operating range: The μCHP system is required to operate within typical grid frequency variations. For example some countries use 60Hz and some 50Hz grid supplies and when connecting to the grid a fuel cell must be within a percentage above or below this value. Typically the frequency will be allowed to vary by ±1Hz.
3) Active power control: Several grid codes require μCHP systems to provide active power control in order to ensure a stable frequency in the system and to prevent overloading of lines, etc. The phase and/or amplitude of the voltage output of the fuel cell should be controllable because it is these two quantities that determine the amount of power being sent to the grid or being received from the grid.
4) Frequency control: Several grid codes require μCHP systems to provide frequency regulation capability to help maintain the desired network frequency. Should something happen to change the frequency of the system a controller must exist to detect a change in frequency and adjust the output of the inverter to the correct frequency.
5) Voltage control: Grid codes require that individual μCHP systems control their own terminal voltage to a constant value by means of an automatic voltage regulator. The voltage amplitude must be monitored and a controller should exist to correct deviations from the desired voltage.
6) Reactive power control: The reactive power input and output must be monitored and corrected should the need arise. Electricity consumers must maintain the reactive within these limits otherwise the electricity supply authority may not physically be able to generate the required reactive power.

7) Low voltage ride through (LVRT): This is the ability of the grid-tied system to maintain connection during below normal dips in grid voltage of a specific duration. A typical value would be 0.1s for a grid voltage dip to 0.1p.u.
8) High voltage ride through (HVRT): This is the ability of the grid-tied system to maintain connection during above normal rises in grid voltage of a specific duration. A typical value would be 0.3s for a grid voltage rise to 1.1p.u.
9) Power quality: This refers to the ability of the grid-tied system to provide constant power with minimal fluctuations and of an acceptable phase factor.
10) Total Harmonic Distortion: This is a percentage measure of how effectively undesired harmonics were mitigated and is typically required to be below 5%.

According to the authors of [31] Total Harmonic Distortion (THD) is defined by equation (2.15):

$$THD = \frac{\sqrt{v_2^2 + v_3^2 + v_4^2 + \cdots + v_n^2}}{v_1^2} \quad (2.15)$$

Where v_n = Voltage Amplitude of the nth Harmonic of the Inverter's sinusoidal output

The standards differ in regard to the values of certain quantities so for the purposes of this thesis project the EN61000-3-2 standard will be adhered to should there be a conflict between the different code requirements.

As can be observed from table 2-4 different standards exist by which to compare the system. According to the authors of [32] systems which are connected to the grid via transformer are more robust and thus have less stringent standards applied to them. Thus the power electronic interface of this thesis has a transformer in not just to boost voltage but also for isolation purposes.

Table 2-4: Harmonic Mitigation Methods Advantages and Disadvantages [29]

Quantity	Standard		
	IEC61727	IEEE1547	EN61000-3-2
Maximum Current THD	5%		-
Power factor at 50% of rated power	0.9	-	
DC Current Injection	Less than 1% of rated output current	Less than 0.5% of rated output current	< 0.22A
Voltage Range for Normal Operation	85%-110%	88%-110%	-
Frequency Range for Normal Operation	50Hz ± 1	59.3Hz to 60.5Hz	-

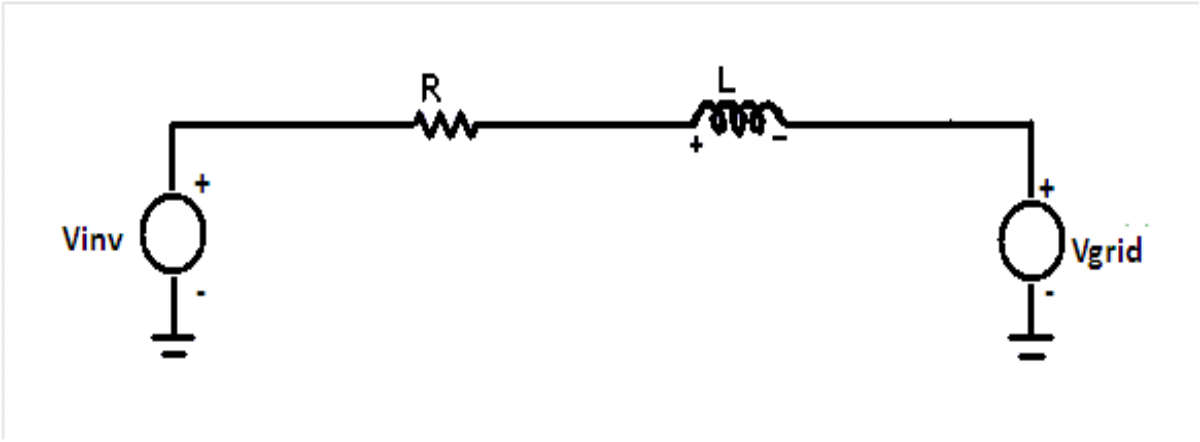

Figure 2-12: Grid-tied inverter model

The final stage of the power electronic interface of the µCHP system is represented by figure 2-12. V_{inv} represents the output of the single phase inverter which is the final stage of the power electronics interface. V_{grid} represents the National Electricity Grid. The power flow direction and magnitude between the two are controlled by the values of the parameters in equations (2.13) and (2.14). In order for power to be transferred to the grid a positive phase angle is required. In

the application of the power electronics interface of this thesis, power will be transferred to the grid and not vice versa in order to avoid current flow into the fuel cell as this will damage it.

$$P = \left(\frac{|Vgrid| * |Vinverter|}{|Xs|}\right) * sin\delta \text{ W} \quad (2.13)$$

$$Q = \left(\frac{|Vgrid| * |Vinverter|}{|Xs|}\right) * cos\delta - \left(\frac{|Vgrid|^2}{|Xs|}\right) \text{ VAR} \quad (2.14)$$

2.10. The Ideal Power Electronic Interface

A three-stage power electronic interface and a two-stage power electronic interface between the fuel cell and the household were implemented in this thesis project and the efficiencies of these topologies were compared. The overall efficiency of the two power electronic interface topologies implemented in this thesis are relatively low compared to inverters discussed in literature. The next step in the development of this interface would be to improve on component efficiency. By comparing efficiency values of similar electronics in literature an estimate on the possible efficiency of this interface can be made. The following points should be noted:

- Transformer efficiencies can be as high as 95.5% discussed as in [33].
- Inverter efficiencies can be as high as 98% with transformerless topologies discussed as in [34].
- DC/DC converter efficiencies can be as high as 95% discussed in [35].

If the efficiency of the AC/DC rectifier stage is assumed to be the equivalent to the efficiency of the transformer (95.5%) because this is the component with the highest losses in this stage of the interface, the highest overall efficiency that can theoretically be achieved is:

Transformerless DC/DC Converter × Transformer Based DC/DC Converter × DC/AC Inverter

=0.95 × 0.955 × 0.98 × 100%= 88.9%

2.11. µCHP Control

The term µCHP control refers to the operating strategy of the µCHP system as a whole and is the regulation of the thermal and electrical operating points (thermal and electrical outputs) of

the µCHP system. The control strategies that are discussed in this section apply to grid-tied residential micro CHP systems and have more complicated control strategies due to the presence of more than one energy source (prime mover and energy purchased from electricity companies) and more than one energy outlet (import and export of electricity, thermal load requirements). Stand-alone residential micro CHP systems are required to meet all heat demand requirements independent of the national grid and thus have simple operating strategies. The focus of the research of this thesis will be on grid-tied systems due to the lower initial investments required to install them. Fuel cell-based µCHP systems as the sole energy source for a household are not ideal due to the need to keep them continuously operational.

The manner in which the µCHP system is used to meet the load requirements will alter the power requirements of the µCHP unit. To reduce the energy cost of the grid-tied system, the system would have to be constantly switching on and off throughout the day. The peak power requirements of the prime mover of the µCHP system will thus differ from the peak energy demand of the household. The current control strategies being implemented on µCHP systems and their effect on power requirements will be investigated. The effect on energy and power requirements for developing control strategies will be discussed.

Table 2-5: Commercially Available µCHP units

Company, Model	Overall Efficiency (LHV)	Price ($US)	System Size (kWe)
Honda(Japan), Ecowill[36]	85%	8815	1
Baxi(UK), Ecogen[37]	91%	8163	1
Eneos (Japan), ENE Farm [16]	>80%	35000	2
ECR(USA), Freewatt [38]	>85%	13000	2

2.11.1. Electricity-led Control

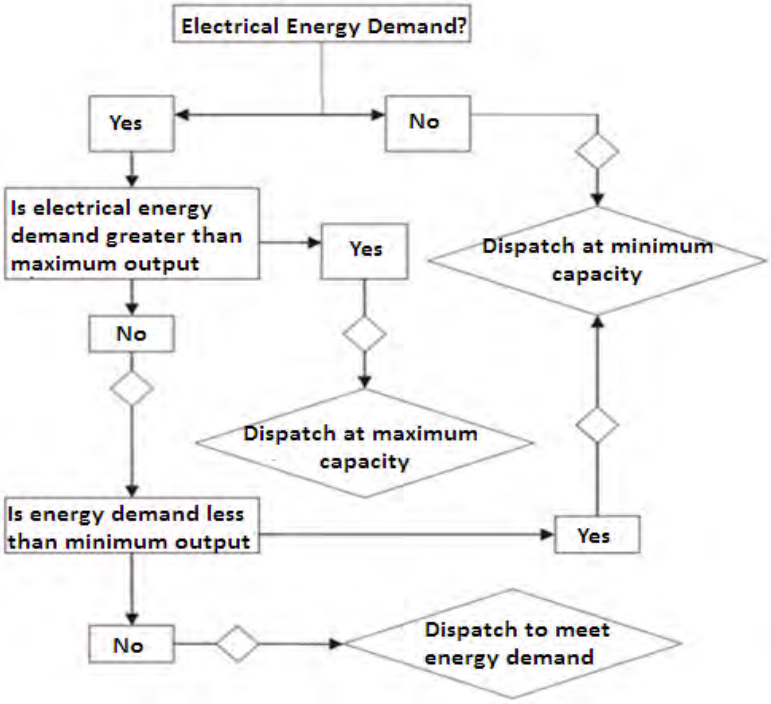

Figure 2-13: Flow Chart for Electricity-led Control [17]

This control strategy refers to when the micro-CHP system's power output is controlled based on the electrical demand. Electrical load following capabilities depend on the characteristics of the prime mover being used. For example, a fuel cell output will not follow the load precisely as turn-off and turn-on of the fuel cell is to be avoided as this leads to degradation. The energy and power requirements of the µCHP system employing this control strategy are determined by the switching strategy of the µCHP system which will be driven by the electrical load. The operating strategy associated with electricity-led control is shown in the flowchart of figure 2-13. There may be slight variations in the operational strategy but most µCHP systems implementing the electricity-led strategy will operate as depicted in figure 2-13.

2.11.2. Heat-led Control

This refers to when the micro-CHP system's power output is controlled based on process heat demand. The accuracy to which the heat load is followed depends on the characteristics of the prime mover being used. The control process in this strategy is controlled by the thermal load. For a process with low thermal load the power and energy requirements will be low even if the

overall process has a high energy demand because a small proportion of this will be heat energy. Heat-led control implements the strategy shown in figure 2-14.

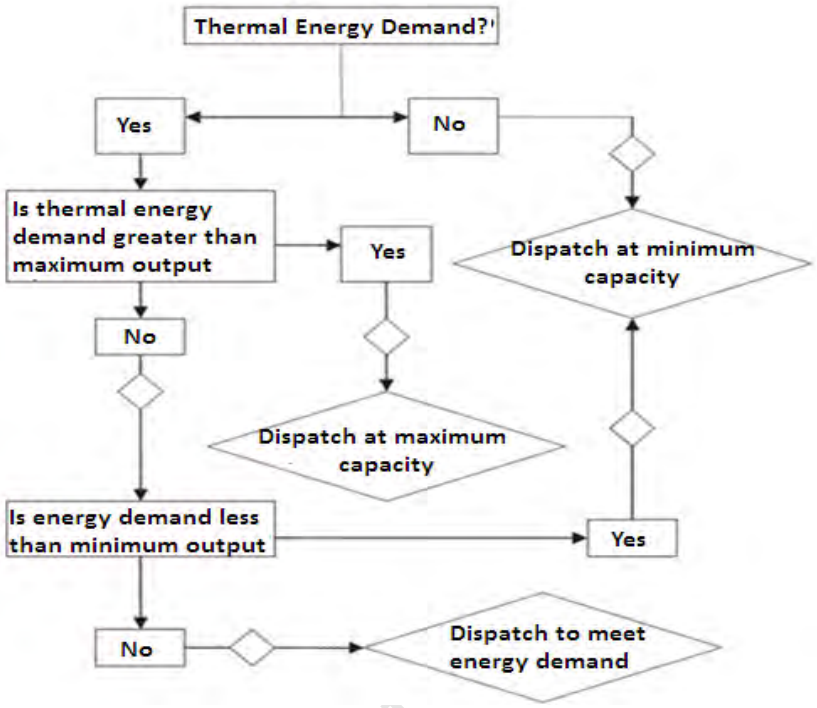

Figure 2-14: Flow chart for Heat-led µCHP Control [17]

2.11.3. Cost-minimizing Control

According to A. D. Hawkes and M. A. Leach, [17] commercially available micro-CHPs are assumed to be heat led. COGEN Europe [39] states that micro-CHP is "a replacement for conventional gas boilers in domestic dwellings, with the micro-CHP unit operating in a 'heat-led' mode". The Energy Saving Trust [40], suggests that electricity is a "by-product" of micro-CHP unit heat production. The heat led operational strategy was used for the first µCHP technology to mass market in the UK: The Stirling Engine operates in a heat led mode, dispatching the engine against heat demand [41], and a supplementary heating unit (either an integrated condensing boiler or other integrated heating unit) where the engine's output is insufficient to meet this demand (the auxiliary burner discussed later). Other micro-CHP technologies are able to modulate output (possibly according to cost signals), and future generations of current technologies may incorporate this feature if it is financially viable.

In addition to the above mentioned strategies, more complex dispatch strategies were investigated in [17], [39], [40] and [41], where the cost of operation and/or other parameters such as emissions are minimised. Some interesting related work, where residential micro-CHP control strategy was optimised to ensure the ability to meet simultaneous loads without recourse to grid electricity or backup thermal systems using fuzzy logic is presented by Entchev in [43].

The concept of price and/or emission minimizing control will now be discussed. The goal of this control strategy is to minimize the variable cost of domestic energy use. Figure 2-15 represents the overall system which equation (2.16) is based on.

This is a control strategy in which a cost function shown in equation (2.16) is minimized in time steps. These costs depend on the gas price p_g, the price of imported electricity p_{imp}, and the price of exported electricity p_{exp}. The gas price is considered to be fixed over time and the evolution of p_{imp} and p_{exp} depends on the relevant tariff structure. Feed-in tariffs are the prices that are paid by the utility for electricity sold back to the grid and reduce the costs of running the µCHP system indicated by the negative sign in equation (2.16).

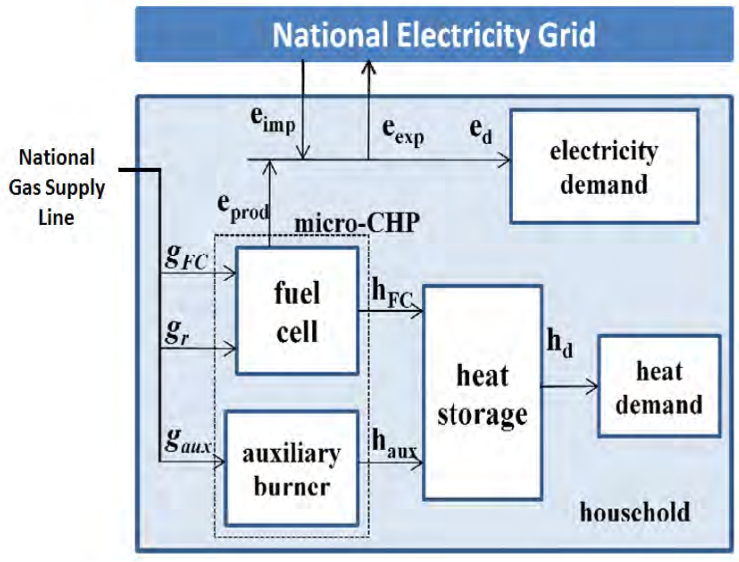

Figure 2-15: Fuel cell-based residential µCHP System [44]

$$C_{chp} = \sum_{k=0}^{M-1}\sum_{l=0}^{N-1}(p_g(g_{FC}[k+l] + g_{aux}[k+l] + g_r[k+l]) + p_{imp}[k+l]e_{imp}[k+l] - p_{exp}[k+l]e_{exp}[k+l] \quad (2.16)$$

Where:

p_g = price of natural gas assumed to be fixed for the day = \$0.16/kWh
g_{fc} = gas used by PEMFC at time [k+l]
g_{aux} = gas used by auxiliary burner at time [k+l]
g_r = gas used by reformer at time [k+l]
p_{imp} = price of imported electricity at time [k+l] = \$0.41/kWh
e_{imp} = moving average of amount of imported electricity at time [k+l]
p_{exp} = price of exported electricity at time [k+l]= \$0.047/kWh
e_{exp} = moving average of amount of exported electricity at time [k+l]
k = hours
l = minutes
M = Hours in a day
N = Minutes in an hour

The control of this system is done in time steps with the minimum value for the cost function being computed in each step. The controller sets the power outputs ($h_{FC,}$ h_{aux} and e_{prod}) of figure 2-15 based solely on the running costs involved in operating the system. The power and energy requirements of the system are influenced heavily by the real-time prices of natural gas and electricity as these are the factors influencing the dispatching of the prime mover of this system. These are the coefficients of the cost function in equation (2.16) and in order to change the operating strategy of the µCHP system when implementing cost-minimizing control all that is required is to change the values of the coefficients of the cost function. The rate at which the fuel cell operating point ramps up or down in voltage prevents an optimal strategy from being implemented in practice.

2.12. Fuel Cell-based Residential µCHP Systems

As stated earlier the prime mover is responsible for generating the electrical and thermal energy in a combined heat and power system. The options that exist for prime movers of residential µCHP are as follows:

1) Stirling Engines
2) Rankine Cycle Engines
3) Fuel cells

4) Internal Combustion engines

The author of [45] highlights the state of fuel cell-based µCHP being used to generate energy for buildings. Future prospects of µCHP system growth are discussed in [46] and governmental support policies for µCHP are discussed by the authors of [47]. Fuel cell-based µCHP differs from other µCHP in that as explained earlier the fuel cell is best operated continuously without switching the device on and off due to the degradation caused by this. As such the operating strategy will differ from that of other µCHP prime movers and a minimum operating point (power output) value is set for the fuel cell. This is best illustrated by showing the actual operating strategy of a residential µCHP system.

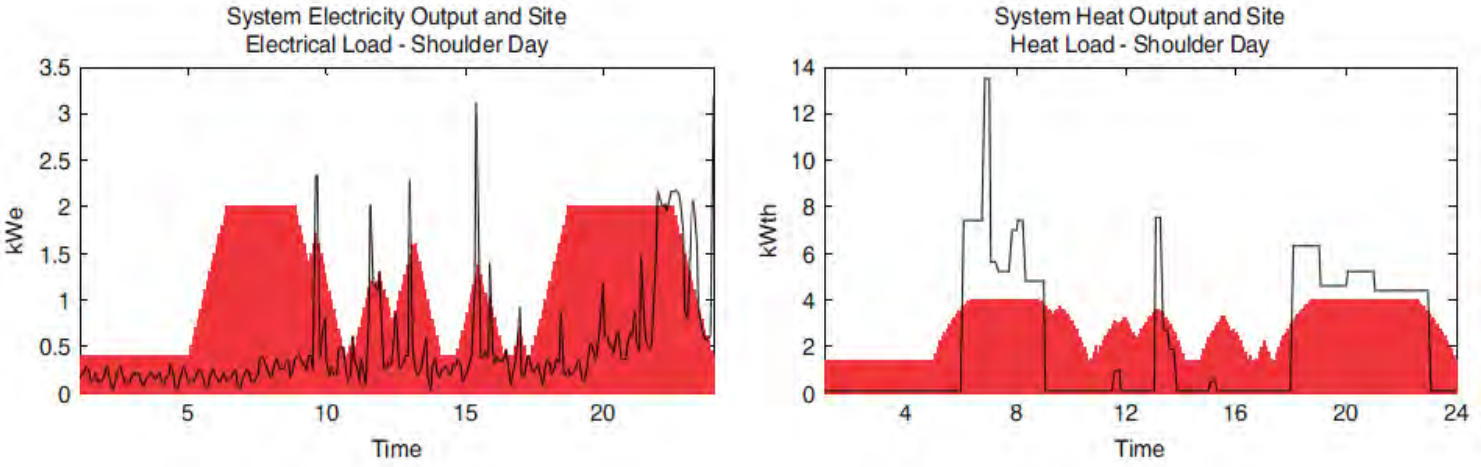

Figure 2-16: Fuel cell-based Residential µCHP System Data (load in black, µCHP output in red) [17]

The SOFC (Solid Oxide Fuel Cell) being tested in the scenario depicted in figure 2-16 has been assigned a maximum and a minimum operating point. The minimum point is at 20% thermal load and maximum operating point of the CHP system is given by the capacity of the µCHP unit. As can be seen from the graphs the rate at which the fuel cell's operating point rises or falls is limited due to the relatively slow dynamics of the fuel cell's chemical reaction. The maximum ramp rate for the fuel cell under investigation in figure 2-15 was 5% of the fuel cell's capacity. The fuel cell is thus unable to accurately follow the thermal and electrical loads of the household and this is taken into consideration in heat-led, electricity-led and cost-minimizing control.

2.13. Conclusion

The above literature provides the necessary background for a study into the successful simulation and subsequent implementation of a fuel cell-based residential µCHP system. The fuel cell-based systems are viewed as more environmentally friendly and less heat constrained than engine-based alternatives. The engine-based µCHP systems have lower initial capital investments and longer average lifespan than fuel cells at the time of preparing this thesis. This literature review highlights the µCHP industry's state at the time of writing this thesis. Methods to control the dispatch of the fuel cell prime mover are outlined and will be used in the sizing method proposed in chapter 4. The system requirements to be met by the power electronic interface before connecting to the grid are outlined and used to ensure safe grid connection in chapters 5 and 6 of this thesis.

Chapter 3

3. µCHP System Model

3.1. Introduction

The components surrounding the fuel cell are known as the balance of plant (BOP) and the µCHP system is considered to be the BOP combined with the prime mover which is a fuel cell in this case. In this chapter a model of a residential µCHP system will be presented.

3.2. System Energy Flow

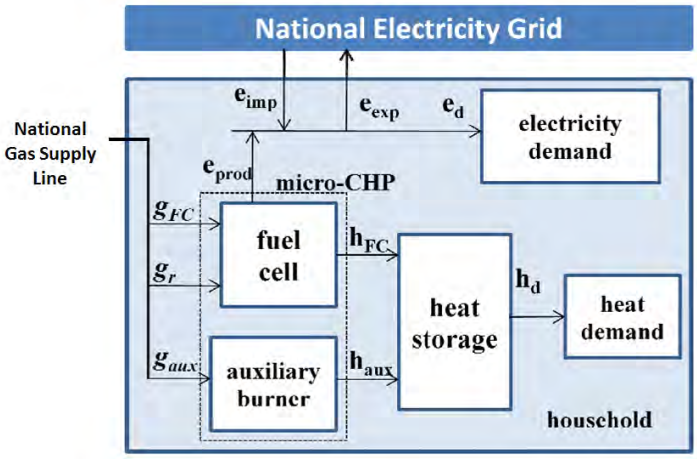

Figure 3-1: Fuel cell-based residential µCHP System [44]

A review of residential µCHP systems that are currently commercially available is given by the authors in [48] and figure 3-1 shows one such system. The system of figure 3-1 is a grid-tied residential µCHP system which occasionally imports energy from the grid as opposed to a standalone system which generates all energy internally. In some European countries, Denmark and England being examples, a gas supply line exists from which natural gas can be obtained for household energy needs and this is the source of g_{FC}, g_r and g_{aux} in figure 3-1. For fuel cell-based µCHP hydrogen is required as the fuel. Systems can be fuelled by pure hydrogen but in general it is usually more viable to use hydrogen that has been extracted from natural gas through a reformer as discussed by the authors in [15]. The µCHP system under investigation will also

have an auxiliary burner, shown in figure 3-1, which meets thermal energy demands not being met by the µCHP system prime mover.

A High Temperature Proton Exchange Membrane (HTPEMFC) will be used as the prime mover of the µCHP system. The HTPEMFC generates thermal energy and electrical energy using a topping thermodynamic cycle, described in [6], in which primarily electrical energy is generated with thermal energy being produced as a bi-product. The thermal energy produced from the exothermic chemical reaction of the fuel cell is used to directly meet the thermal demand of the household and not to generate more electricity.

A Thermal Energy Storage tank (TES) is used in this system since there are occasions when there is a significant electrical load but a negligible thermal load of the household. In situations when there is thermal energy being generated that is not required, the excess thermal energy can be stored in the TES. This contains a good thermal conducting fluid such as ammonium and is insulated to prevent heat loss. The thermal energy stored in the TES is slowly dissipated over time and thus storing thermal energy should be done short term.

3.3. Fuel Cell

The prime mover of the µCHP system, as explained in section 2.4, is responsible for the thermal and electrical energy generation within the system. Fuel cell-based µCHP systems differ from Internal Combustion (IC) and Stirling engine-based systems in that there is no combustion involved in the energy generating process.

An HTPEMFC is considered as the prime mover for the residential µCHP system. A method for determining the size of the fuel cell to use in a µCHP system is discussed in chapter 4.

The aim of the project is to explore the applicability of HTPEMFCs for µCHP applications.

3.3.1. Fuel Cell Dynamics

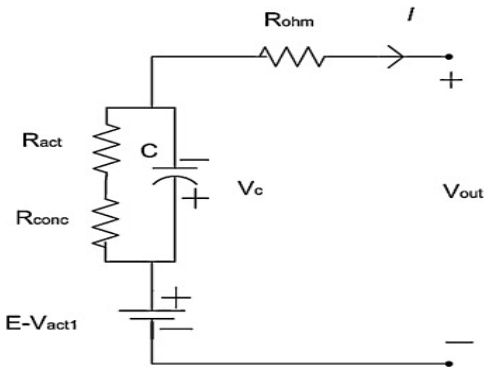

Figure 3-2: Fuel cell Equivalent Circuit [23]

The equivalent circuit of a PEMFC will be discussed to determine the dynamics of the fuel cell. The dynamics of the fuel cell may be characterised by equations (3.1) and (3.2) taken from [21].

$$C\,\frac{dv_c}{dt} + \frac{v_c}{R_{act} + R_{conc}} = i \tag{3.1}$$

$$v_{fc} = E - v_c - iR_{ohm} \tag{3.2}$$

$$v_c = v_a + v_{conc} \tag{3.3}$$

Where
- R_{act} = Equivalent Activation Resistance of fuel cell
- R_{conc} = Equivalent Concentration Resistance of fuel cell
- R_{ohm} = Equivalent Ohmic Resistance of fuel cell
- v_{conc} = Concentration overvoltage
- v_a = Activation overvoltage
- v_o = Open circuit voltage of fuel cell
- i = Current density of fuel cell
- v_c = Voltage across theoretical bybass capacitor

The activation voltage losses of the fuel cell are caused by reactants in the fuel cell not having sufficient energy to react and since bond breaking is endothermic energy is required by reactants to take part in the fuel cell chemical reaction. The ohmic voltage losses are caused by the resistance to electrons crossing the membrane separating the anode and cathode chambers of a fuel cell. The concentration voltage losses occur when reactants cannot be replaced fast enough to keep up with the pace of the reaction and these losses are proportional to current density of the fuel cell. When the current through the fuel cell changes rapidly, the ohmic

voltage drop quantity, iR_{ohm} in equation (3.2), changes instantly. It takes longer for the activation overvoltage and concentration overvoltage to respond to the changes in current. There is therefore a time constant associated with changes in the voltage across the fuel cell. The author in [22] reported the time constant to be 10^{-19}s which is fast dynamics but this value is believed to be for a single fuel cell. The dynamics of the balance of plant is much slower. The concentration of reactants of the fuel cell's chemical reaction, for example, will not change this fast. As a result of this a maximum ramp rate of 25% of the capacity of the fuel cell per 5 minutes is assumed based on these assumptions as well as the same assumptions being made by the authors of [17].

3.3.2. Fuel Cell Operating Conditions

The operating parameters of the fuel cell are determined by the output capacity of the fuel cell. In chapter 4 a sizing methodology in which an appropriate fuel cell size is determined. For the practical implementation of the converters in chapters 5 and 6, a 1kWe HTPEMFC will be used as the basis for all parameter assumptions. Experimental data was available for a 1kWe HTPEMFC and in order to use the data from this fuel cell stack a system of this size was chosen. Table 3-1 gives the corresponding operating parameters of this 1kWe model.

Table 3-1: Fuel cell model input variables for 1kW HTPEMFC [49]

Parameter	Unit	Value
Active area	cm^2	100
Coolant Temperature	°C	100 to 180
Air Pressure	Atm	3
H_2 Pressure	Atm	3
Number of cells in stack	-	48
Air flow rate	lpm	31.9
H_2 flow rate	lpm	8

Since the steady state operation of the fuel cell-based µCHP system is what is being considered. The following assumptions will be made:

- When simulating this fuel cell model a constant coolant temperature of 120°C will be assumed which is feasible at steady state operation.
- The flow rate of air and fuel (hydrogen) are considered constant
- Flow rate of hydrogen and oxygen are determined by the reaction rate.

3.3.3. Fuel Cell Output

The theoretical and experimental polarisation curves for the 1kWe HTPEMFC assumed to be used in the simulations and laboratory work of chapters 5 and 6 fuel cell are shown in figure 3-3 where both the theoretical and practical values for a 1kWe HTPEMFC are considered. The practical results will be used as the basis for the assumption that the 1kWe HTPEMFC output will vary between 20V and 48V. This range can be decreased but the fuel cell's output characteristics change over the lifespan of the fuel cell. A MATLAB programme for determining the theoretical polarisation curve of a given fuel cell is given in Appendix B of this document and this can be used to determine the polarisation curves of the fuel cells used in the simulations of chapter 4.

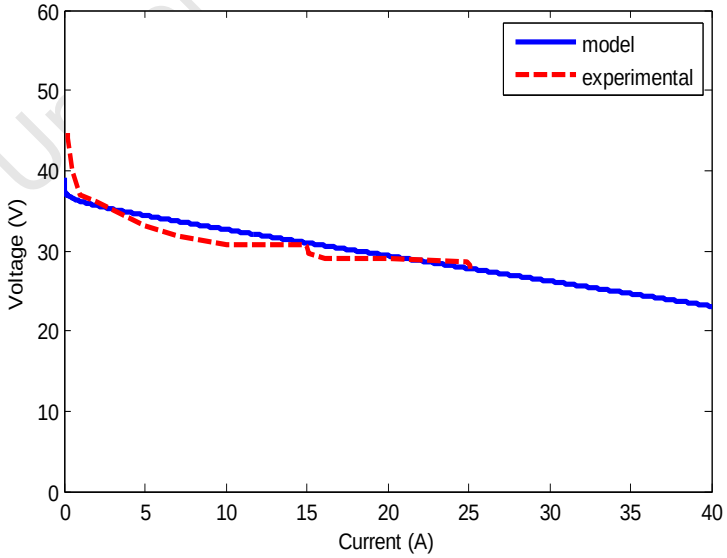

Figure 3-3: 1kWe HTPEMFC Fuel Cell Polarisation Curve

3.3.4. Fuel Cell Efficiency

The efficiency of the fuel cell unit is the ratio of output to input power. In CHP systems, electrical power and thermal power are both utilised so the overall efficiency of a CHP unit, as stated earlier, is given by adding the electrical efficiency and thermal efficiency.

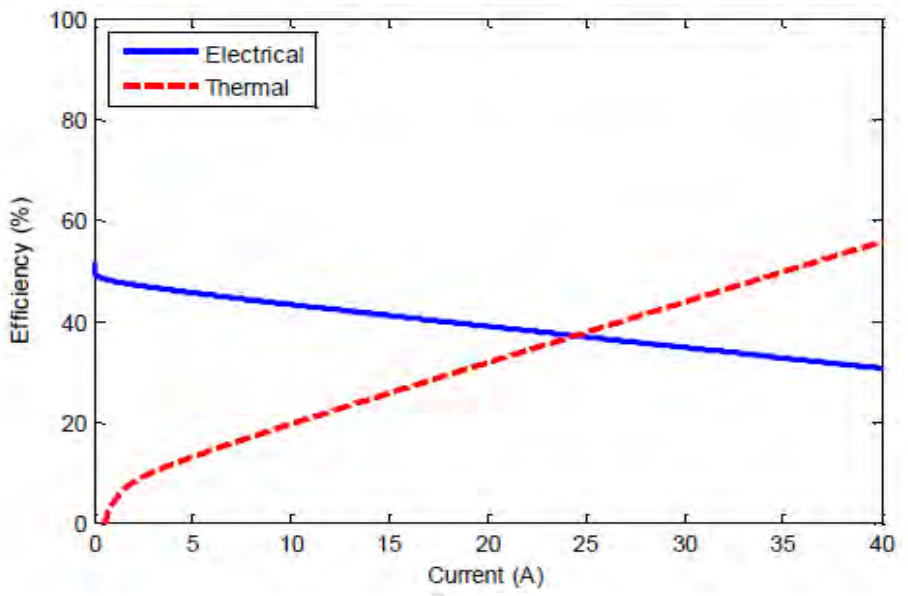

Figure 3-4: Thermal and Electrical Efficiency for a 1kWe HTPEMFC [49]

The electrical and thermal efficiencies of the fuel cell change with operating current and an example of the relationship between electrical and thermal efficiency is shown in figure 3-4. Electrical efficiency for this fuel cell stack varies from approximately 30% to 58.6% having done a line of best fit approximation through the data points on the graph of figure 3-4. Thermal efficiency varies from approximately 5% to 56% using the same approach. These values can be used to obtain an approximate mathematical relationship between the load and the efficiency of the fuel cell.

For example, using the methodology outlined in section 2.8 of this thesis, when the current is 0A (0% of the rated load), the electrical efficiency is 58.6%. When the load is 100% of the rated load the electrical efficiency is 30%. The value of the electrical efficiency at 0% rated load is the y-intercept and assuming a linear efficiency as did the authors of [17] a linear equation is derived for the electrical efficiency of the fuel cell of figure 3-4 which is to be used in the simulations of chapters 4 and 6.

Thus the electrical efficiency of this fuel cell is given by equation (3.4):

$$\text{Electrical efficiency} = -0.286x + 0.586 \quad (3.4)$$

Where x = fraction of rated load of the fuel cell

When the load is 0% the thermal efficiency is 5%. When the load is 100% the thermal efficiency is 56%. Thus, using the same method used to derive equation (3.4), the thermal efficiency of this fuel cell stack is given by equation (3.5):

$$\text{Thermal efficiency} = 0.56x + 0.05 \quad (3.5)$$

Where x = fraction of rated load of the fuel cell

3.4. Auxiliary Burner

This is a natural gas-fuelled burner used to meet heat demand of the household in instances where the fuel cell will not meet this demand. This occurs when either the thermal demand exceeds the thermal rating of the fuel cell or the μCHP control strategy, discussed in section 2.11, requires the fuel cell operating point below the required value to reduce cost. Commercial μCHP systems include the burner in its system. The auxiliary burner provides faster warm up and top-up during periods of high thermal energy demand. The efficiency of this burner will be assumed to be a constant 80%. This is the estimated average efficiency of many burners on the market and this is also a value assumed by the authors of [17] in their μCHP simulations. The efficiency of the burner does decrease with time however the fuel cell has an estimated lifespan of 40000 hours and in this time the efficiency of the auxiliary burner will not have decreased significantly hence the decrease in efficiency will not be incorporated in cost calculations.

3.5. Thermal Energy Storage Tank (TES)

This is a tank filled with a good heat conducting liquid, ammonium being an example, which absorbs heat and is a sealed, insulated container. Tanks of this nature are discussed by the authors of [50]. The size of the heat storage tank is to be determined by the methods outlined in chapter 4. There is a general decrease in the amount of energy stored in the tank over time

even when the tank is idle. When thermal energy is sent to storage instead of being used directly, energy is lost in storage. Therefore there is an efficiency of the storage tank given by equation (3.6):

$$\eta_{sto} = \frac{thermal\ energy\ retrieved\ from\ storage\ tank}{thermal\ energy\ placed\ in\ storage\ tank} \quad (3.6)$$

Thus, thermal energy placed in storage will cost more than that generated and used directly. The efficiency of the thermal energy storage tank will be assumed to be 90% which is the same efficiency for the TES of [17]. The maximum rate at which the storage tank can be charged or discharged will be assumed to be 0.5kWth. In order to evaluate the impact of heat storage on capital cost, it will be assumed that the storage tank price is proportional to the size of the tank even though in practice certain specific tank sizes exist and being able to purchase a heat storage tank of the exact size required is not always possible.

3.6. Electricity Import

Grid-tied μCHP systems are connected to the National Electricity Supply Authority of the country and so electricity can either be imported from the National Grid or generated by the μCHP prime mover. The tariff structures vary from country to country and for the purposes of this thesis, the Danish electricity prices will be assumed since because Denmark is a country with a gas supply network and electricity feed-in scheme required for the implementation of this system. Load data from Denmark was readily available and was required as input to simulations. The average electricity price will be used instead of the varying prices of electricity throughout the day. The average price of electricity at the time of publishing this thesis was found to be US$0.41/kWh (according to [51]) and this will be used in the calculations of chapters 4 and 6. It can be assumed that all prices in this thesis will be in United States dollars.

3.7. Electricity Export

In chapter 4 there are scenarios when the fuel cell is generating more electrical energy than is actually required by the household. The excess electricity will be assumed to be sold back to the electricity supply authority for profit. This is what is known as a feed-through scheme discussed in [44]. The price at which the electricity is sold back to the supply company is known as the

feed-in tariff. The average Danish feed-in tariff at the time of publishing was US$0.0467/kWh (according to [51]) and is what will be assumed in the calculations of chapters 4 and 6. All prices in this thesis will be in United States Dollars.

3.8. Conclusion

To simplify the calculations, certain assumptions have been made with regard to the components of the system under investigation. The assumptions made have been explained in this chapter whereby critical reasoning has been provided in justifying these assumptions. This chapter lays the foundation for the following chapters whereby simulations for optimising and evaluating different control strategies for µCHP systems will be explored.

Chapter 4

4. µCHP Sizing Strategy

4.1. Introduction

As discussed earlier µCHP (micro combined heat and power) systems are defined as CHP systems below 10kWe (10kW electrical power output). It is important to size these systems optimally to avoid higher operational and installation costs than are necessary. Systems that are too large will result in wasting of generated energy especially heat which is difficult to store over long periods of time. Systems that are undersized will not meet the residential heat and electricity demands which will then have to be met by other, less efficient means.

4.2. Industrial CHP Sizing Strategies

Knowledge of Combined Heat and Power Systems of an industrial magnitude is more developed than that of µCHP systems. Some of the principals of the sizing strategies used for industrial CHP systems can be used to size the residential µCHP system and in this section an industrial CHP sizing method will be referenced.

Figure 4-1 shows the flow chart for an optimal sizing strategy for industrial CHP discussed in detail in [52]. The factors taken into consideration when sizing this system are the costs (both capital costs and running costs) and constraints under which the system is to operate. In order to determine the optimal sizing strategy a cost function is proposed which is made smaller in magnitude with each iteration of the flow chart in figure 4-1. The system size that yields the lowest cost function value, whilst operating within the constraints of the system, is the optimal size of the system. For the system of [52] the cost function is given by the equation:

$$Min = Cc + Cr \quad (4.1)$$

Where Cc = Capital Cost

Cr = Running Costs

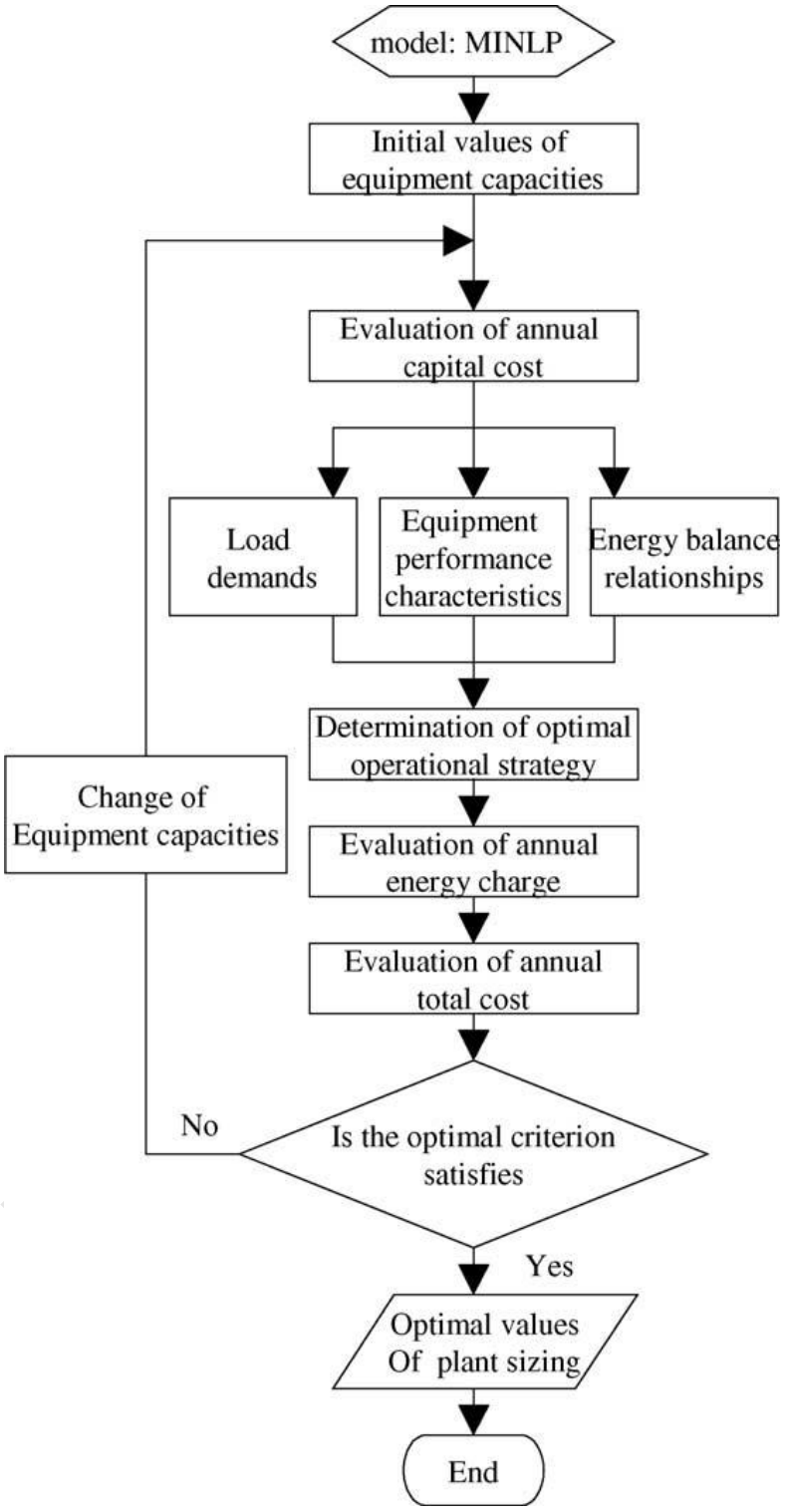

Figure 4-1: Industrial CHP System Sizing Strategy [52]

In order to actually get the capital costs of the system the depreciation of component values with time must be taken into consideration. The yearly capital cost (Cc) of the system is thus given by:

$$Cc = R \times \Sigma (N_i C_i) \quad (4.2)$$

Where N = Number of components

C = Purchasing cost of components

R = Capital recovery factor

The capital recovery factor (R) is used to evaluate the yearly capital cost of the system. In order to be able to determine the optimal size the rate at which the system depreciates in value plays a major role in determining which size of system to buy. If the depreciation in value of the equipment is too rapid then the lifespan of the system will be less than the payback period and it would be unfeasible to purchase the system. The payback period is the amount of time it takes for the savings realized by implementing the system to be equivalent to or greater than the investment into the system. The capital recovery factor is given by:

$$R = \frac{i(1+i)^n}{(i+1)^n - 1} \quad (4.3)$$

Where *i* = interest rate

n = lifetime

The running costs of the µCHP system are given by:

$$\mathrm{Cr} = \sum_{\mathrm{D}} \sum_{\mathrm{H}} \mathrm{C_k}\,(\mathrm{X_k}, \mathrm{Y_K})\mathrm{T_k} \quad (4.4)$$

Where Ck = Hourly energy charge

Xk = On/off status

Yk = Energy flow rate

Tk = On Time period

D = Days

H = Time period length

Equation (4.4) is used to calculate the running cost of the system by summing the energy generated over a period of time and multiplying this by the cost of generating this energy.

The system size that yields the lowest cost function value evaluated over the lifespan of the system is the optimal system size. When evaluating the system it must be noted the exact value of the optimal size may not be feasible in practice due to constraints. The value closest to this optimal value is chosen instead. This industrial method will now be applied to the residential scenario.

4.3. Residential µCHP Sizing Strategy

The system with the optimal operating capacity is the one which yields the lowest cost. This cost is a sum of the running costs and capital costs of the system. The industrial sizing strategy of the previous section can be adapted to the residential scenario bearing in mind the differences between the two scenarios. As stated in the previous chapter in industry heat storage is not an option due to the large amounts of thermal energy generated. Thus industrial systems are designed to avoid excess heat at all costs whereas in the residential scenario storage of heat can lead to reduction in running costs. Industrial CHP can be assumed to be grid-tied whereas residential µCHP comes in two forms: standalone and grid-tied.

The size (maximum power output) of a stand-alone residential µCHP system can be determined much easier than that of a grid-tied system required to meet similar thermal and electrical energy demands. A standalone system is required to meet the entire energy requirements of the household and so the prime mover of the µCHP system together with an auxiliary burner should be capable of meeting the maximum electrical load and thermal load of the residence. That maximum value of electrical and thermal demand of that household is what the size of the stand-alone system will have to be.

The determining of the size of a grid-tied residential µCHP system is complicated by the fact that the µCHP prime mover does not have to generate all the electrical and thermal energy. To size the system according to the maximum load would, in most cases, results in a system too large. This would result in excessive capital costs and wasting of energy that the system is unable to store leading to excessive running costs as well. Figure 4-2 shows a residential version

of the sizing strategy discussed in section 4.2 previously. A step by step explanation of this algorithm now follows.

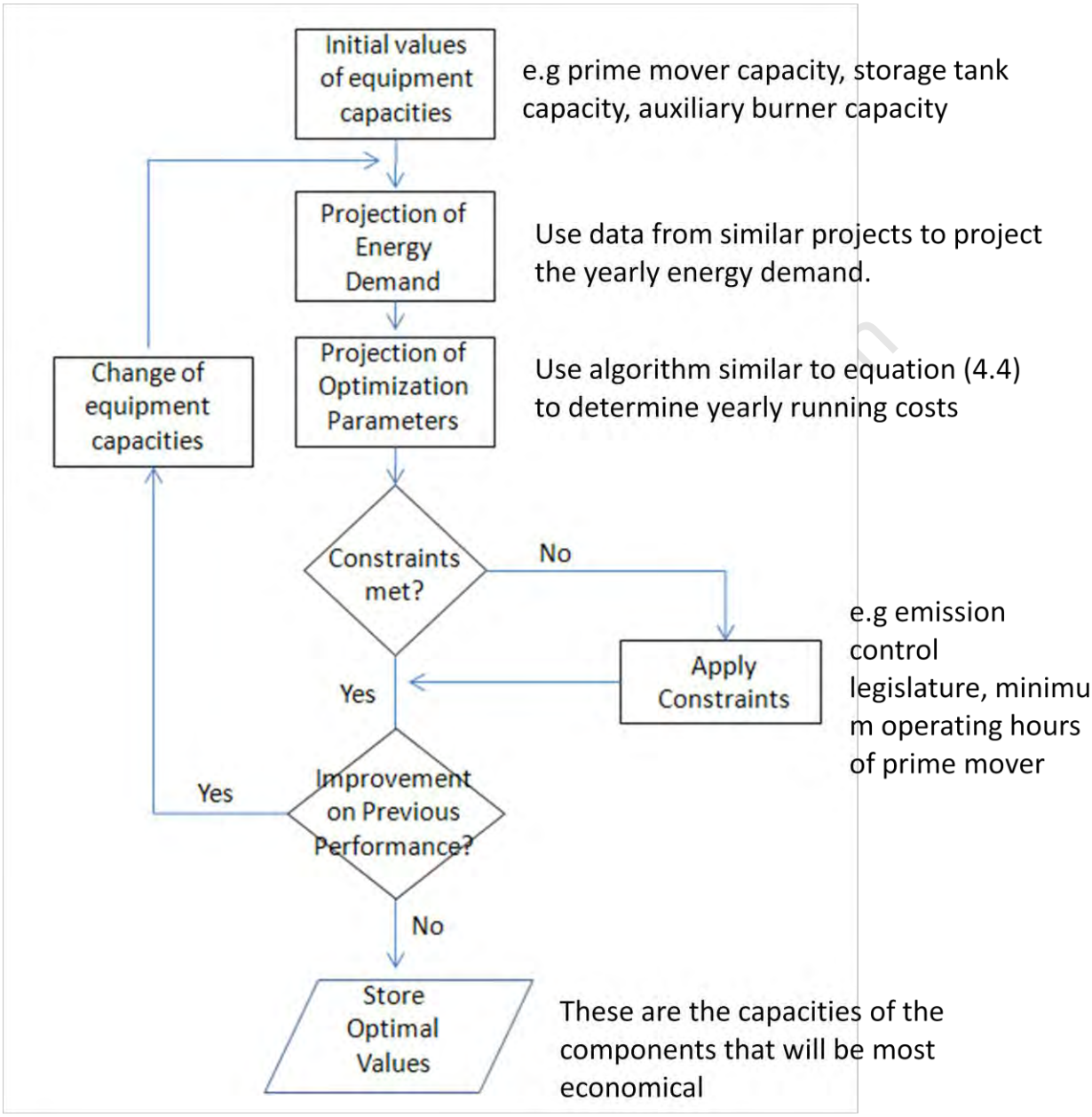

Figure 4-2: Residential µCHP Sizing Strategy

Step 1: Initial values of equipment

The worst case scenario of sizing is the one in which the entire thermal and electrical energy loads of the µCHP system are to be generated by the µCHP system. At no point will there be a need to have the operating point of the µCHP prime mover (an HTPEMFC in this case) to go

above the maximum demand values. The initial values for the fuel cells capacity will be the maximum demand value of the households typical load profile.

Step 2: Projection of energy demand

It will be assumed that the average load profile of a household in the region the system is being designed for will predict the thermal and electrical load of the household. This will not always be 100% accurate but deviations from this will not be extreme due to the fact that the statistics being dealt with are for one household and not a group of households. The energy demand is relatively small in magnitude resulting in relatively small deviations from the average demand which can be updated.

Step 3: Constraints meet?

The constraints of the system are determined by the limitations of the prime mover, legislation and financial considerations. The fuel cell is not to be turned off and on repeatedly during operation because to do so will contribute to degradation explained in [53] which puts a minimum value on the fuel cell operating point which is above zero. Every nation has its own set of allowable residential area noise level and pollution level values which should be taken into consideration when determining the operating point value. Financially, there is an operating point value of the fuel cell at which it is more financially feasible to not purchase the µCHP system which will be highlighted via an example.

Step 4: Improvement on previous performance?

The optimal size of the system is the one that yields the lowest cost function value. Therefore simulations are run over a fixed time period using projected load profile data to determine the cost function value over a year and if this is an improvement on the value from the previous iteration of the flow chart loop then the previous values are replaced with the new ones.

Step 5: Store Optimal Values

The cost function will converge to a value and the sizes of the components of the µCHP system associated with this cost function value are the optimal values. These are the ideal values for the systems size and during construction these are the target values for the size of components.

It may not be possible to attain these exact values in practice due to reliance on manufacturers of various components to supply these. Manufacturing companies may not supply the desired components in the desired proportions.

4.4. Residential µCHP Sizing Example

As discussed in the previous section the cost function used to determine optimal system size takes capital costs and running costs of the µCHP system into consideration. In order to determine these, the power and energy requirements of the system need to be defined.

The factors affecting the power and energy requirements of µCHP system are the profile of the household, the grid-connection and the µCHP control strategy being used by the system and these will be discussed briefly.

4.4.1. Household Load profile

The Danish Single Family Household model will be used to evaluate the theory in this thesis. The data is taken from an average of 25 Danish households over a calendar year available in [54]. The thermal and electrical loads are given by figure 4-4 and 4-5.

The thermal load of the household is the combined hot water storage load and space heating load of the household. The assumption that electrical energy is not to be used to heat the hot water or for space heating is made. This is reasonable given that natural gas-based burners are used to perform these tasks in many household including the ones used to collect the data. As expected a high thermal load is observed in winter as seen in figure 4-4. The fuel cell is advantageous as a prime mover in summer when there is a low thermal load because of the fuel cells low heat-to-power ratio because there will not be a large amount of unused heat to store in the TES.

The electrical load is the energy required by all appliances connected to the plugs of the household electrical network. Electricity is imported from the electricity supply authority and generated by the fuel cell. Excess electricity can be sold back to energy retailer which is depicted by e_{exp} in figure 3-1.

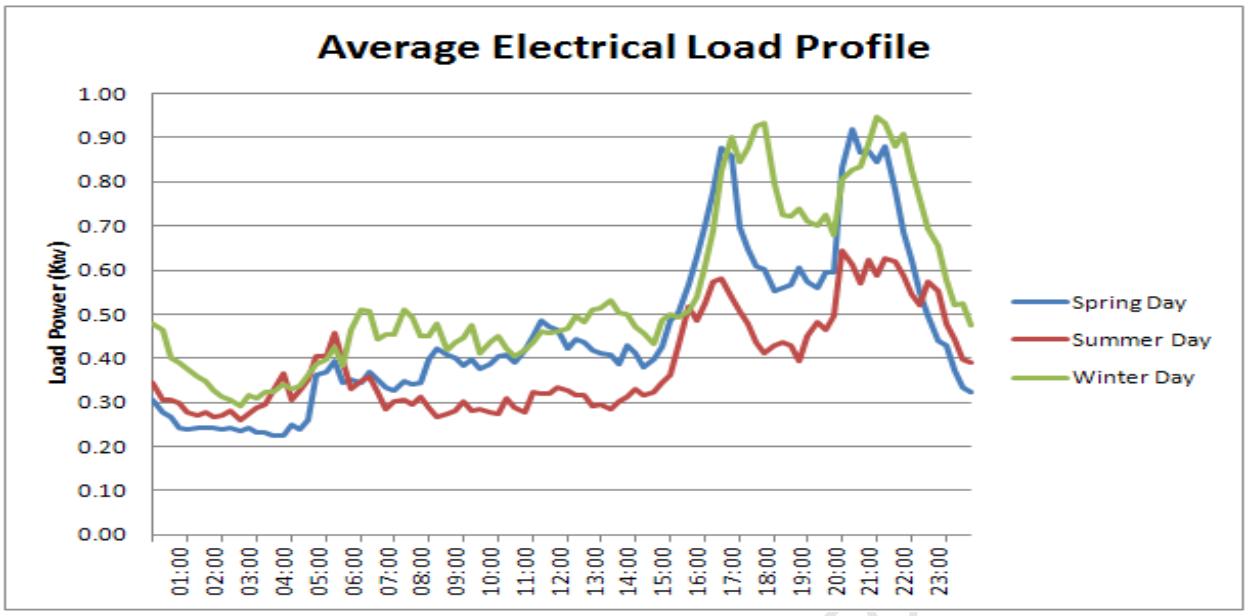

Figure 4-3: Electrical Load Profile of a typical Danish Single Family House [54]

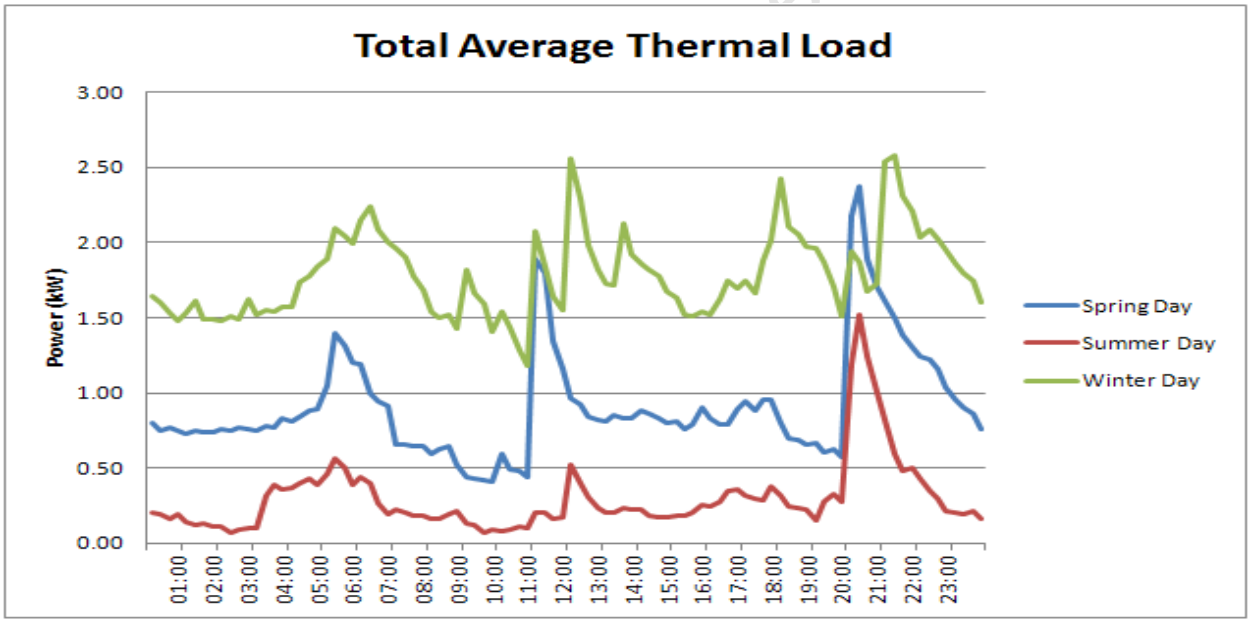

Figure 4-4: Thermal Load Profile of a typical Danish Single Family House [54]

The factors affecting the load profile are:

1) The age of the building

Using Europe as an example, older buildings have poorer insulation. They lack cavity insulation and double glazing which are newer insulation techniques that result in better retention of space heat. Older buildings tend to have higher thermal load.

2) The location of the building

The climate of the household is determined by the location and the space heating and hot water storage requirements depend on the climate. Hotter climates require less thermal energy and have lower thermal demand.

3) Number of occupants

The more inhabitants a household has, the greater the electrical and thermal demand of the household because of the higher sum of individual energy needs.

4.4.2. Grid Connection

As stated in section 2.7 if a system is stand alone the entire thermal and electrical energy demands of the household are to be met by the prime mover of the residential µCHP system and the auxiliary burner. If the system is grid-tied the control strategy of the µCHP system determines what proportions of electrical energy and thermal energy are generated by the µCHP system. Some thermal energy will be generated by the fuel cell s exothermic reaction while some of the thermal demand will be met by the auxiliary burner of the µCHP system.

4.4.3. µCHP Control Strategy

As stated in section 2.7 the µCHP control strategy determines the operating point of the µCHP prime mover (fuel cell) and this plays a major role in determining the size of the µCHP prime mover. The maximum load does not have to be met by the fuel cell and due to the control strategy being implemented the required maximum power output from the fuel cell may be considerably less than the maximum demand value which would require a smaller fuel cell unit.

4.4.4. Running Cost Calculations

In this section the equation to evaluate the daily running costs of a residential µCHP will be introduced by way of three examples.

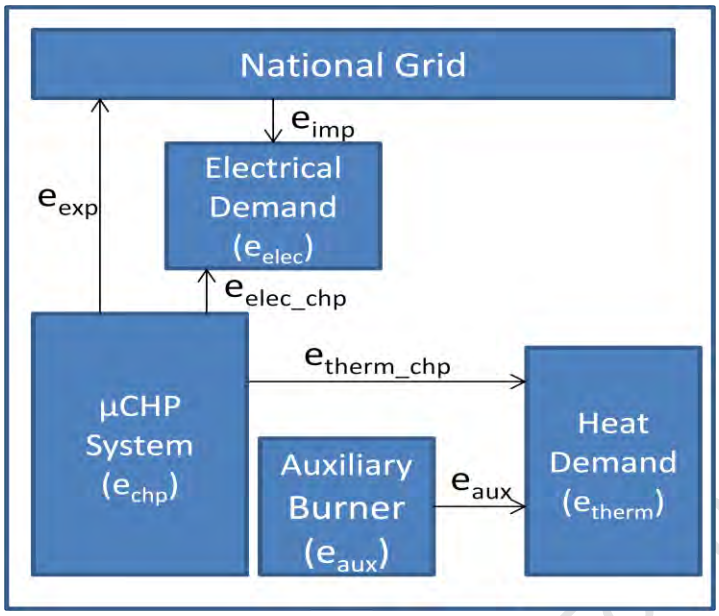

Figure 4-5: Residential µCHP System

Figure 4-5 shows the energy flows of the fuel cell-based residential µCHP system. The daily running costs are given by applying equation (4.5) which is an adaptation of equation (2.16). All energy quantities can be deduced from moving average values of electrical and thermal power taken from load profile data. The area under the load profile graph will yield the energy demanded by the household over that period of time. The area under an operating point vs. time graph will yield energy generated by the fuel cell prime mover. In the calculations to follow 'C' denotes costs, 'e' denotes energy and 'η' denotes efficiency. The following assumptions will be made for the running cost calculations in this section of this thesis project:

1) The electrical and thermal efficiencies of the fuel cell will vary according to equations (2.6) and (2.8) where the constants of these equations are determined by the data of [54].
2) Unless otherwise stated a heat to power ratio of 1:1 will be assumed for constant operating point tests. Fuel cells operate at low heat-to-power ratio so this is a reasonable assumption and simplifies calculations.
3) Constant prices for natural gas, imported and exported electricity are assumed. Thus the average prices of these are used in calculations and not the maximum or minimum prices of a time varying tariff system which will simplify calculations but not significantly affect the overall sizing of the system.

4) Unless specifically stated storage will not be incorporated.

The following equations will be used to determine the running costs of a fuel cell-based μCHP system in 3 examples based on the Danish Single Family household discussed in [54].

$$C = C_{chp} + C_{aux} + C_{elec} = \text{Daily running costs of μCHP system} \quad (4.5)$$

Where : $C_{chp} = (e_{therm\_chp} + e_{elec\_chp})/\eta_{chp}$ (4.6)

$= \text{Energy output of fuel cell}$

$C_{aux} = (e_{therm} - e_{therm\_chp}) \times C_{gas}/\eta_{aux} = \text{Output of auxiliary burner}$ (4.7)

$C_{elec} = (e_{elec} - e_{elec\_chp}) \times p_{feed\_in}\ (\text{if } e_{elec} - e_{elec\_chp} < 0)$ (4.8)

$= \text{electricity imported}$

$= (e_{elec} - e_{elec\_chp}) \times p_{imp}\ (\text{if } e_{elec} - e_{elec\_chp} > 0)$ (4.9)

$= \text{electricity exported}$

Where:

$e_{exp} = e_{elec} - e_{elec\_chp} = \text{electrical energy imported from the grid}$

$e_{imp} = \text{electrical energy sold back to the electrical utility at } p_{feed\_in} \text{ price.}$

$e_{therm\_chp} = \text{Thermal output of fuel cell}$

$e_{elec\_chp} = \text{Electrical output of fuel cell}$

$\eta_{aux} = \text{efficiency of auxiliary burner}$

$\eta_{elec} = \text{electrical efficiency of fuel cell}$

$\eta_{therm} = \text{thermal efficiency of fuel cell}$

$\eta_{chp} = \eta_{elec} + \eta_{therm}$

$= \text{overall efficiency of fuel cell}$

The term C_{chp} is a combination is the cost of running the prime mover of the μCHP system. This is basically the cost of the electric and thermal energy generated by the prime mover. The

prime mover is not assumed to be ideal so energy is lost and the total cost is increased by 1/(efficiency of prime mover).

The term C_{aux} is the cost of running the auxiliary burner of the µCHP system. The auxiliary burner is not assumed to be ideal so energy is lost and the total cost of running the auxiliary burner is increased by 1/(efficiency of auxiliary burner).

The term C_{elec} is the cost of importing electrical energy from the grid into the µCHP system. This has two components: The cost of importing electricity and the cost of exporting electricity. The terms e_{exp} and e_{imp} indicate the amount of electrical energy entering and leaving the µCHP system. The term e_{exp} has a negative value meaning money is made when electricity is exported.

Three examples have been chosen to demonstrate how the daily running costs of a household whose load profile we know can be obtained using equation (4.5).

Example 1:

Equation (4.5) will now be applied to a heat-led µCHP system operating at base-load, no storage:

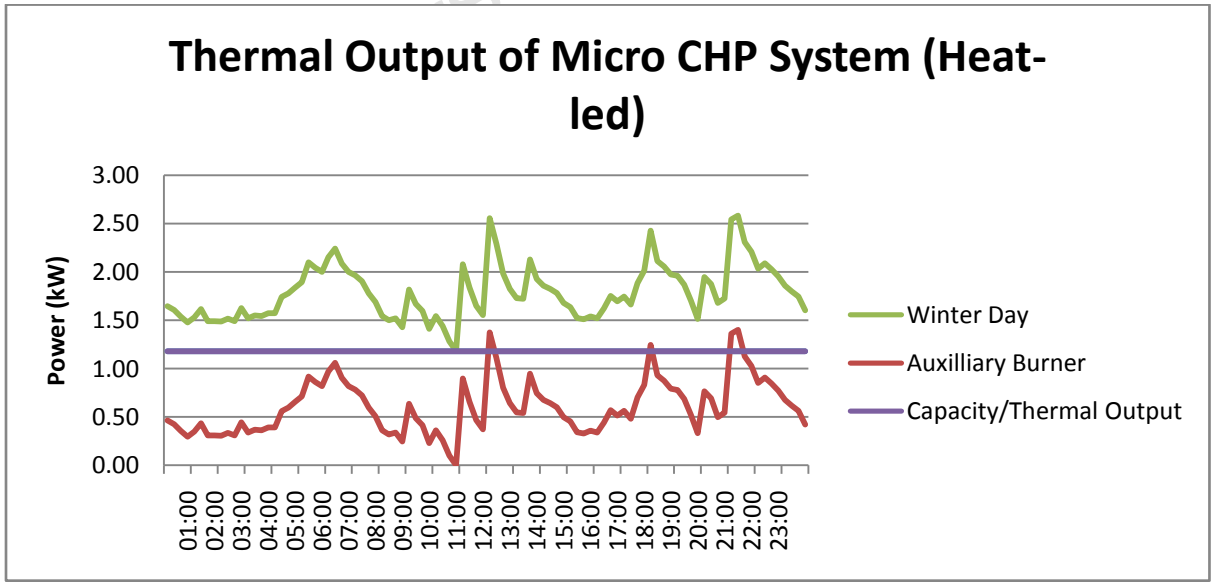

Figure 4-6: Electrical Output of Thermal Base-load operating µCHP System

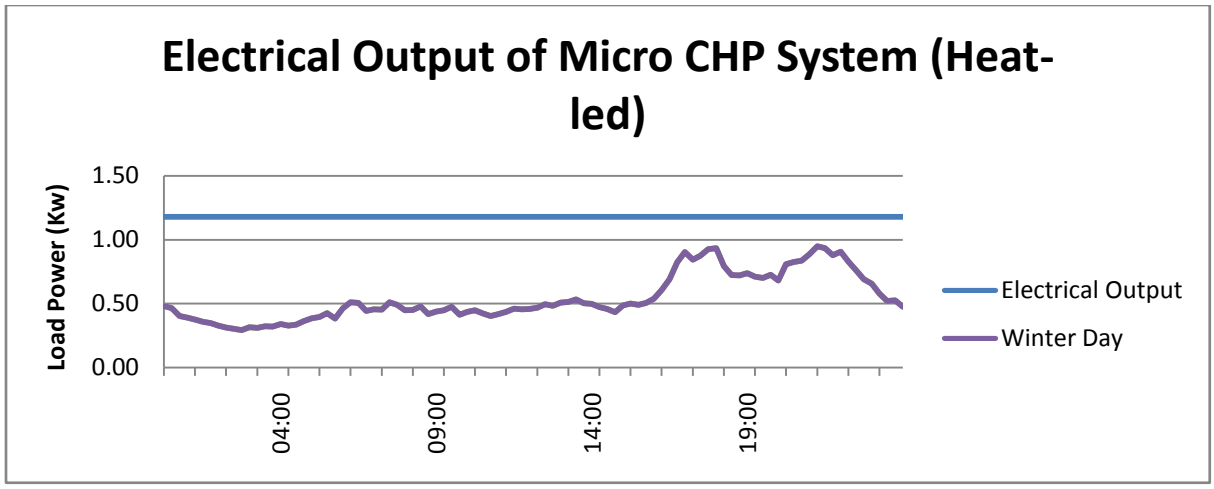

Figure 4-7: Electrical Output of Thermal Base-load operating µCHP System

C = $C_{chp} + C_{aux} + C_{elec}$

= (1.18kW × 24h + 1.18 × 24h) × \$0.16 / 0.8 + (14.52kWh × \$0.16 / 0.86) - (1.18kW × 24h – 13.00kWh) × \$0.0467/kWh)

= \$13.314/day

Example 2:

A residential µCHP system with the electrical operating point at average electrical load:

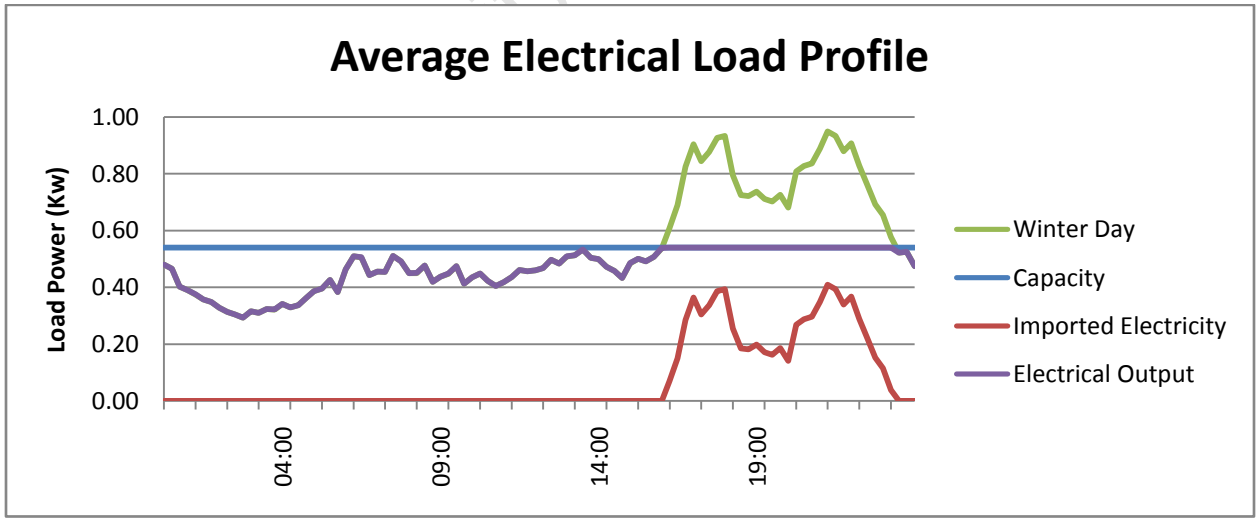

Figure 4-8: Electrical Output of Electricity-led operating µCHP System

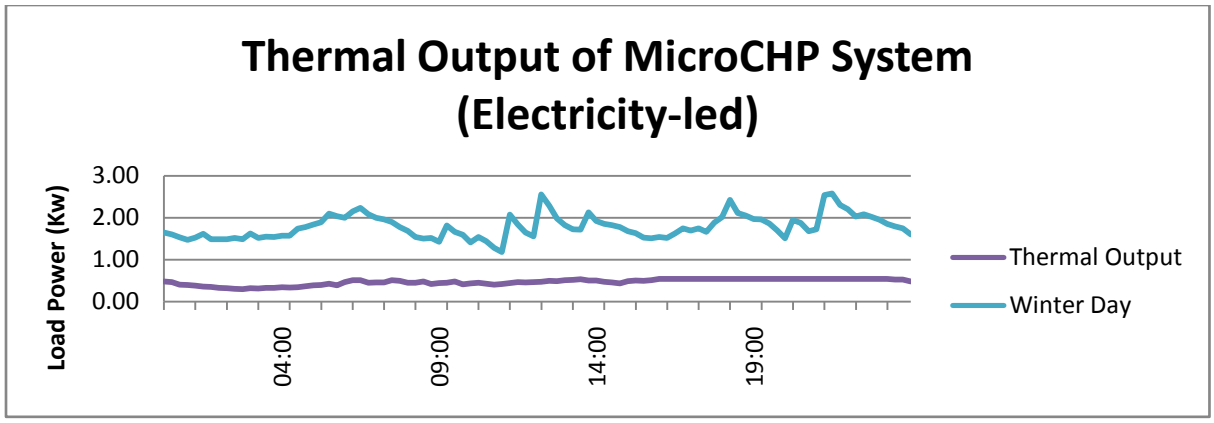

Figure 4-9: Thermal Output of Electricity-led operating µCHP System

$C = C_{chp} + C_{aux} + C_{elec}$

= (12.96kWh + 12.96kWh) × \$0.16/kWh / 0.8 + (29.88kWh × \$0.16/kWh) / 0.86 + 1.82kWh × \$0.41/kWh – 1.78kWh × \$0.0467/kWh)

= \$11.41/day

In this case electricity is exported from midnight to 1500hrs and exported from 1500hrs to 2330hrs meaning C_{elec} will have two components 1.78kWh × \$0.0467/kWh for export and .82kWh × \$0.41/kWh for import. If the export and import price of electricity were the same then these could simply be added to find the net electricity export/import.

Example 3:

A residential µCHP system with electrical operating point at base electrical load:

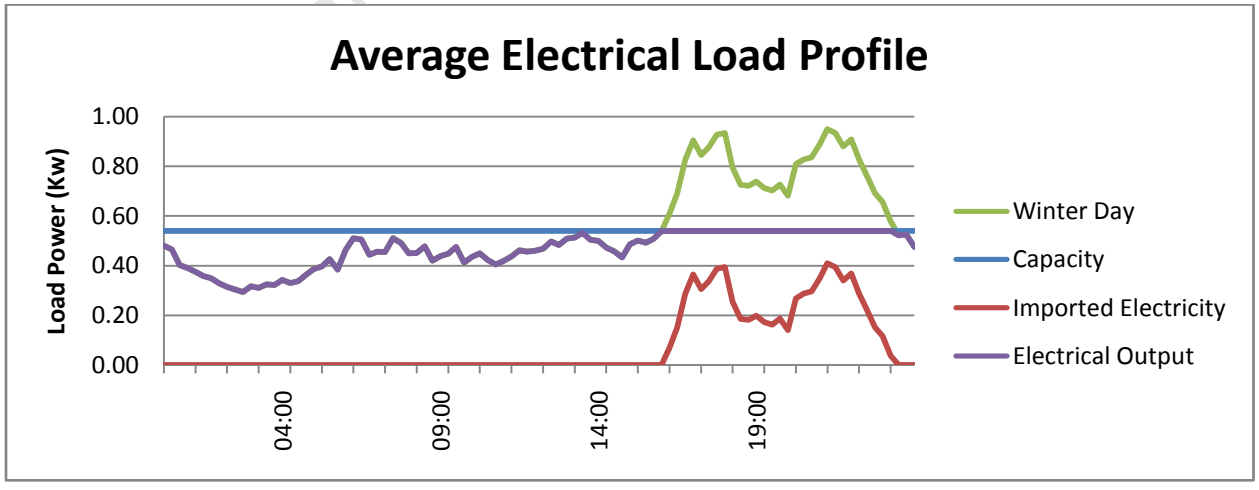

Figure 4-10: Electrical Output of Electrical Base-load operating µCHP System

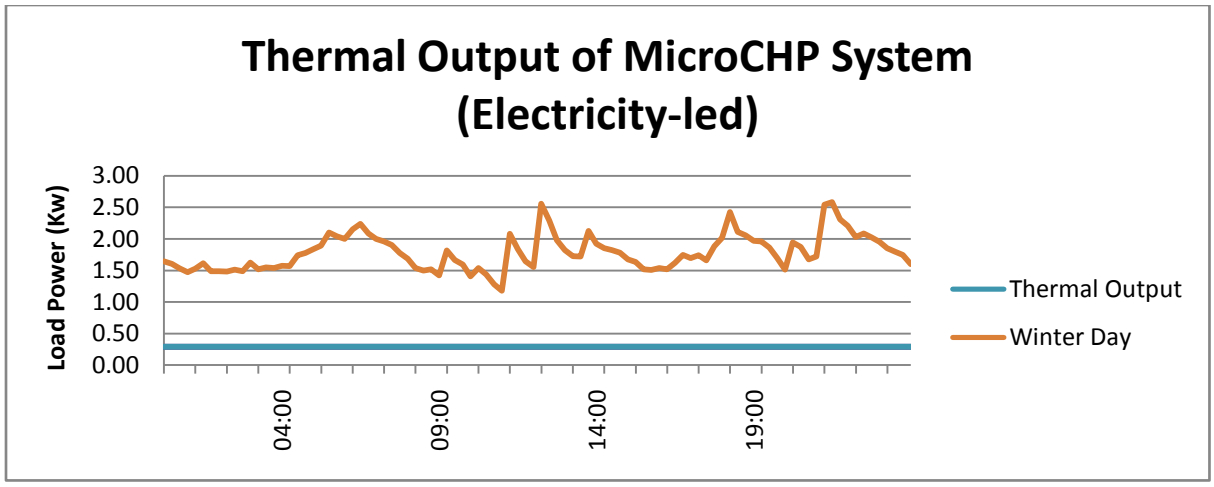

Figure 4-11: Thermal Output of Electrical Base-load operating µCHP System

$C = C_{chp} + C_{aux} + C_{elec}$

$= (0.29kW \times 24h + 0.29kW \times 24h) \times \$0.16/kWh / 0.8 + (35.88kWh \times \$0.16/kWh) / 0.86 + 6.04kWh \times \$0.41/kWh$

$= \$11.94/day$

It is expected that the result of example 1 should be less than that of example 2 and 3 because electricity is being sold back to the grid however the price of this electricity paid by the utility is not enough to compensate for the cost of the extra natural gas required to produce heat along with this electricity.

In order to determine what price of natural gas will result in lower costs, the total energy without the µCHP system will be calculated that is the amount using electricity imported from the grid and thermal energy from the auxiliary burner.

$C_{withoutchp} = C_{imported\_elec} + C_{aux}$ (4.11)

$= \text{electrical energy} \times p_{imp} + \text{thermal energy} \times C_{gas} / \eta_{aux}$

$= 13kWh \times \$0.41 + 42.84kWh \times \$0.16 / 0.86$

$= \$13.30$

This is lower than the electricity-led chp case. In order for benefits to be derived from the electricity-led scenario C should be ≤ $13.30

$C \leq C_{withoutchp}$

$C \leq \$13.30$

$C_{chp} + C_{aux} + C_{elec} \leq \$13.30$

$(1.18kW \times 24h + 1.18 \times 24h) \times \$0.16 / 0.8 + (14.52kWh \times \$0.16 /0.86) – (1.18kW \times 24h – 13.00kWh) \times p_{feed\_in} \leq \$13.30$

$14.03 - 15.32 \times p_{feed\_in} \leq \$13.30$

Therefore:

$p_{feed\_in} \geq \$0.04765 / kWh$

Any feed in tariff lower than this will result in it not being feasible to implement CHP in the case of Example 1. Calculating running costs is a step taken in sizing the system and in the next section sizing of the system will be demonstrated via examples.

4.4.5. µCHP Sizing Assumptions

In order to be able to evaluate the control strategies and sizing of the system some assumptions will be made about the system's parameters:

1) The heat to power ratio of the fuel cell is equivalent to the ratio of thermal efficiency to electrical efficiency as in equation (2.10).
2) Thermal and electrical efficiency of the fuel cell will vary as the operating point varies. The values of these quantities can be determined by equations (2.6) and (2.8).
3) Auxiliary burner efficiency will be assumed to be 80%.
4) Efficiency of the heat storage tank will be assumed to be 90% (thus 10% of thermal energy placed in storage is lost).
5) There is no electrical energy stored. Energy is either being imported from the grid or exported to the electricity supply authority.

4.4.6. Fixed Operating Point Heat-led µCHP Sizing Example

A common way of operating fuel cell-based µCHP systems is to maintain the operating point at a predetermined value often the base load. Figure 4-12 illustrates the concept of fixed

operating point. The horizontal purple coloured line is the thermal operating point of the fuel cell.

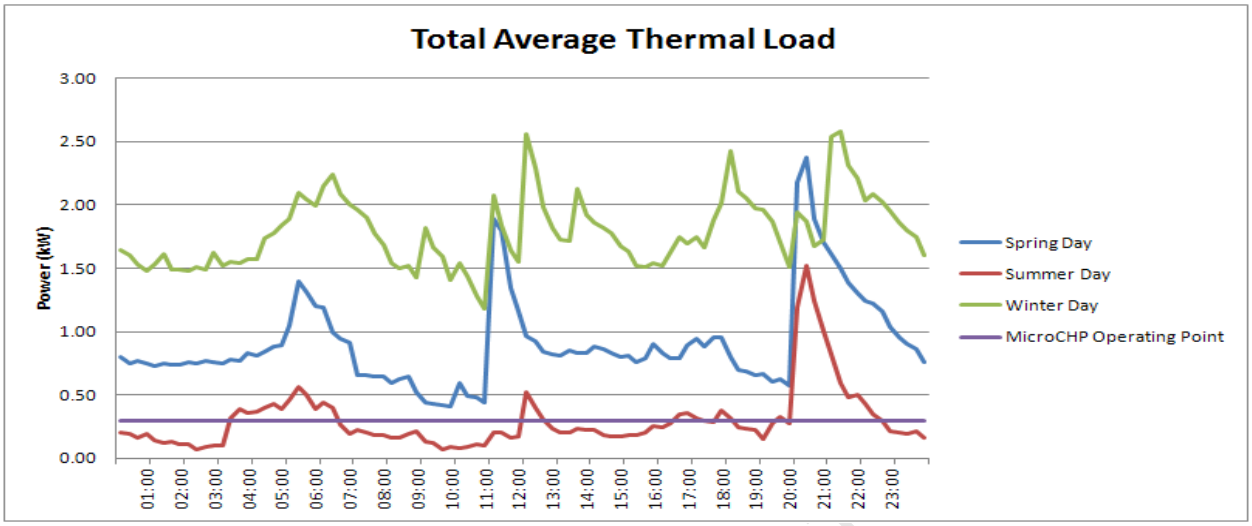

Figure 4-12:Thermal Load Profile of a typical Danish Single Family House [54]

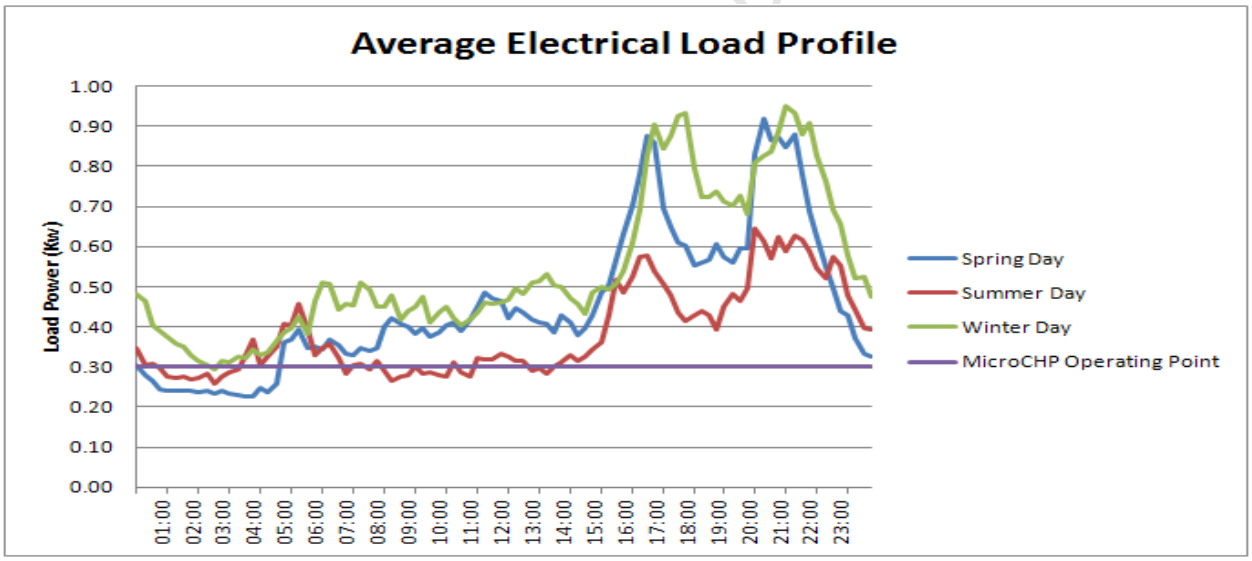

Figure 4-13: Electrical Load Profile of a typical Danish Single Family House [54]

A 1:1 heat-to-power ratio 1:1 is assumed in this scenario the electrical operating point has the same value as shown in figure 4-13.

In order to determine the optimal system size, the running costs and capital costs of the system are to be determined. A MATLAB Simulink simulation of the fuel cell-based µCHP system is coded the code of which is available in Appendix C. The operating point is changed from 3kWth

(3kW thermal output) all the way down to 0kWth which is a residential system without a µCHP unit attached and running costs values are determined for each of these operating points. The daily running costs for each of the 0.1kWth steps is recorded and plotted in figure 4-14. The spring load is the one that is under investigation in this example. The lowest daily running cost was achieved at 0.4kWth operating point. The daily running cost in spring at this operating point is $7.17. This is very close to the thermal base load indicated by the green vertical line on figure 4-14 indicating that base load operation is preferable in this season for this set of load data. Beyond 1kWth operating point the daily running cost of implementing µCHP in this household exceeds the running costs of a household operating without a µCHP system and it is no longer feasible to implement µCHP. As the operating point increases so too does the thermal storage required for the excess thermal energy being generated which contributes to the overall capital cost of the system below base load (to the left of the green line) no storage is required which is expected because the output of the µCHP prime mover will not have exceeded the load.

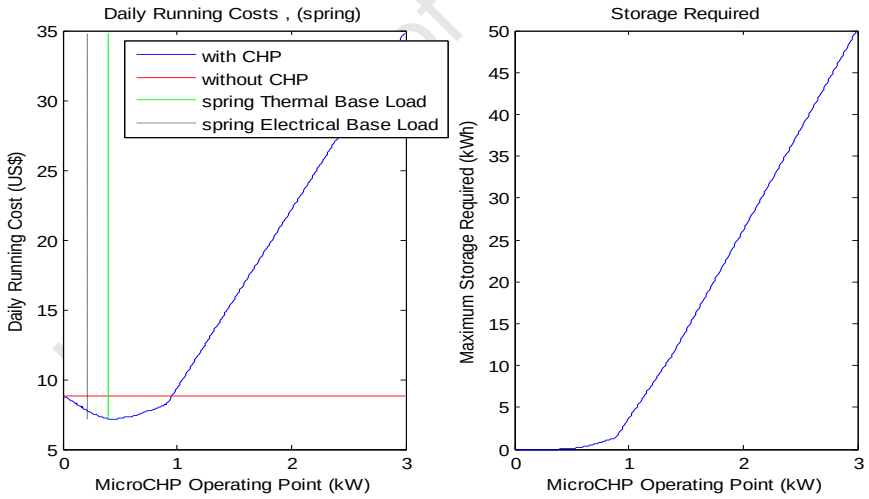

Figure 4-14: Electrical Load Profile of a typical Danish Single Family House [54]

In this scenario base load operating point is the ideal operating point of the µCHP system. A system which has a thermal output of 0.4kWth operating at a heat-to-power ratio of 1:1 is the size of the system that will be recommended in this scenario since a low heat-to-power ratio is desirable.

4.4.7. Varying Operating Point Heat-led µCHP Sizing Example

Varying the operating point of the fuel cell can reduce the need for storage because there will be less scenarios where the fuel cell's output is larger than that of the energy demand at any particular time. It must be stated however that the fuel cell will not follow the load precisely because of the delay in the increase and decrease of the operating point of the fuel cell. The authors of [17] stipulate a maximum ramp rate of 5% of the capacity of the fuel cell per 5 minutes. This limits the extent to which the fuel cell operating point can match the load. There are also maximum and minimum values placed on the fuel cell operating point. The minimum point is above zero to avoid turning off the fuel cell regularly which would lead to degradation as discussed in [53]. The upper limit is set by the capacity of the fuel cell. Figure 4-15 shows results of the varying operating point method in spring.

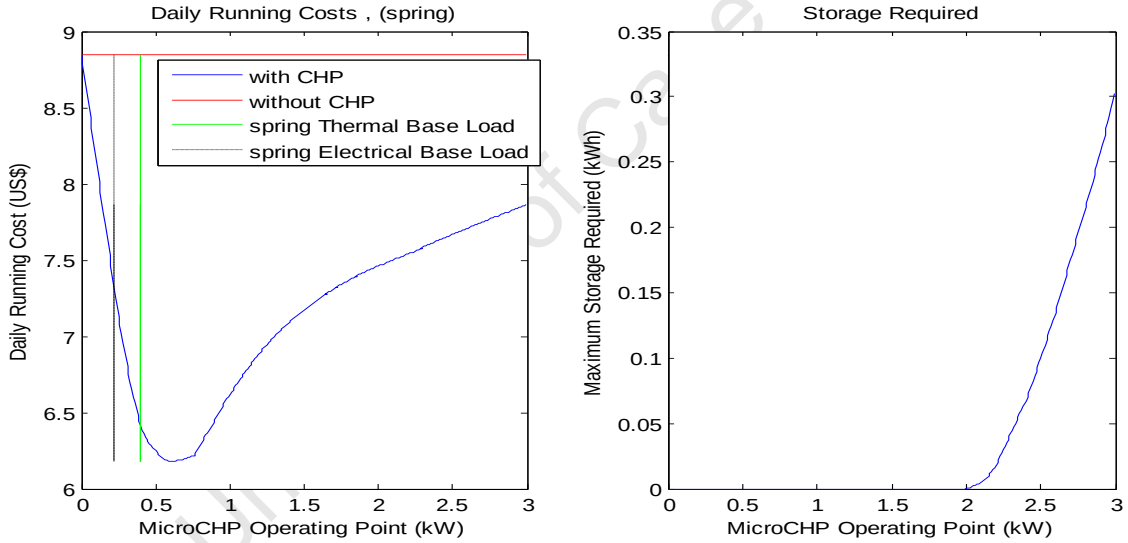

Figure 4-15: Electrical Load Profile of a typical Danish Single Family House [54]

The minimum running costs of this system are found to be $6.18 and occur at 0.6kWth operating point. Storage is not required for low operating point values because the upper limit of the thermal operating point (because this is heat-led control) does not exceed the demand. When the load is in between the minimum and maximum operating point values, the fuel cell output matches the load profile as closely as is possible. As the capacity of the fuel cell increases, the maximum and minimum values of the fuel cells operating point increase as well. The minimum operating point will exceed the demand at 2kWth hence the need for storage at

that point as shown by figure 4-16. The varying operating point yields a lower running cost and requires a slightly larger capacity µCHP unit and all factors taken into consideration is preferable for this load data.

4.4.8. Cost-minimizing µCHP Sizing Example

As discussed in the previous chapter cost minimizing control is not influenced by the heat or electrical demand but rather by the cost function of equation (2.16). The objective of this control strategy is to, by varying the operating point of the fuel cell, minimize this cost function. As can be seen from figure 4-16 the operating point of the fuel cell is not constant and varies unpredictably.

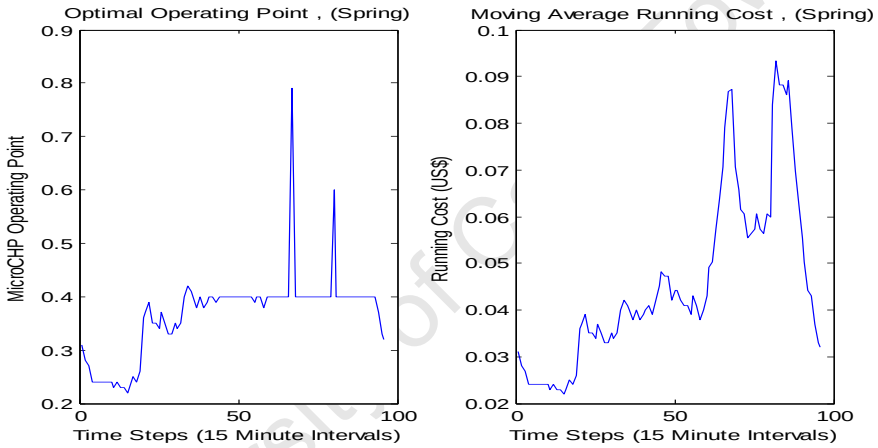

Figure 4-16: Electrical Load Profile of a typical Danish Single Family House

The left of figure 4-16 shows the actual value of the operating point over 96 time steps (15 minutes each over 24 hours). The daily running costs are given by the area under the graph to the right of figure 4-16 and this is $4.36 which is lower than that for the varying operating point heat-led and fixed operating point heat-led operating strategies.

4.4.9. Comparison of Control Strategies

In order to determine which operating strategy is best for the load profile data of [54] the method discussed in section 4.3 will be used. The results of the MATLAB simulations are displayed in Table 4-1.

The data for spring is assumed to be identical to that of autumn in the simulations in this section. In order to determine the Capital Cost for the µCHP system it is necessary to define the cost per kW of capacity of the µCHP system. The Honda Eneos ENE Farm will be used as the example upon which this figure is taken. This is fuel cell-based and a 1kW unit costs $35000. Therefore the cost per kW of µCHP capacity is $35000. Using the thermal storage discussed in [50] the cost of thermal energy storage is $14.9/kWh. The Capital Recovery Factor (R) will be assumed to be 0.2775 assuming an interest rate of 12% and system lifespan of 5 years. The yearly capital cost is calculated using equation (4.2):

$$Cc = R \times \Sigma \text{ (Capital cost of components)} \quad (4.2)$$

Cost minimizing control yields the lowest cost function value as expected however variable operating point operation is less effective than that of constant fuel cell operating point operation. This is due to a larger capacity fuel cell being required to operate using this control strategy which outweighs the lower storage costs.

Table 4-1: Calculation of cost function for different µCHP operating strategy

	Fixed Operating Point	Variable Operating Point	Cost Minimizing Control
Running Cost (Spring)	$7.17	$6.18	$4.36
Running Cost (Summer)	$3.80	$3.79	$3.69
Running Cost (Winter)	$11.80	$10.67	$5.15
Yearly Running Cost (Cr)	$2732.03	$2447.33	$1602.35
Maximum Thermal Output Required	0.49kW	0.69kW	0.55kW
Storage Required	1.223kWh	0	0.4kWh
Total Capital Cost = Cost of prime mover + cost of storage	$17168.22	$24150	$14000
Yearly Capital Cost (Cc)	$4764.15	$6701.63	$3885.00
Cost function value(Min)	$7496.18	$9148.96	$5487.35

4.5. Conclusion

The major factors affecting the sizing of a µCHP system are the projected load profile, µCHP control strategy being used and the connection of the system to the grid or lack thereof. In order to determine the optimal size of a µCHP system the performance of the system in all possible weather seasons needs to be taken into consideration as well as the prices associated with natural gas and electricity so there is not one optimal size for residential µCHP systems. Once the potential running costs and potential capital costs of a residential system are obtained the appropriate system size can be determined. If the system size is too large energy will be wasted if the system size is too small energy requirements of the household will not be met. Fuel cell-based µCHP systems have the potential to completely replace engine-based µCHP system and other forms of Distributed Generation as the primary generators of household electrical and thermal energy.

Chapter 5

5. Power Electronic Interface Design

5.1. Introduction

In Chapter 3, the theory behind residential µCHP operation was discussed and a system model proposed. The focus of the practical aspect of this thesis is on the interfacing power electronics between the HTPEMFC and the single-phase household circuit and this chapter will discuss the design of an interface of which simulations will be conducted and a practical system will be implemented. Two topologies are to be considered via simulation and practical implementation. It is assumed, as stated in chapter 3, that a 1kWe HTPEMFC fuel cell will be used as an example.

5.2. Three stage Power Electronics Interface

5.2.1. System Overview

The 1kWe HTPEMFC fuel cell voltage output varies non-linearly as depicted by the polarisation curve in section 3.3 of this thesis. The voltage output varies between approximately 20V and 48V during operation. This presents a problem in that the household load requires a constant $220V_{rms}$ sinusoidal supply and to achieve this, the varying DC output of the fuel cell needs to be regulated and inverted to AC.

Figure 5-1 is a schematic of the proposed three-stage power electronic interface between the fuel cell and household grid. The low fuel cell voltage is boosted by the DC/DC Forward Boost Converter from a value between 20V and 48V to a value of 48V. By maintaining the output of the Boost Converter stage at 48V using the control strategy shown in figure 5-2 and discussed in section 5.2.2, the option of connecting a 48V battery to this stage of the interface is made available. The authors of [55]- [57] discuss bidirectional DC/DC Converters in which a battery is used as an energy storage mechanism and provide examples of how 48V batteries can be applied to an interface such as this one. The DC/DC Full-bridge Boost Converter Stage discussed

further in section 5.2.3 consists of a DC-chopping H-bridge, a step up high frequency transformer and a full-bridge voltage rectifier. The 48V DC is chopped via the H-Bridge made up of switches Q1 to Q4. The resultant AC is then stepped up via the transformer and the output of the transformer is rectified by diodes D1 to D4. In the grid-tied inverter stage discussed in section 5.2.4, switches Q5 to Q8 are used to converter the DC from the DC/DC Full-bridge Boost Converter Stage into a PWM AC signal which, when filtered by the LC low pass filter made up of *Lf* and *Cf*, results in a $220V_{rms}$ at the output of the interface being sent to the grid.

The advantage of this topology when interfacing the fuel cell to the household grid is that:

1) It is modularised making it easier to maintain and manufacture.
2) Adequate isolation is provided for the fuel cell via the transformer discussed in [58].
3) Energy storage can be implemented via the regulated DC/DC Converter output. The Boost Converter Stage which is regulated to 48V a common battery operating voltage.
4) Control is simplified and is applied via a reliable easy to design and implement PI Controller as discussed by the authors of [59].

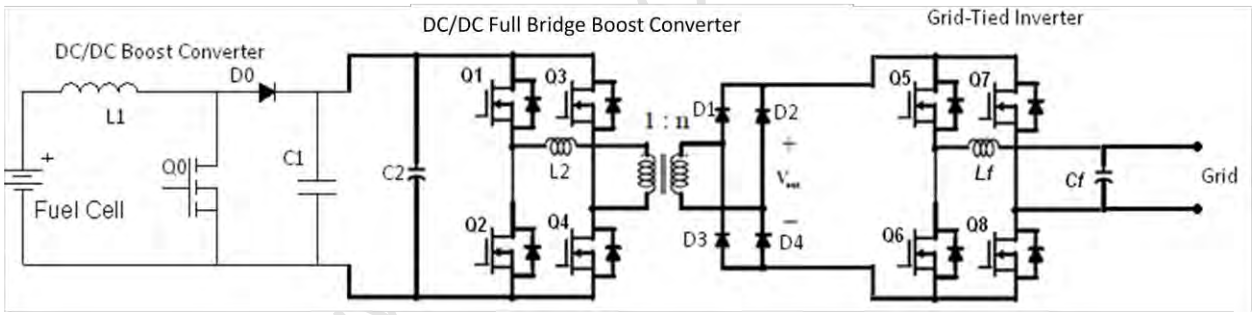

Figure 5-1: Three Stage Power Electronic Interface Schematic

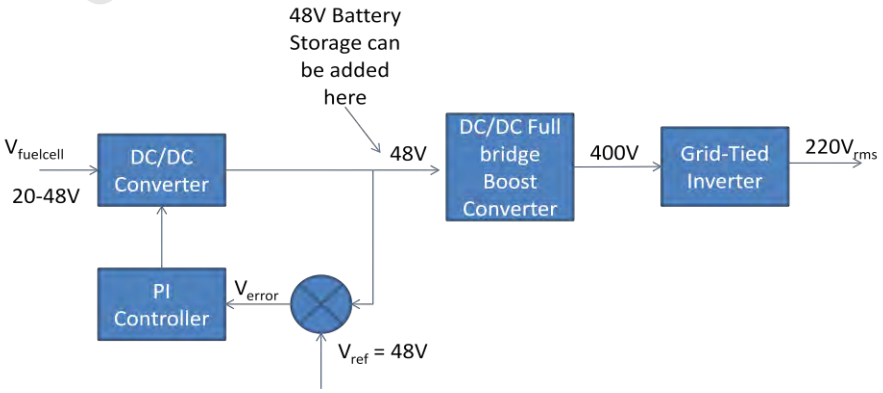

Figure 5-2: Three-stage Fuel Cell to Household Grid Power Electronic Interface

5.2.2. DC/DC Forward Boost Converter Stage

The role of the DC/DC converter in the power electronic interface is to boost the low fuel cell voltage and regulate the fuel cell voltage to the desired 48V for reasons mentioned in the previous section. The principles of operation of this stage of the interface are discussed in section 2.8 of this thesis. In brief, the MOSFET switch Q0 opens and closes a current path to ground. When switch Q0 is on the current through the inductor rises and when Q0 is off the energy in the inductor discharges through D0 into C1. By controlling the rate at which Q0 is switched on and off, the voltage across C1 which is proportional to the energy stored in the capacitor can be controlled. This is done by controlling the duty cycle of Q0 switching.

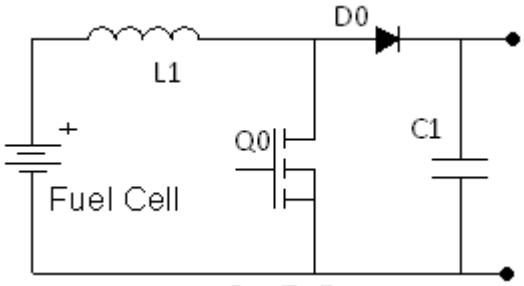

Figure 5-3: DC/DC Forward Boost Converter Schematic

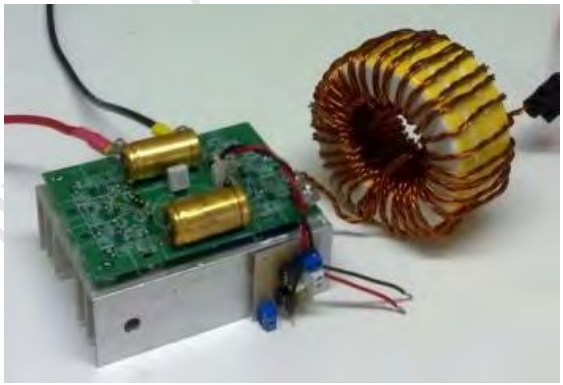

Figure 5-4: DC/DC Forward Boost Converter

The voltage output of a boost converter is larger than or equal to the input voltage to the converter. The equation for the output of the boost converter is given by:

$$Vout = \frac{1}{1-D} Vin \quad (5.1)$$

Where D - duty cycle ratio of switch

The duty cycle is the ratio of on-time to the switching period and has a value between 0 and 1. The minimum value of *Vout* is therefore *Vin* according to equation (5.1). In order to ensure a stable voltage at the output of the converter the duty cycle is varied in response to changes in voltage at the input (i.e from the fuel cell). A negative feedback loop compensates for variations in the voltage at the output of the fuel cell. Figure 5-5 shows the implementation of this closed loop controller.

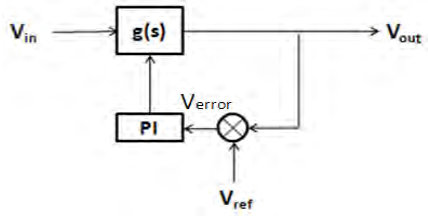

Figure 5-5: Closed loop duty cycle ratio control

A Proportional Integral (PI) controller is placed in the feedback loop to mitigate transients within the feedback loop. Inspection of equation (5.1) reveals that as long as the input to the DC/DC converter never rises above the regulated voltage then the feedback loop will adjust the duty cycle to regulate the voltage. The voltage is regulated at $48V_{DC}$ because this is a value of voltage the 1kW PEMFC will not rise above during normal operation. If the voltage were to overshoot above the 48V value the boost converter output will be more than 48V and there is no control action that can correct this.

When tuning a PID controller the following four factors are taken into consideration:

1) Rise Time: the time it takes for the plant output (where the plant is the DC/DC Converter) to rise beyond 90% of the desired level for the first time.
2) Overshoot: how much the peak level is higher than the steady state.
3) Settling Time: the time it takes for the system to converge to its steady state.
4) Steady-state error: the difference between the steady-state output and the desired output.

The PID controller transfer function has a proportional term, an integral term and a differential term. A PI controller is a PID controller where the differential term is zero in magnitude.

The PID controller is represented by equation (5.2)

$$C(s) = K_P + \frac{K_I}{s} + K_D s \qquad (5.2)$$

Where K_P = Proportional gain

K_I = Integral gain

K_D = Differential gain

Table 5-1 gives indications of the effect changing the values of these gains has on the rise time, overshoot, settling time and steady-state error. A controller of low rise time, low overshoot, low settling and minimal steady-state error was desired. Compromises had to be made improving one characteristic of the plant would result in degrading another characteristic of the plant.

Table 5-1: Results of increasing the parameters of the PID transfer function [60]

Response	Rise Time	Overshoot	Settling Time	Steady-state Error
K_p	Decrease	Increase	No trend	Decrease
K_I	Decrease	Increase	Increase	Eliminate
K_D	No Trend	Decrease	Decrease	No trend

Though these are guidelines to tuning of the PID Controller, competent initial values are required to begin tuning with. An open-loop step-test of the system is stable with oscillations as shown in figure 5-6. Therefore the Zeigler-Nichols approach to PID tuning was used. Appendix E explains the DC/DC Converter can be approximated to second order.

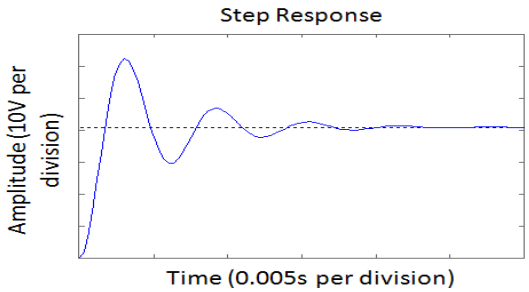

Figure 5-6: DC/DC Converter Open Loop Response

If the system is proportionally closed-loop controlled and the proportional gain is adjusted until the point where it is at the limit of stability the gain (G) and period of oscillation (T_P) can be used to determine initial PID values. (T_P = 0.01s and G = 1)

$$\text{Initial values: } K_P = 0.6G;\ K_I = 2K_P/T_P;\ K_D = K_PT_P/8$$

$$K_p = 0.6;\ K_I = 120;\ K_D = 0.00075$$

Using the guidelines of table 5-1 the coefficient values of the PID controller coefficients, after tuning in MATLAB Simulink were found to be:

$$K_p = 0.4;\ K_I = 0.5;\ K_D = 0$$

The I value was decreased significantly because the initial value of 120 resulted in saturation of the PI controller whose output was limited to a value between 0 and 1. This PI controller was implemented via the DSpace DS1004 kit which enables implementation of MATLAB Simulink blocks in real time by the using of ADCs and DACs. The Simulink block for PID is used and the dialog box where these coefficients are set is shown in figure 5-7. Figure 5-8 shows the method used to limit the output which is necessary because the duty cycle being controlled will be a value between 0 and 1. Thus figure 5-8 shows how the upper and lower saturation limits of the controller are set. The anti-windup mechanism discharges the integrator when the output is limited and this is set up in figure 5-8 as well.

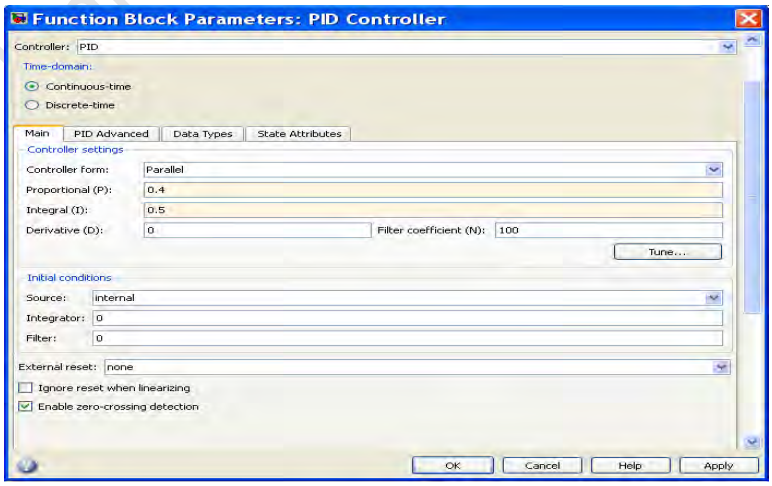

Figure 5-7: PID Controller Coefficient Values

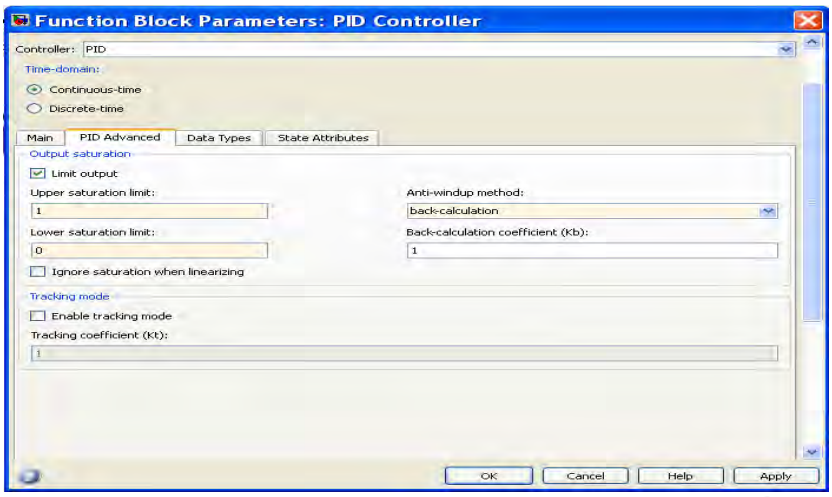

Figure 5-8: PID Controller Saturation Limiting

5.2.3. DC/DC Full-bridge Boost Converter Stage

This circuit appears in both the two-stage and three-stage power electronic interface topologies and provides isolation for the fuel cell and DC voltage gain.

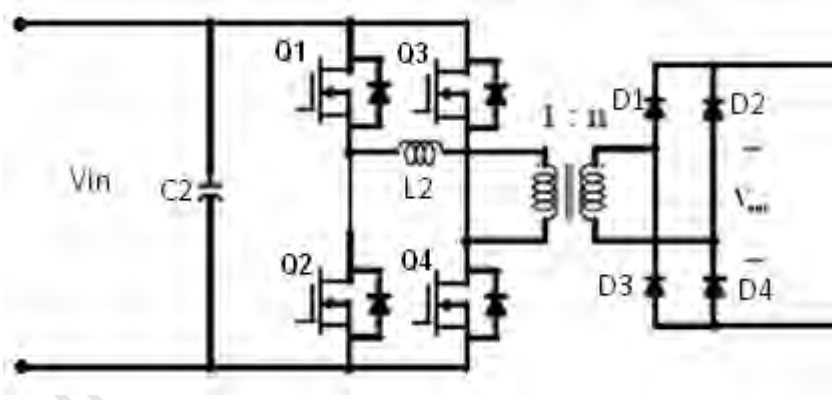

Figure 5-9: DC/DC Full-bridge Boost Converter Stage Schematic

Figure 5-10: DC/DC Full-bridge Boost Converter Stage of the Power Electronic Interface

Figures 5-9 and 5-10 show the stage of the interface in which the voltage level is boosted significantly to a value above that of the fuel cell in preparation for the inverter stage. It comprises a DC-chopping H-bridge on the bottom-left, a high frequency transformer in the middle of the diagram and a rectifier at the top right of the diagram. The chopping DC H-bridge is made up of four IRF260 MOSFET switches and these switches are driven by SKHI22B Semikron drivers directly from the DSpace DS1104 kit. MOSFETs are used instead of IGBTs because at this stage in the interface voltages are low and high voltage rating switches are not required. In the two-stage version of the interface, as will be discussed in section 5.3, the DC/DC Converter stage is not present and there is a need for an increase in the voltage gain of the transformer. E67 core type transformers are design for both topologies with different gains.

The transformer for the two-stage topology is designed using the following procedure: According to Faraday's law of electromagnetic induction the voltages induced in the primary and secondary coils of the transformer are equal and are given by equations (5.7) and (5.8).

$$V_{primary} = N_1 \frac{d\varphi}{dt} \quad (5.7)$$

$$V_{secondary} = N_2 \frac{d\varphi}{dt} \quad (5.8)$$

The maximum currents allowable through the primary and secondary coils are determined by evaluating the current at the lowest allowable voltage levels in equations (5.9) and (5.10).

Primary side: $i_{max\,,primary} = \frac{Pin}{Vin} = \frac{1000}{48} = 20.83A$ (5.9)

Secondary side: $i_{max\,,secondary} = \frac{Pin}{Vout} = \frac{1000}{400} = 2.5A$ (5.10)

The wires used in the primary and secondary coils should be able to sustain these currents hence the primary coil is made up of 0.5mm multi-stranded wire. Single strand 0.5mm wire will be adequate for the secondary wire.

The required gain of the transformer is determined by the proposed turns ratio. When determining this ratio the voltage drops across the diodes of the rectifier stage must be taken into account because the output is required to be at the required levels after this diode voltage

drop has occurred. This is accounted for in equation (5.11). There is some dead time in-between the switching pulses of the full bridge hence a MOSFET H-bridge gate switching signal duty cycle of 0.9 will be assumed.

$$\frac{N_1}{N_2} = \frac{V_{in}}{V_{out} + Voltage\ \ drop} \times duty\ cycle = \frac{48}{400 + (2 \times 0.7)}\ 0.9 \tag{5.11}$$

Therefore, the turns ratio and gain of the transformer is given by equation (5.12)

$$n = \frac{N_2}{N_1} = 9.33\text{turns} \tag{5.12}$$

Having found the required gain for the transformer the number of turns to be used is determined by equation (5.13).

$$V_{primary} = N_1\, f\, \varphi_{pk-pk} \tag{5.13}$$

Where: $V_{primary}$ = Voltage across primary winding of the transformer

N_1 = Number of turns in primary coil of transformer

f = frequency of change of flux

φ_{pk-pk} = peak-to-peak flux

$$\varphi_{\mathrm{pk-pk}} = BA_{eff} \tag{5.14}$$

B = Flux density

A_{eff} = Effective Cross-sectional area covered by flux

Because current in the coils flows in both directions so too does the flux hence,

$\varphi_{pk-pk} = 2 \times \varphi_p$, considering that the flux moves from the positive to the negative cycle, as shown in figure 5-11.

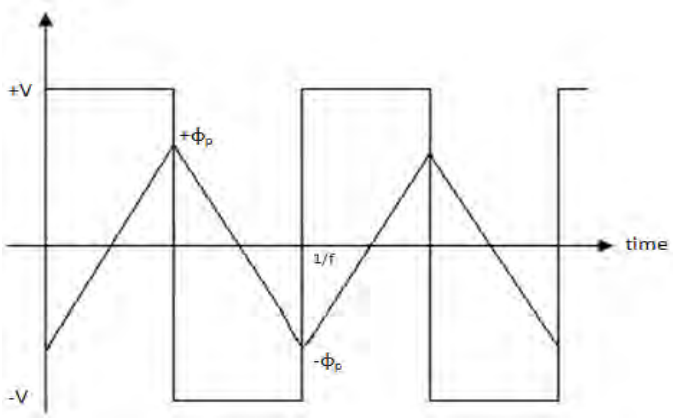

Figure 5-11: Peak to peak flux, [61]

As a result, when selecting B, the magnetic flux density, the value obtained must be halved (to ensure saturation is not reached). A flux density value below 0.24T is used because this is the point where N87 E-core saturates. A value of 0.2T was selected.

$$\therefore N_1 = \frac{V_{primary}}{f\,(2\times B\times A_{eff})} = \frac{48}{20000\times(2\times 0.2\times 683\times 10^{-6})} = 9\ turns \text{ (rounded up)} \quad (5.15)$$

$$N_2 = N_1 \times \frac{N_2}{N_1} = 6\ \times 15.93 = 84\ turns \text{ (rounded up)} \quad (5.16)$$

Table 5-2: Transformer Gain Requirements

	Original Transformer (Three-stage topology)	New Transformer (Two-stage topology)
Primary Turns	9	6
Secondary Turns	84	92
Gain	9.333	15.333

5.2.4. DC/AC Inverter Stage

A single-phase 220V_{rms} AC signal is required by the household and the 400V_{dc} from the output of the DC/DC Full-bridge Boost Converter is inverted by the circuit of figures 5-12 and 5-13. The output of this circuit is connected to one phase of the grid labelled L_{grid} in figure 5-12 via an inductor enabling power to be sent to and from the grid via the power electronic interface.

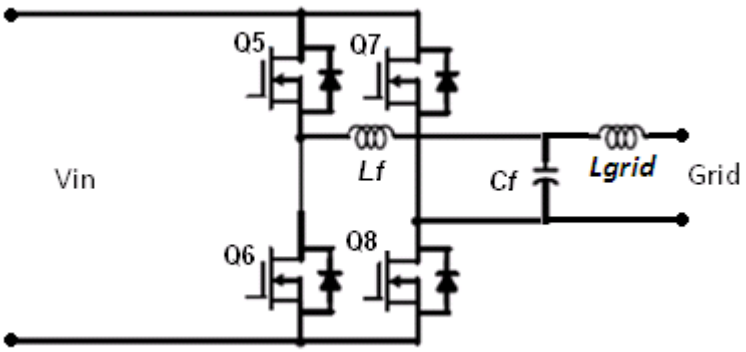

Figure 5-12: Grid-tied Inverter Schematic

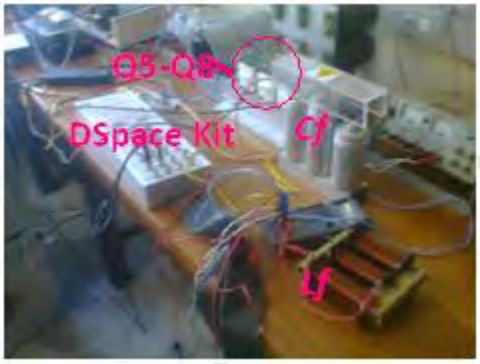

Figure 5-13: Grid-tied Inverter Laboratory Setup

The theory of the grid-tied shown in figure 5-13 inverter is discussed in section 2.8 of this thesis. The role the inverter plays in the power electronic interface is converting the 400 V DC voltage of the previous stage to the required $220V_{rms}$ AC voltage. An H-bridge is used to create a Pulse Width Modulation (PWM) waveform at the output. High-voltage Semikron SKM 150 GB IGBT modules (Q1 to Q4) are used and driven by SKHI21A Semikron drivers. These modules are capable of handling voltages of up to 1200V and 150A of current. The signals triggering the IGBTs come from the DSpace kit in the left of figure 5-10 via a transistor inverter circuit to increase the voltage level from the 5V DSpace output to the 15V required to trigger the SKHI21A drivers. The circuit for this is shown in figure 5-14. The supply voltage Vcc of these inverters is 15V and only one signal is required from the DSpace kit because the circuit of figure 5-14 has two complimentary outputs. This reduces the computational requirements of the DSpace kit. The gain of the transistor inverter circuit is given by equation (5.17):

Transistor inverter gain = $-\frac{R_c}{R_b}$ (5.17)

The values of the components chosen to attain a gain of at least 3 were: Rc = 10kΩ, Rb(Transistor 1) = 1kΩ, Rb(Transistor 2) = 1kΩ. The gain is more than three but the output is then saturates to the supply voltage which is 15V.

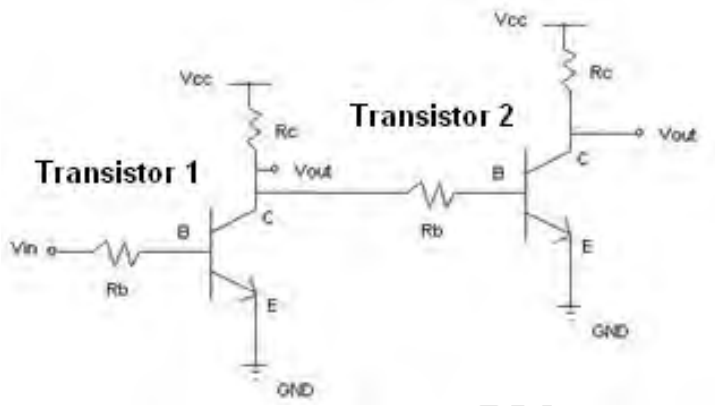

Figure 5-14: Schematic representation of the BJT Inverter Circuit (adapted from[62])

The PWM waveform undergoes harmonic mitigation in order to eliminate the undesired harmonics of the PWM and eventually remain with the 50Hz sine wave output. Having considered all the harmonic mitigation methods mentioned in section 2.8 of this thesis the passive LC low pass filter was chosen.

The cut-off point of the LC low-pass filter is determined by the inductance of the inductor and capacitance of the capacitor in the circuit.

Dahono et al in [63] derives a comprehensive LC filter design method that eliminates the need for the duty cycle parameter. The method he develops is based on the minimisation of the filter reactive power. This criterion has the benefit of "directly minimising the size, losses, and cost of the filter" [63].

In order to determine the sizes of the inductor and capacitor to be used in the LC filter Dahono's method of filter design was applied.

Dahono's design method can be summarised as follows:

- Based on nominal DC source voltage E_d and the nominal load voltage V_0 calculate the nominal modulation index using equation (5.18)

$$k = \frac{\overline{V_o}}{E_d} \tag{5.18}$$

- This value of *k* is used to calculate *K* in equation (5.19):

$$K = \left[\frac{k^2 - \frac{15}{4}k^4 + \frac{15}{4}k^5 - \frac{5}{4}k^6}{1440}\right]^{1/2} \tag{5.19}$$

- Based on the nominal load current I_o the fundamental output frequency f_r, the switching frequency f_s, and the specified voltage ripple $V_{o1,av}$ calculate the optimum filter inductance using equation (5.20):

$$L_f = \frac{\overline{V_o}}{\overline{I_o} f_s}\left\{K \frac{E_d}{V_{o1,av}}\left[1 + 4\pi\left(\frac{f_r}{f_s}\right)^2 K \frac{E_d}{V_{o1,av}}\right]\right\}^{1/2} \tag{5.20}$$

- Having found the inductance the filter capacitor can be found using equation (5.21).

$$C_f = K \frac{E_d}{L_f f_s^{\,2} V_{o1,av}} \tag{5.21}$$

- The values of the inductance and capacitance required in this thesis are obtained using this method and actual values used in the laboratory will be as close to these as possible. The result of this process is a single phase sinusoid to be supplied to the household electricity grid.

The MATLAB program used to implement this method and obtain the L and C values is given in Appendix A. The results of running that program are:

L_f = 20.0mH and C_f = 38.43μF.

A capacitor of 50μF was what was available and was feasible because it was above the required 38.43μF capacitance. The values of capacitance and resistance used are large and can possibly be reduced by operating at higher frequency however in the choosing of operating frequency th filter size was not taken into consideration.

5.3. Two stage Power Electronics Interface

5.3.1. System Overview

As is discussed in the literature review chater of this thesis there are a number of options available when choosing the components of each stage of the power electronics interface. Should there be no need for the inclusion of a regulated 48V signal in the circuit then the DC/DC Converter stage can be removed with a possible increase in efficiency. A two-stage power electronics interface is proposed in which the unregulated DC from the fuel cell is boosted via the DC/DC Full-bridge Boost Converter stage and the resultant unregulated DC inverted to an AC signal. The amplitude of this AC signal will be controlled by varying the modulation index of the PWM signal of the Grid-tied inverter. Figures 5-15 and 5-16 show the proposed arrangement for the two-stage power electronics interface.

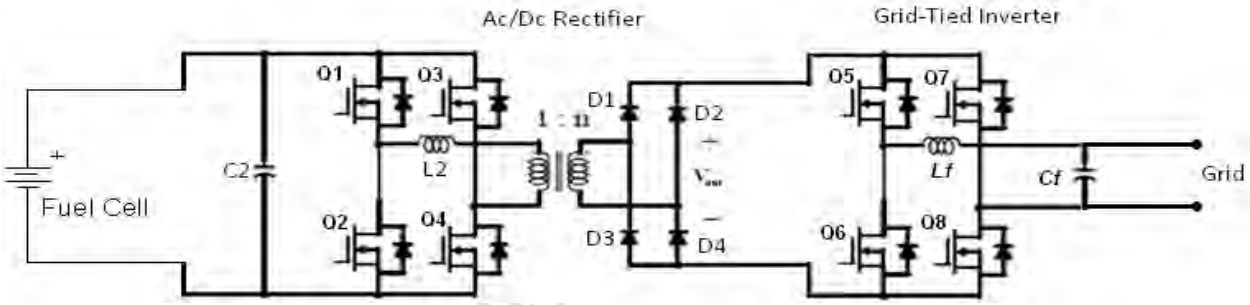

Figure 5-15: Two-stage Fuel Cell to Household Grid Power Electronic Interface Schematic

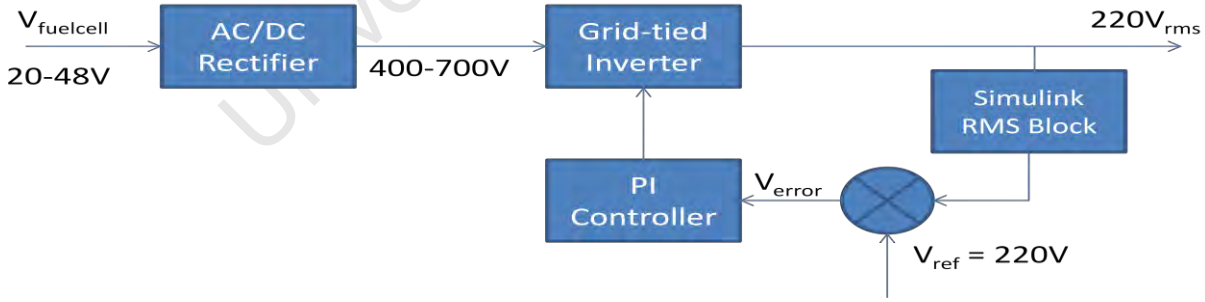

Figure 5-16: Two-stage Fuel Cell to Household Grid Power Electronic Interface

5.3.2. The DC/DC Full-bridge Boost Converter Stage in the Two-stage Interface

The DC/DC Full-bridge Boost Converter stage of the two-stage system has the same H-Bridge (Q1-Q4) as discussed in section 5.2.3 chopping the input DC signal. This signal is coming from the fuel cell and is unregulated as opposed to in the three-stage topology where it is regulated

by the Boost Converter. Since there is no voltage gain from a Boost Converter in the two-stage topology, a new transformer of greater gain is required to achieve a DC/DC Full-bridge Boost Converter output of at least 330V.

The transformer for the two-stage topology is designed using the following procedure: According to Faraday's law of electromagnetic induction the voltages induced in the primary and secondary coils of the transformer are equal and are given by equations (5.7) and (5.8).

$$V_{primary} = N_1 \frac{d\varphi}{dt} \quad (5.7)$$

$$V_{secondary} = N_2 \frac{d\varphi}{dt} \quad (5.8)$$

The maximum currents allowable through the primary and secondary coils are determined by evaluating the current at the lowest allowable voltage levels in equations (5.9) and (5.10).

Primary side: $i_{max\,,primary} = \frac{Pin}{Vin} = \frac{1000}{28} = 35.7A$ (5.9)

Secondary side: $i_{max\,,secondary} = \frac{Pin}{Vout} = \frac{1000}{400} = 2.5A$ (5.10)

The wires used in the primary and secondary coils should be able to sustain these currents hence the primary coil is made up of 0.5mm multi-stranded wire. Single strand 0.5mm wire will be adequate for the secondary wire.

The required gain of the transformer is determined by the proposed turns ratio. When determining this ratio the voltage drops across the diodes of the rectifier stage must be taken into account because the output is required to be at the required levels after this diode voltage drop has occurred. This is accounted for in equation (5.11). There is some dead time in-between the switching pulses of the full bridge hence a MOSFET H-bridge gate switching duty cycle of 0.9.

$$\frac{N_1}{N_2} = \frac{V_{in}}{V_{out} + Voltage\ \ drop} \times duty\ cycle = \frac{28}{400 + (2\times 0.7)}\ 0.9 \quad (5.11)$$

Therefore, the turns ratio and gain of the transformer is given by equation (5.12)

$$n = \frac{N_2}{N_1} = 15.93 \tag{5.12}$$

Once again using equations (5.13) and (5.14):

$$V_{primary} = N_1 f \varphi_{pk-pk} \tag{5.13}$$

Where: $V_{primary}$ = Voltage across primary winding of the transformer

N_1 = Number of turns in primary coil of transformer

f = frequency of change of flux

φ_{pk-pk} = peak-to-peak flux

$$\varphi_{\mathrm{pk-pk}} = BA_{eff} \tag{5.14}$$

B = Flux density

A_{eff} = Effective Cross-sectional area covered by flux

Using the same method applied in section 5.2.3:

$$N_1 = \frac{V_{primary}}{f\,(2\times B\times A_{eff})} = \frac{28}{20000 \times (2\times 0.2\times 683\times 10^{-6})} = 5.12\ turns \tag{5.15}$$

N_1, the number of primary turns, was rounded up to 6 turns.

$$N_2 = N_1 \times \frac{N_2}{N_1} = 6 \times 15.93 = 91.8\ turns \tag{5.16}$$

N_2, the number of secondary turns, was rounded up to 92 turns.

The input to the DC/DC Full-bridge Boost Converter is unregulated and since no control is implemented in this stage the output is also unregulated because control is going to be implemented in the grid-tied converter unlike in the three-stage scenario where control is implemented in the DC/DC Forward Boost Converter Stage. It is possible to implement control in the DC/DC Full Bridge Converter Stage to produce a regulated DC output but this was not implemented because that would require varying of the MOSFET switch duty cycles. The transformer of the two-stage topology was designed for constant duty cycles and changing this

could result in saturation and decreased efficiency. Controlling the modulation index leaves the duty cycle of the MOSFET switches constant at 50% which the transformer is designed for.

5.3.3. The DC/AC Inverter Stage Control in the Two-stage Interface

The same DC to AC inverter hardware is used for the two-stage power electronic interface topology as was used for the three phase topology. The voltage of the DC Bus of the inverter will be higher and in some cases lower than the 400V for the three-stage topology due to lack of control being implemented by the DC/DC Forward Boost Converter not present in the two-stage topology. Therefore in order to produce a sinusoidal output of $220V_{rms}$ the modulation index needs to be changed. The peak amplitude of the output waveform is given by equation (5.22).

$$\text{Inverter output amplitude} = \text{modulation index} \times \text{DC bus voltage} \quad (5.22)$$

The DSpace kit is thus used to control the modulation index and hence the sinusoidal output amplitude of the inverter. The set-point is $220V_{rms}$ and since the rms value is the set-point the MATLAB Simulink RMS block is used to find the rms value of the output signal which is subtracted from the set-point to find the signal error. As long as the signal remains at 50Hz then the RMS value can be obtained. The MATLAB Simulink model used by the DSpace kit to control the inverter is shown in Appendix C.

The inputs to this block are the frequency of the input waveform which is 50Hz and the output waveform of the inverter read into the DSpace kit via an ADC. A PID-based closed-loop control loop is implemented using the same method as in section 5.2.2 in which the initial Zeigler-Nichols inputs were found to be:

$$\text{Initial values: } K_p = 0.9;\ K_I = 98;\ K_D = 0.0045$$

$$\text{Final values: } K_p = 0.7;\ K_I = 0.5;\ K_D = 0$$

Just as was the case with the PI controller of the DC/DC Converter the I value was decreased significantly because the initial value of 120 resulted in saturation of the PI controller whose output was limited to a value between 0 and 1. The inverter can be approximated to a third

order system whose PI controller can be tuned via the Zeigler Nichols method of PID tuning. The average small signal system model for the inverter is given in appendix E.

5.3.4. Synchronising to the Grid

In order to connect to the grid the output sinusoidal waveform needs to be in phase with the grid waveform or out of phase by a predetermined amount. One way of doing this is to capture the grid waveform via an ADC and use this waveform to generate a PWM that is then used in the Grid-tied inverter H-Bridge (Q5-Q8) and the result of low pass filtering the output would be a sine wave in-phase with the grid. The disadvantage of doing this would be that any imperfections in the grid waveform would be transferred to grid-tied inverter output. So an internally generated sine wave must be used that is in-phase with the grid waveform. A phase locked loop is thus required and the 'single phase PLL' Simulink block is used to generate a sine wave signal that is in-phase with the grid waveform and is at the correct frequency (50Hz in this thesis). The Simulink model displayed in Appendix C of this thesis shows the application of the 'single-phase PLL' block.

5.4. Conclusion

There are novel adaptations to the power electronics interfacing topologies used in this thesis but these are known tried and trusted methods of interfacing. The non-linear nature of the fuel cell makes interfacing somewhat complex and by regulating the fuel cell voltage before reaching the inversion stage of the interface, the control problem is greatly simplified. The thermal power of the fuel cell prime mover is not dealt with as this is beyond the scope of this thesis. The methods used to design the system are applicable to a number of different prime mover sizes. Should a larger fuel cell stack be used the voltage output of the voltage regulating DC/DC Forward Boost Converter must be adjusted and the turns ratio of the transformer must also be adjusted in order to achieve the desired sinusoidal output voltage.

CHAPTER 6

6. Simulation and Experimental Results of Power Electronic Interface

6.1. Introduction

Before verifying the design procedure of chapter 5 via the practical implementation of the power electronic interface of this thesis project, simulation of the system was done to predict the practical performance of the system and avoid operational errors which would prove damaging and/or costly. Two topologies were formulated: A three-stage power electronic interface and a two-stage power electronic interface. In this chapter the simulation and experimental results will be discussed. MATLAB Simulink program is used to simulate the two configurations under consideration in this project. The control required to practically implement the system was done via a DSpace RTI1104 system.

6.2. Three-stage Power Electronics Interface Results

6.2.1. DC/DC Forward Boost Converter

Figure 6-1 shows the open loop model of the DC/DC Forward Boost Converter. As discussed in section 2.8.6, the capacitor is charged when the switch is in the 'off' position and the diode prevents the discharge of the capacitor when the switch is in the 'on' position resulting in an output voltage higher or equal to the input voltage. The value of the voltage at the output of the boost converter is determined by the duty cycle of the switching element labelled 'SW1' in figure 6-1. The output voltage should be consistent with equation (5.1) in the previous chapter.

Figure 6-2 shows the open loop voltage output of the DC/DC Forward Boost Converter at a duty cycle of 75% immediately at the point of connection.

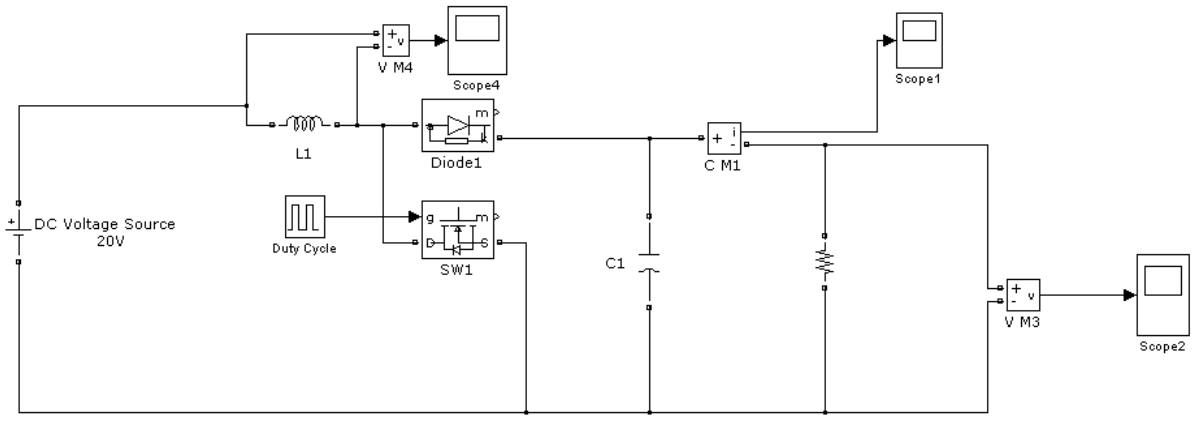

Figure 6-1: Open-loop DC/DC Forward Boost Converter Model

The gain of the forward boost converter is given by the expression ($\frac{1}{1-D}$) and it is important to determine the limits of this gain which can, in theory, tend to infinity. The gain of the boost converter was tested for 9 different duty cycle values for both simulation and practical implementation and the results are plotted in figures 6-2 and 6-3.

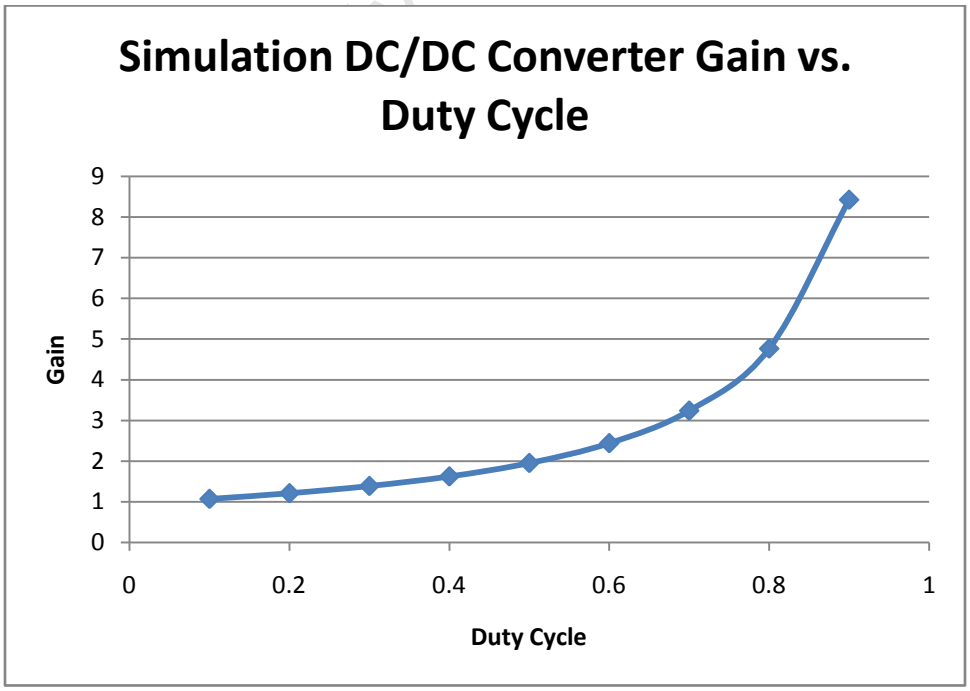

Figure 6-2: DC/DC Gain vs. Duty Cycle (Simulation)

In the simulation results it was observed that the gain converged to infinity as the gain corresponds with the relationship 1/ (1-D). The larger D, the duty cycle, gets the smaller the gain becomes. The MATLAB simulation will not take into account saturation of the inductor of the forward boost converter and component power, voltage and current limitations.

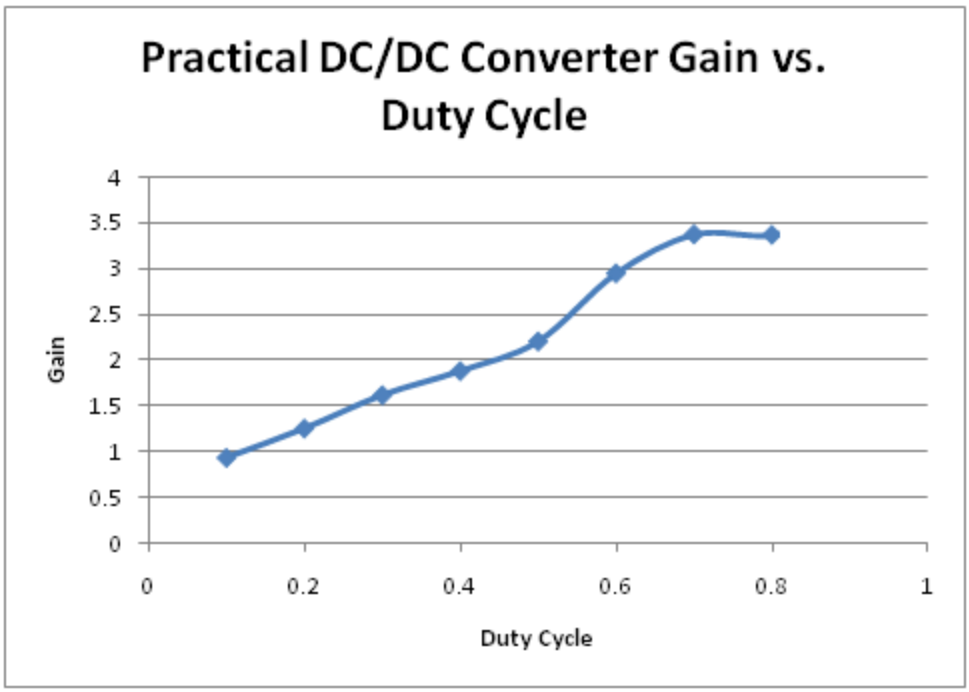

Figure 6-3: DC/DC Gain vs. Duty Cycle (Practical)

Unlike in the simulated results, the practical gain is not infinite. The gain actually begins to decrease at 80% duty cycle. In reality the theoretically infinite gain of the boost converter is limited by the saturation of the inductor. When high currents are reached the inductor behaves more like a short circuit losing its energy storage abilities. This energy storage of the inductor is what makes high voltages across the capacitor, higher than the input voltage, attainable in this circuit.

Figure 6-4 represents the MATLAB Simulink model of the closed-loop DC/DC Forward Boost Converter that was used in the three-stage power electronic interface. The components encircled in the bottom left corner produce the MOSFET switching pulses in this simulation. In the practical implementation these pulses are produced by the DSpace PWM module. The

output of the PI controller is the duty cycle of the converter switch. The component sizes are as discussed in the chapter 5 design process.

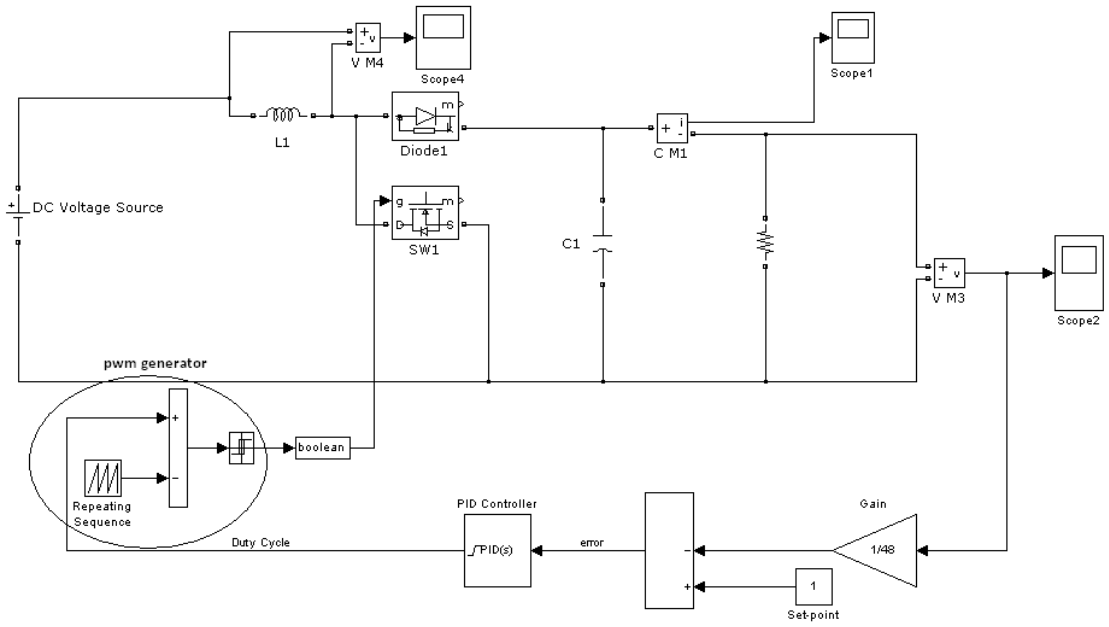

Figure 6-4: DC/DC Forward Boost Converter Incorporating Closed-Loop Control

The tuning of the PID Controller coefficient values is discussed in chapter 5 of this thesis project. Using the same methodology of section 5.2.2 the PID Controller coefficient values chosen for the Forward Boost Converter controller were:

$$K_p = 0.4;\ K_I = 0.5;\ K_D = 0$$

The output of this converter is expected to be regulated at 48V for a DC input ranging from 20V to 48V as to be expected of the 1kWe HTPEMFC. In order to validate this, the input voltage to the converter was stepped from 20V to 40V and then from 40V to 10V to ensure large ranges of output dynamic displayed by the fuel cell are catered for. The resultant outputs were recorded and are displayed in figures 6-5 and 6-6.

An initial overshoot peak of 60.33V is observed in figure 6-7 which is within the component operating limits of the converter components. This overshoot is approximately 25.7% of the steady state value which is high but the simulations do not incorporate the stray capacitances and inductances which will have an effect on the transient behaviour of the system but will not

affect the steady state value of the system. The possibility of adding poles to the system to curb this will be considered if the experimental results show similar overshoot. As expected in figure 6-7, the output settles at 48V when the input voltage is stepped from 20V to 40V at time 0.5s due to the closed-loop set-point tracking control. Overshoot is observed at time 0.5s and the peak of this overshoot is 55.12V and it takes the output of the converter 0.023 seconds to settle to within ±2% of the 48V set-point.

An initial overshoot peak of 106.9V is observed in figure 6-7 which is within the component operating limits of the converter. As expected, in figure 6-7 the output settles at 48V when the input voltage is stepped down from 40V to 10V at time 0.5s due to the closed-loop set-point tracking control. Undershoot is observed at time 0.5s and the minimum value of this undershoot is 37.42V and it takes the output 0.028 seconds to settle to within ±2% of the 48V set-point.

As was discussed in section 2.11, the authors of [17] find there is a maximum ramp rate that a fuel cell operating point in this µCHP application will adhere. As such, all transients observed were within acceptable amplitude and time limits based on [17]. In both tests the output of the forward boost converter was maintained at 48V during steady-state operation which is the voltage required in order to incorporate electricity storage mechanisms as discussed by the authors of [55] to [57].

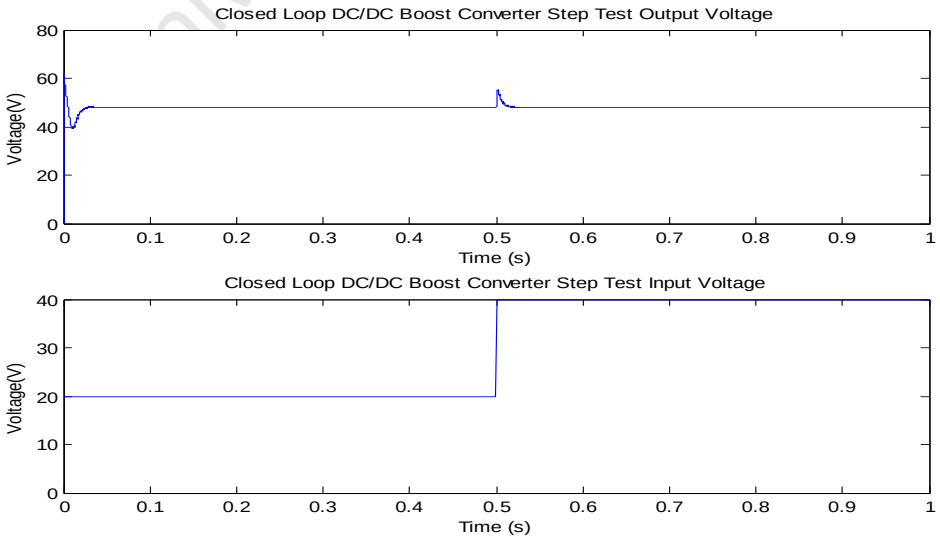

Figure 6-7: Boost Converter Step Test (20V to 40V)

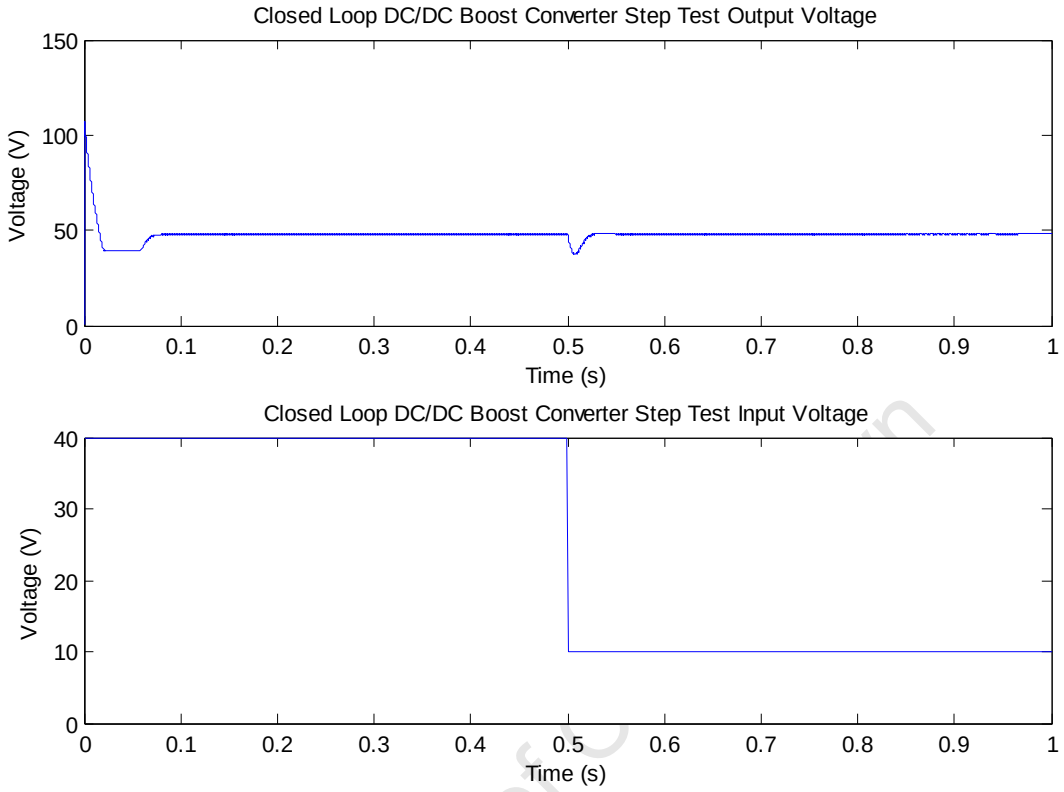

Figure 6-8: Boost Converter Step Test (40V to 10V)

The same step-tests that were conducted on the simulated closed-loop forward boost converter were conducted on the practical forward boost converter. The output of the closed-loop DC/DC Forward Boost Converter settled to 48V after stepping the input voltage up from 20V to 40V as shown in figure 6-9. This indicates that the PID-based closed-loop controller regulates the output of the fuel cell as expected during steady-state operation. A 5.2V overshoot was observed which was less than the 7.12V of overshoot that was observed in simulation. The settling time observed was approximately 125ms which was longer than the 23ms settling time observed in simulation indicating some dead-time was introduced in the practical implementation of the circuit. This can be attributed to the computational delay of the ADC and DAC used by the DSpace kit to control the converter as well as stray inductance and capacitance in the circuit.

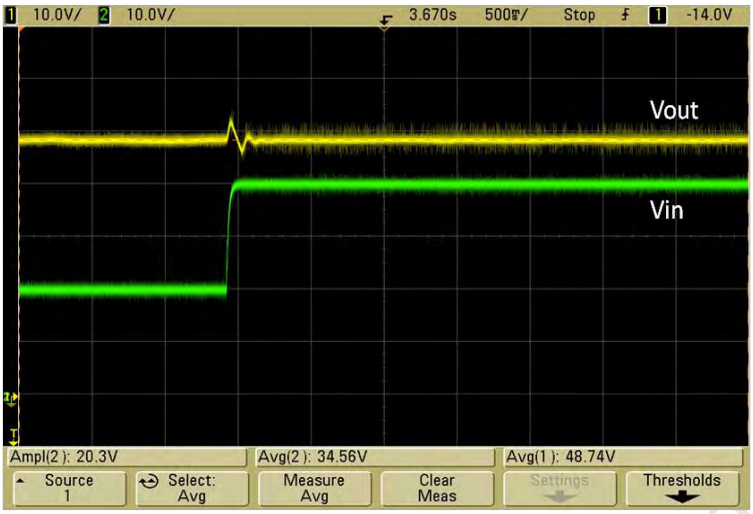

Figure 6-9: Step-test of Closed-loop DC/DC Forward Boost Converter

The initial voltage is stepped down to establish the performance of the closed-loop control of the DC/DC Forward Boost Converter with regards to dips in fuel cell voltage. Figure 6-10 shows the results of this step-test in which the fuel cell voltage was stepped down from 40V to 10V. In the simulations an undershoot of 10.42V and a settling time of 0.028s was observed. In the practical results an undershoot of 4.1V was observed as well as a settling time of 600ms due to ringing. The ringing is more pronounced in the practical results than in the simulations due to slower dynamics of the practical circuit caused by the stray inductance and capacitance of the circuit. The long settling time can also be attributed to saturation of the PID controller.

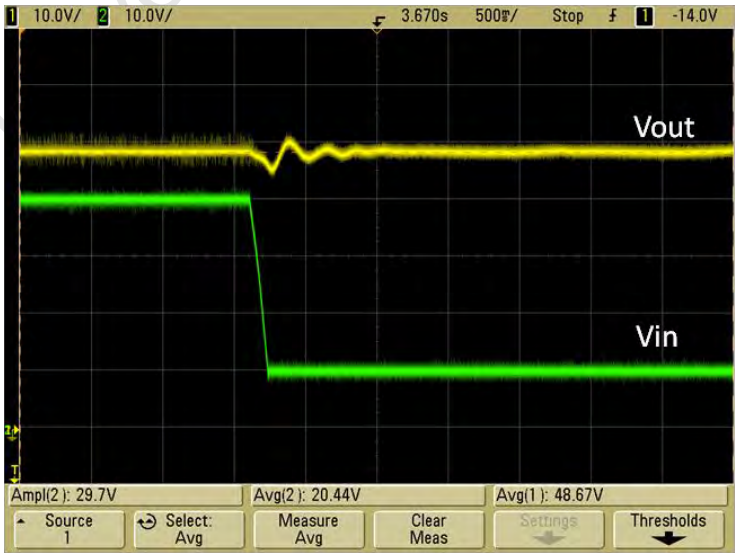

Figure 6-10: Step-test of Closed-loop DC/DC Forward Boost Converter

The dynamics of the actual laboratory DC/DC Converter are slower than the simulation results which results in decreases in the magnitude of the undershoot but also results in an increase in settling time. Given that the fuel cell will not be required to change operating point as rapidly as was the case in these step-tests the decrease in decrease in the magnitude of undershoot but increase in settling time is an acceptable trade-off resulting in adequate voltage regulation of the fuel cell in preparation for the next stage in the three-stage power electronic interface.

6.2.2. DC/DC Full-bridge Boost Converter

This stage of the three-stage interface takes the voltage output of the forward boost converter and boosts the voltage further in preparation for inversion of the DC output to AC by the inverter. A 20kHz, 50% duty cycle square wave signal is fed to the gates of the H-bridge switches which are used to convert the DC voltage from the forward boost converter to a high frequency AC voltage. The high frequency AC voltage is fed to the primary coil of the high frequency step-up transformer. The output of the transformer is then rectified to produce a DC output voltage which is higher in value than the DC input voltage. This stage of the power electronic interface was simulated in MATLAB Simulink as indicated in figure 6-11.

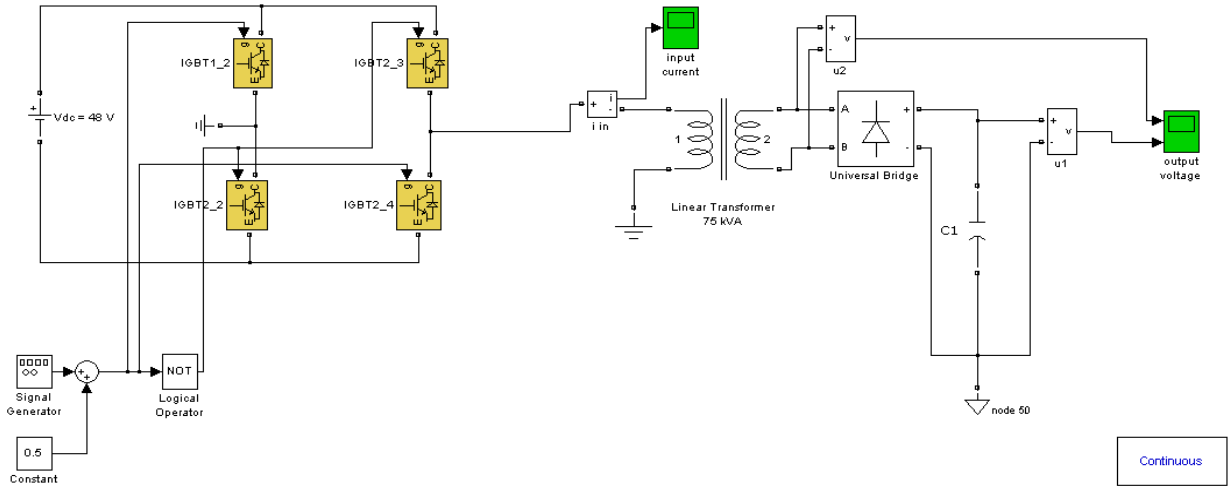

Figure 6-11: Simulink Model of DC/DC Full-bridge Boost Converter Stage of the Power Electronic Interface

The simulated results of the converter are shown in figure 6-12. In the three-stage topology, the input to the DC/DC Full-bridge Boost Converter is the voltage output of the DC/DC Forward

Boost Converter which is regulated at 48V. The output voltage of the secondary side of the high frequency transformer was found to be 409V. The output of the DC/DC Full-bridge converter stage after rectification was 407V which is acceptably close to the 400V value required because a higher voltage as the input to the inverter stage of the topology will mean the modulation index has to be adjusted to a lower value in order to get the $220V_{rms}$ which is a relatively simple task. The higher values can be attributed to voltage overshoot caused by the circuits inductance not accounted for in calculations.

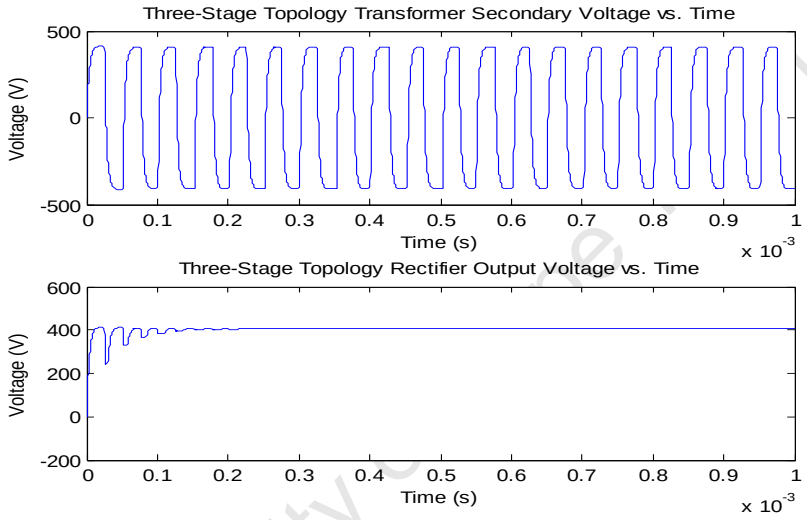

Figure 6-12: Simulated DC/DC Full-bridge Boost Converter Output for Three-Stage Topology

The output of the practically implemented DC/DC Full-bridge Boost Converter stage of the three-stage topology is shown in figures 6-13, 6-14 and 6-15 where the input voltage is 48V from the forward boost converter and the overall output is approximately 400V as expected which is consistent with what was observed in simulation. The requirements for the output of this stage of the interface are that the output of the inverter must not drop below 330V otherwise a $220V_{rms}$ will not be possible at the output of the inverter. The fuel cell voltage input will be between 20V and 48V. Control is not implemented in this stage of the power electronics interface since the input voltage to the three-stage topology DC/DC Full-bridge Boost Converter is regulated at the Boost Converter. Figure 6-13 indicates the transformer is providing a voltage gain of approximately 8.3 which is what is consistent with what was observed in simulation. Figure 6-14 shows the rectified output voltage of $400V_{DC}$ with figure 6-

15 showing the overall input and output of the DC/DC Full-bridge Boost Converter stage of the three-stage power electronics interface topology.

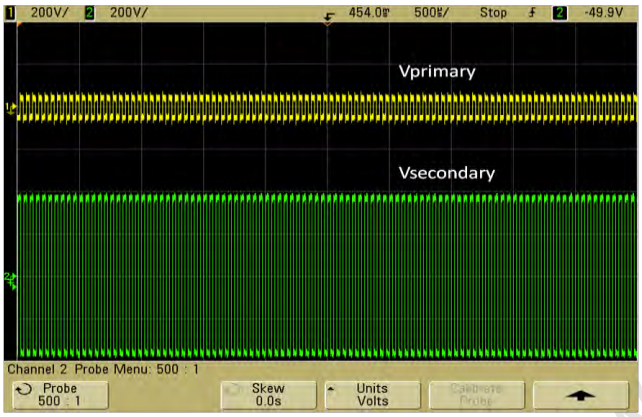

Figure 6-13: High Frequency Transformer Primary and Secondary Voltages (Three-stage Topology)

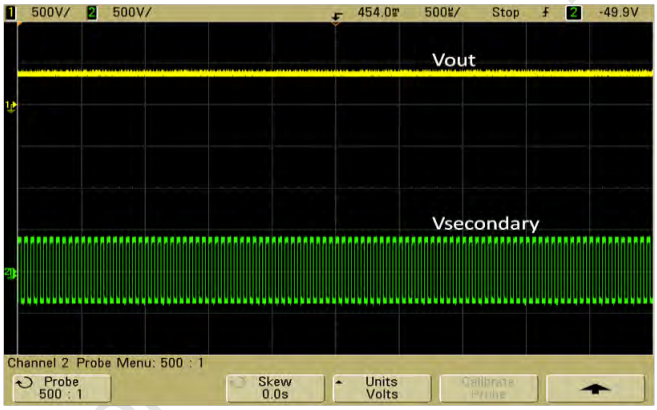

Figure 6-14: DC/DC Full-bridge Boost Converter Output and Secondary Voltage of High Frequency Transformer (Three-stage Topology)

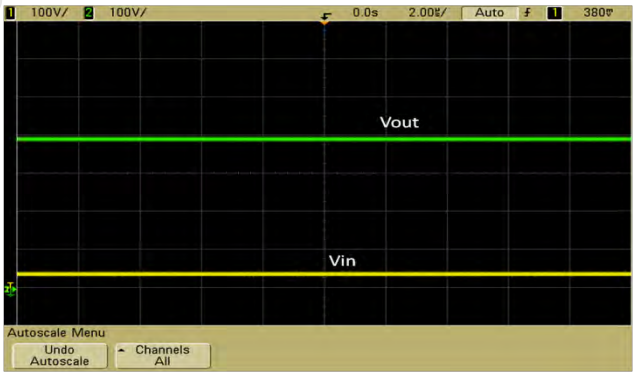

Figure 6-15: DC/DC Full-bridge Boost Converter output (Three-stage Topology)

6.2.3. DC/AC Full Bridge Inverter

The final stage of both the two-stage and three-stage power electronics interfaces is a single-phase DC/AC inverter. A MATLAB Simulink model of the H-Bridge converter is shown in figure 6-16. The three-stage topology provides a regulated DC voltage to the input of the inverter unlike the two-stage topology which is unregulated

In the three-stage interface, the input to this inverter stage is approximately $400V_{DC}$ from the rectified DC/AC converter output. This is converted to a 50Hz, sinusoidal, AC signal of $220V_{rms}$ magnitude by using an H-Bridge with a sinusoidal PWM switching scheme. Two complimentary PWM signals are fed to the four gates of the H-bridge switches. To ensure the sinusoidal PWM is in-phase with the Electricity Grid a single-phase Phase-Locked Loop (PLL) is employed. The PWM output of the H-bridge is bipolar which is discussed by the authors of [64]. The harmonics of the PWM above 50Hz are attenuated by the linear filter designed in chapter 5 which resulted in the sinusoid of figure 6-16. No further control is implemented in this stage of the interface in the three-stage topology and a constant modulation index of 0.785 is maintained.

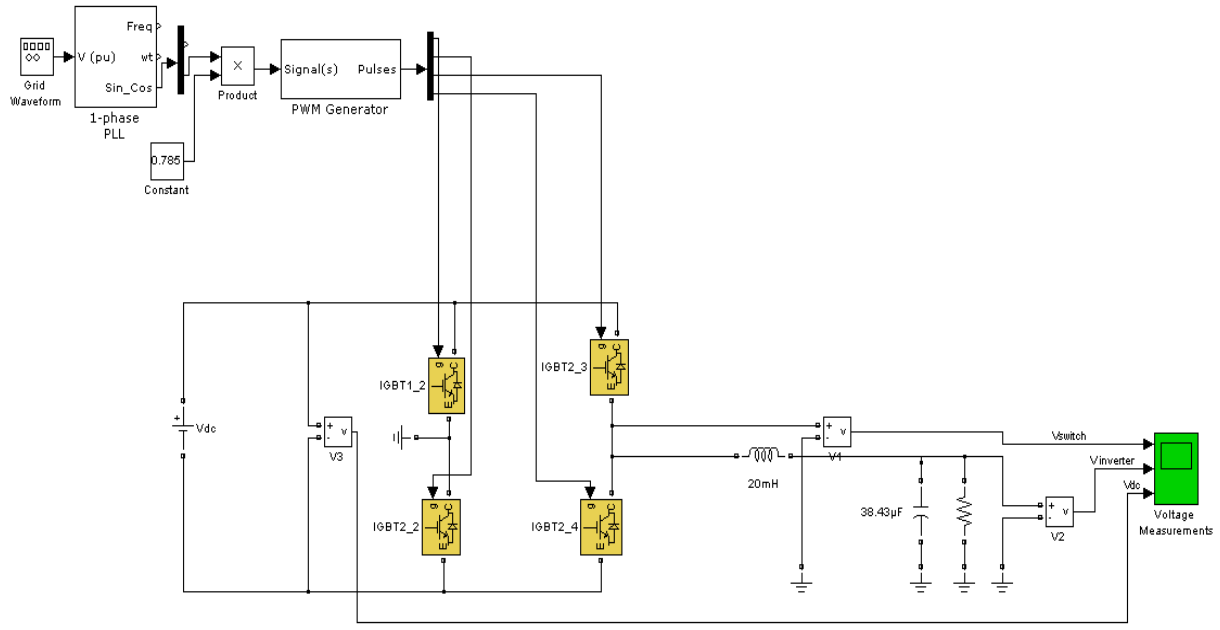

Figure 6-16: Single Phase Grid-tied Inverter Simulink Model (Three-stage)

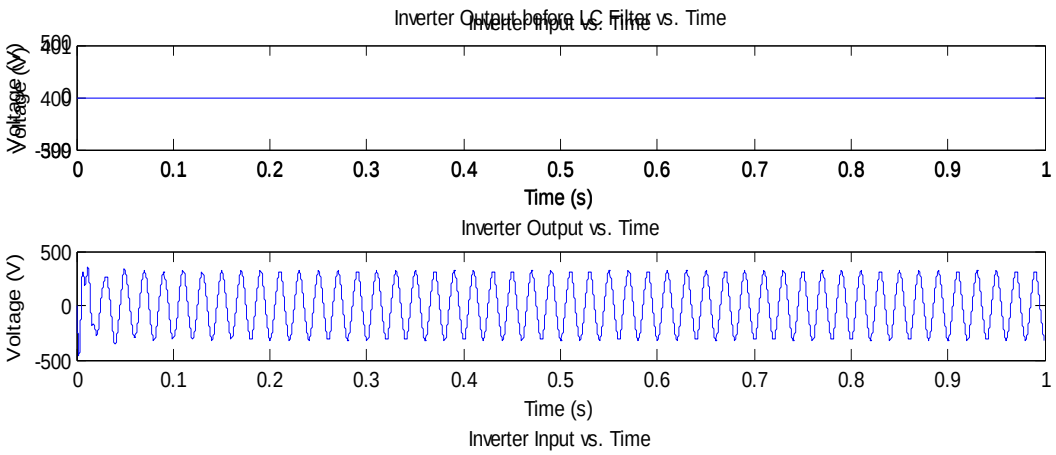

Figure 6-17: Grid Tied Inverter Output Waveforms Vin = 400V

The sinusoidal inverter output went slightly above 314V at start-up due to overvoltage caused by inductances within the grid-tied inverter circuit. The output did not rise above 410V which is well within the rated limits of the proposed electronic components. In the case of the three-stage interface as long as the input to the grid-tied inverter is regulated at 400V the output will be $220V_{rms}$.

Figure 6-18 shows the regulated DC input voltage to the inverter and the filtered output of the inverter. The output is the required $220V_{rms}$ and the modulation index of the PWM generated by the DSpace is maintained constant at 0.785 to achieve this.

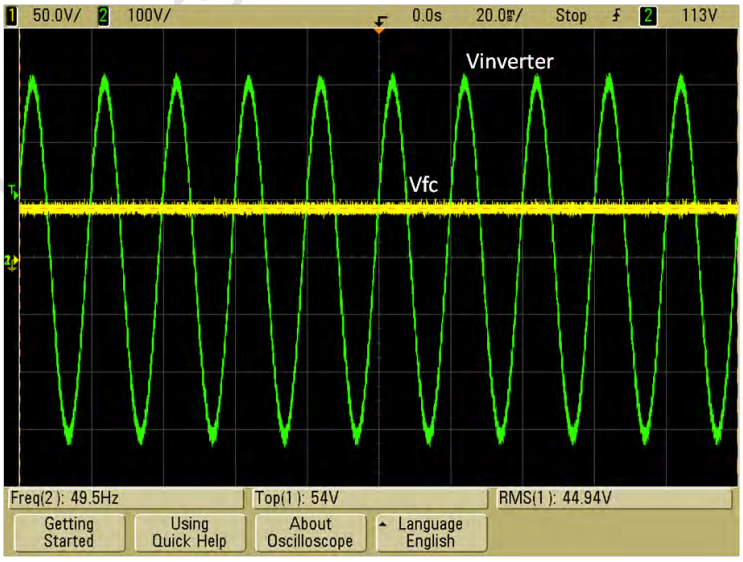

Figure 6-18: Grid-tied inverter output for V_{FC} = 48V

The phase of the sinusoided voltage relative to the grid is controlled by the PLL as discussed in section 5.3.4. The DSpace kit PLL ensures that the inverter output is in phase with the grid waveform as shown in figure 6-19, whereby full control of the phase difference is attainable.

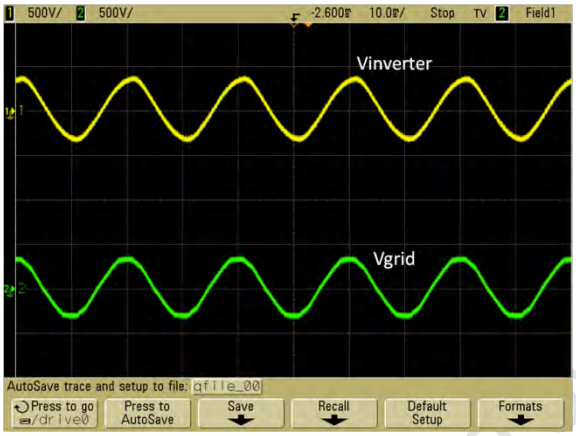

Figure 6-19: Inverter output in-phase with grid waveform

6.3. Two-stage Interface

6.3.1. DC/DC Full-bridge Boost Converter

The high frequency transformer for the two-stage topology must have a higher voltage gain than that of the three-stage topology because of the absence of a forward boost converter stage. In the two-stage topology, the input to this stage is not regulated at 48V since it is directly connected to the fuel cell. The fuel cell voltage will be between 20V and 48V.

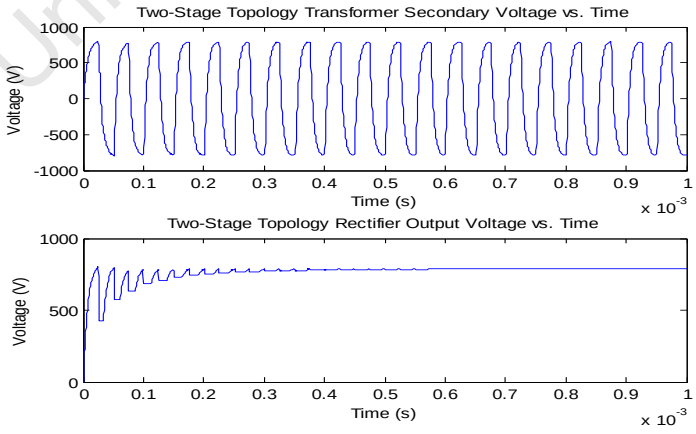

Figure 6-20: Simulated DC/DC Full-bridge Boost Converter Output for Two-Stage Topology

The voltage gain of the transformer for the two-stage topology was designed for 13.33 as discussed in section 5.2.3. Since control in the three-stage topology is achieved using the forward boost converter, which is absent in the two stage topology there is a need for control to be implemented either in this stage or the inverter stage. It was decided against using the H-bridge for control since the high-frequency transformer is designed at 50% duty cycle using the method of section 5.2.3 and thus implementing this control method would have required redesign of the transformer and resulted in poor efficiency and possible transformer saturation over certain duty cycle values. Thus the PWM signals driving the H-bridge remained constant with 50% duty cycle for both the three-stage and two-stage interface topologies and control was implemented on the inverter for the two stage topology.

The experimental results of implementing the higher gain transformer are displayed in figures 6-21, 6-22 and 6-23, indicating higher gain.

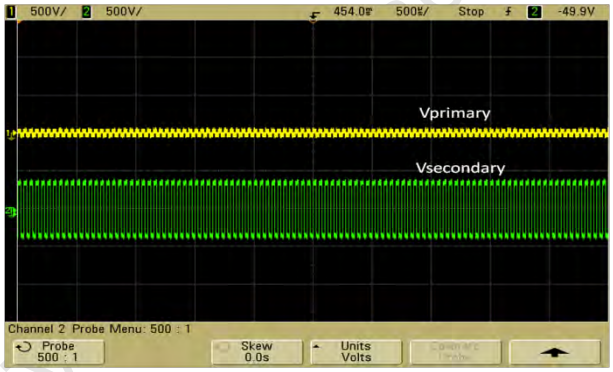

Figure 6-21: High Frequency Transformer Primary and Secondary Voltages (Two-stage Topology)

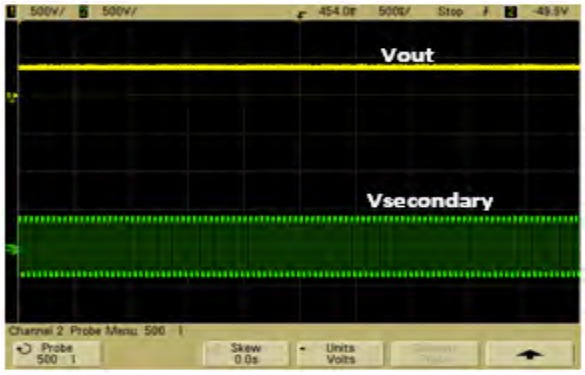

Figure 6-22: DC/DC Full-bridge Boost Converter Output and Secondary Voltage of High Frequency Transformer (Two-stage Topology)

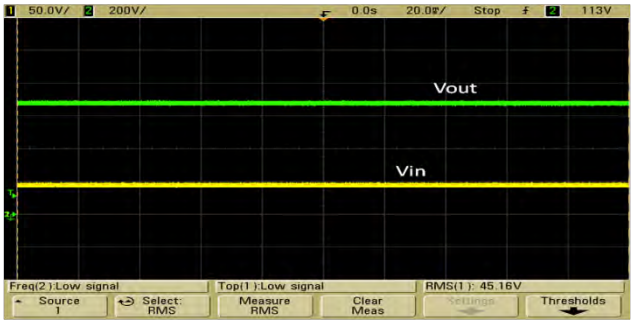

Figure 6-23: DC/DC Full-bridge Boost Converter output (Two-stage Topology)

The primary and secondary voltages of the high frequency transformer shown in figure 6-21 indicate higher voltage gain was successfully implemented practically since these values are higher than that of the two stage interface transformer in figure 6-13. The DC/DC Full-bridge Boost Converter is tested for the lowest expected input voltage from the fuel cell of 20V as can be observed by the 20V peaks of the transformer primary coil in figure 6-21. Figure 6-22 shows the rectified output of the secondary side of the high frequency transformer. Figure 6-23 shows the input and output to this stage of the two-stage topology and indicates an adequate gain is achieved with the final output being 680V which is above the minimum 330V required to generate a $220V_{rms}$ signal. The practical implementation of the DC/DC Full-bridge Boost Converter is sufficiently close to simulated results and expectations from the design procedure of chapter 5.

6.3.2. DC/AC Inverter

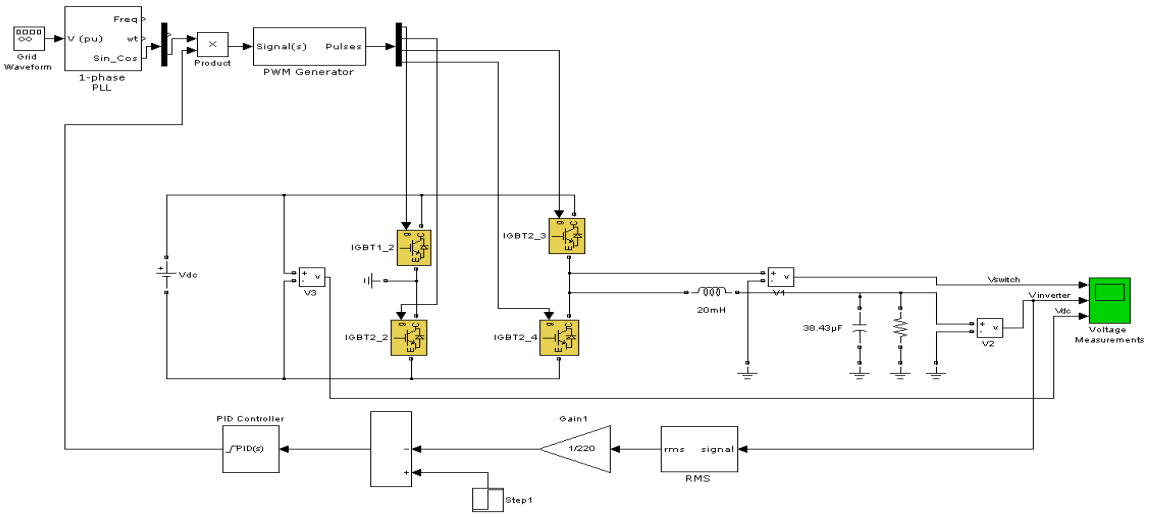

Figure 6-24: Single Phase Grid-tied Inverter Simulink Model (Two-stage)

The control of the inverter of the two-stage topology is carried out via the closed-loop PID control shown in figure 6-24. In order to obtain an error value to feed into the PID controller a constant value for the output is required and since the output of the inverter is sinusoidal, the root mean square value is taken (RMS). When subtracted from the set-point, the error is used to determine the amount by which to change the modulation index. By changing the amplitude of the sinusoidal reference waveform the value of the modulation index is varied. The output of the PID controller is not the modulation index but rather a multiplication of the modulation index.

The simulated inverter output waveforms before the LC filter are shown in figures 6-25 and 6-26. Though the input voltage to the grid-tied inverter is different in both cases (500V and 600V) the output remains at $220V_{rms}$. This is an indication that the closed-loop control is functioning correctly.

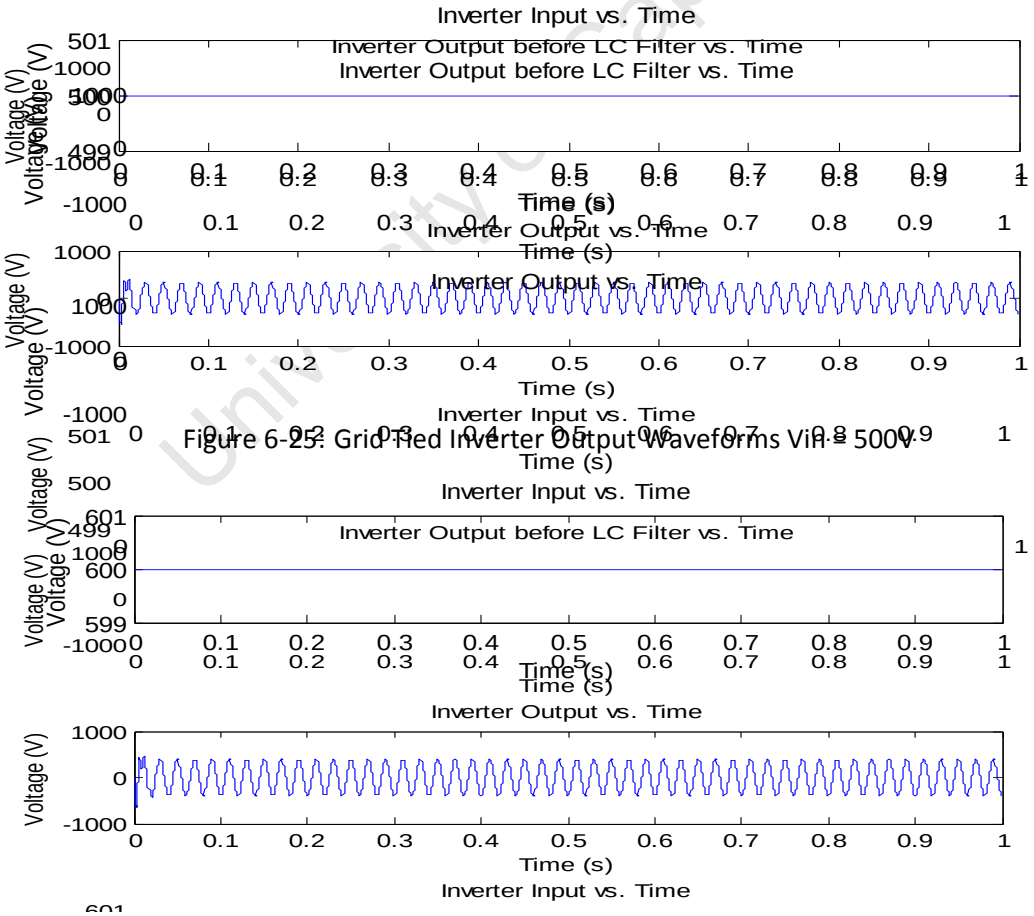

Figure 6-25: Grid Tied Inverter Output Waveforms Vin = 500V

Figure 6-26: Grid Tied Inverter Output Waveforms Vin = 600V

Equation (6.2) gives the definition of the modulation index as discussed by the authors of [64].

$$Modulation\ index\ = \frac{amplitude\ \ of\ carrier\ \ signal}{amplitude\ \ of\ reference\ \ signal} \tag{6.2}$$

Figures 6-27 and 6-28 show the post-filter outputs of the grid-tied inverter for inputs to the power electronic interface of 30V and 35V. The LC low pass filter removes the harmonics above 50Hz in the pre-filter output of the grid-tied inverter resulting in a 50Hz 220V_{rms} sinusoidal output. The modulation index for the PWM signal of figures 6-25 and 6-27 is 0.628 and the modulation index for the PWM signal for figures 6-26 and 6-28 is 0.523.

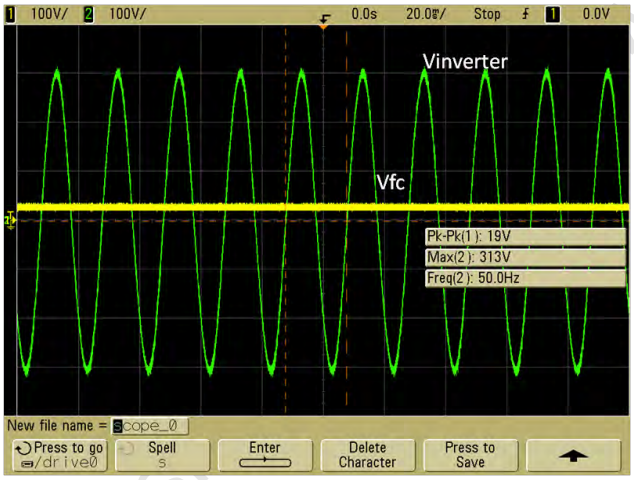

Figure 6-26: Grid-tied inverter output for V_{FC} = 30V

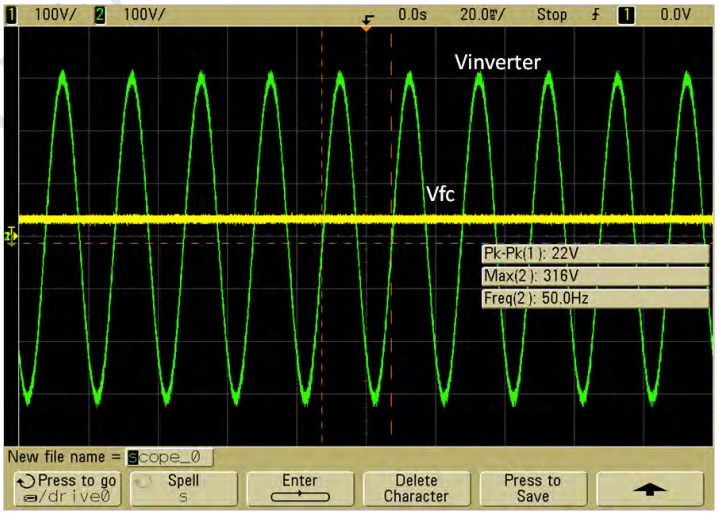

Figure 6-28: Grid-tied inverter output for V_{FC} = 35V

Just as in the case of the three-stage interface, the phase of the inverter output relative to the grid should be controlled and the Phase-locked Loop discussed in section 5.3.4 and implemented via the DSpace kit ensures that the inverter output is in phase with the grid waveform as shown in figure 6-29.

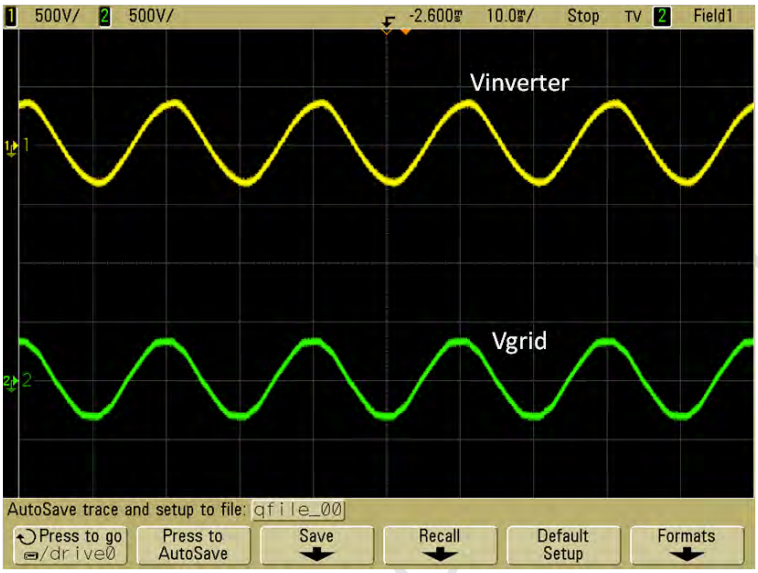

Figure 6-29: Output waveform of grid-tied inverter in-phase with grid waveform

Before connecting to the grid, the output of the inverter should adhere to the grid codes highlighted in section 2.9 of this thesis and the testing of the inverter in adherence to these standards is done in the following section.

6.4. Grid Code Adherence

6.4.1. Power Flow

In order to transfer power to or from the grid either the phase angle (δ) between the grid signal and inverter signal must be altered or the amplitude of the inverter output $|V_{inverter}|$ must be altered as indicated by equations (2.13) and (2.14).

$$P = (|Vgrid| * |Vinverter|/|Xs|) * sin\delta \text{ W} \quad (2.13)$$

$$Q = (|Vgrid| * |Vinverter|/|Xs|) * cos\delta - |Vgrid|^2/|Xs| \text{ VAR} \quad (2.14)$$

For this project, the phase angle between the grid waveform and the inverter is varied while keeping the amplitude of the inverter voltage output, $V_{inverter}$, constant. There is a need for a phase-locked loop (PLL) to lock onto the phase angle, δ, of the grid constant and this is implemented in the DSpace software package. To transfer real power to the grid the $V_{inverter}$ should lead V_{grid} and the amount required would determine the phase difference, δ, as indicated:- Figure 6-30 is a scenario in which the phase angle is shifted to 90°.

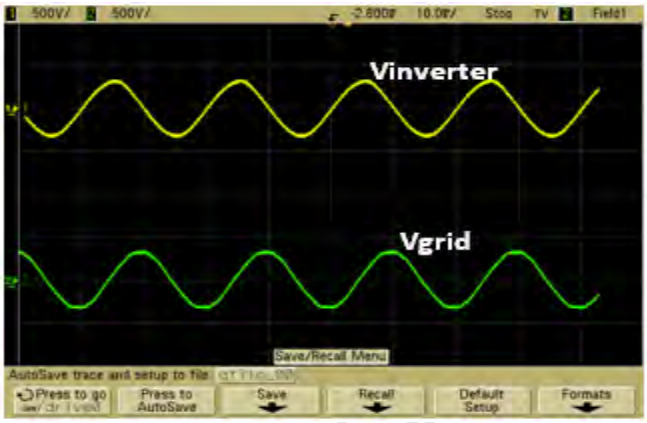

Figure 6-30: Output waveform of grid-tied inverter 90° out-of-phase with grid waveform

Figure 6-31 shows the transfer of real power to the grid as a function of the phase difference between *Vinv* and *Vgrid* (δ). These tests were done for an inverter output of 220Vrms and current of 25A from the fuel cell which is the maximum fuel cell power point being investigated and is discussed section 6.5.

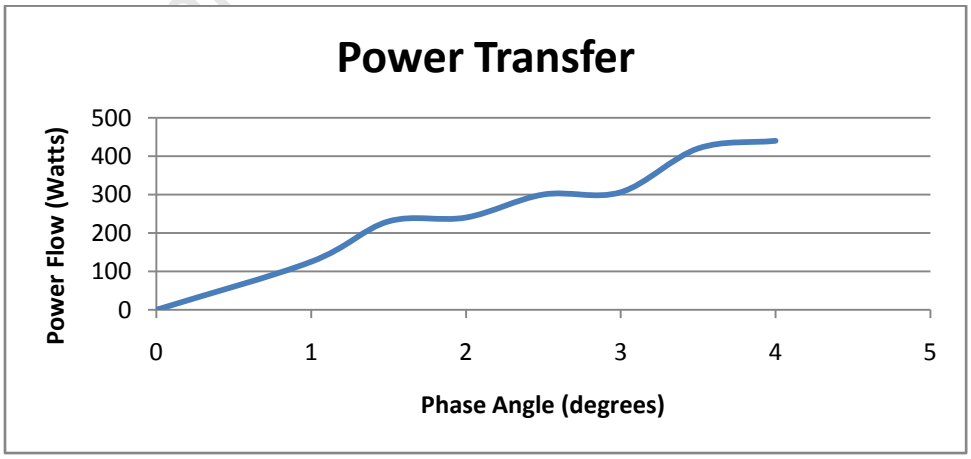

Figure 6-31: Real Power Transfer from the Grid-tied Inverter to the Grid

6.4.2. DC Current Injection

This is defined as the magnitude of the DC (0Hz) frequency component present in an AC signal. Figure 6-31 indicates the FFT of the inverter waveform when connected to the grid. The FFT is a logarithmic value and the DC Current Injection can be determined from this.

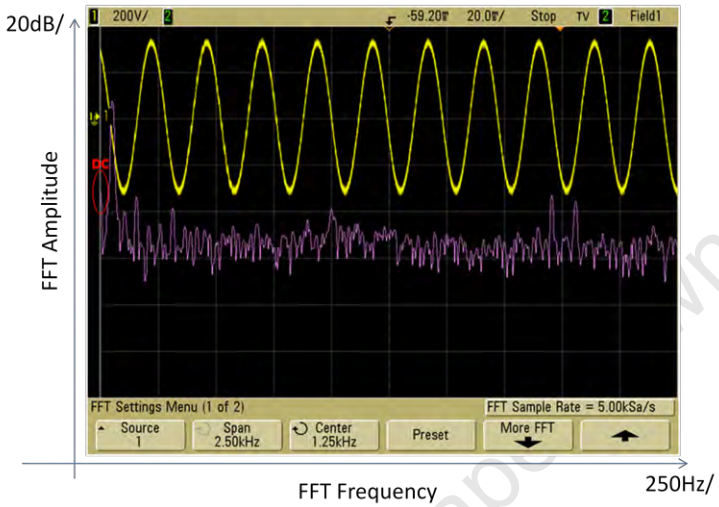

Figure 6-32: FFT of Inverter Output

The EN61000-3-2 standard discussed in section 2.9 states that the DC current Injection of the grid-tied inverter must not exceed 0.22A. The DC Current Injection values obtained for different power flow values are shown in figure 6-33.

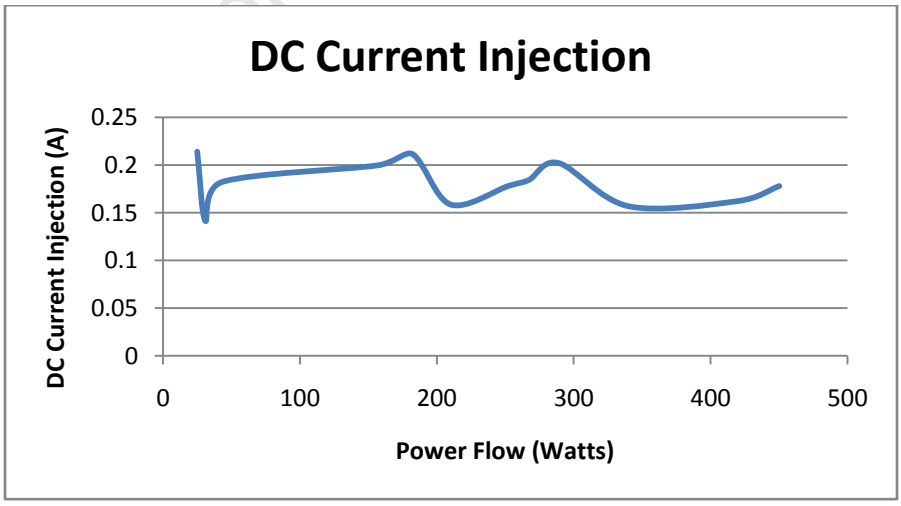

Figure 6-33: DC Current Injection

The power flow shown in figure 6-33 indicates flow into the grid and is achieved by varying the phase angle between the grid waveform and the inverter waveform as discussed in section 2.9. The highest value of DC Injection was 0.21A which is close to the 0.22A limit. The EN61000-3-2 is met but a DC suppression loop such as that discussed in [65] is necessary to ensure code adherence.

6.4.3. Total Harmonic Distortion

The total harmonic distortion discussed in section 2.9 is a means of quantifying the distortion present in a sinusoidal output such as the output signal of the grid tied inverter. Equation (2.15) is used to evaluate THD.

$$THD = \frac{\sqrt{v_2^2 + v_3^2 + v_4^2 + \cdots + v_n^2}}{v_1^2} \qquad (2.15)$$

Figure 6-33 shows the FFT of the inverter output waveform and the first five harmonics are labelled in red on the diagram. The THD values are analysed for when the inverter is connected to the grid and there is power being sent to the grid by the grid-tied inverter.

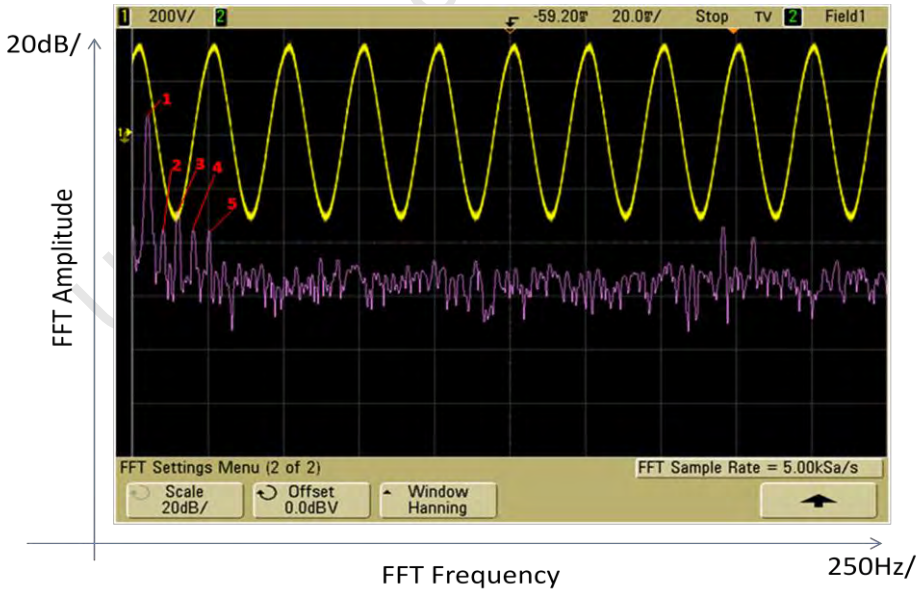

Figure 6-34: FFT of Grid tied Inverter Output

Equation (2.15) of section 2.9 was used to determine the THD of the inverter output over the rated power range and the results are shown in figure 6-35. The first 7 harmonics were used to determine the values of THD displayed in figure 6-35.

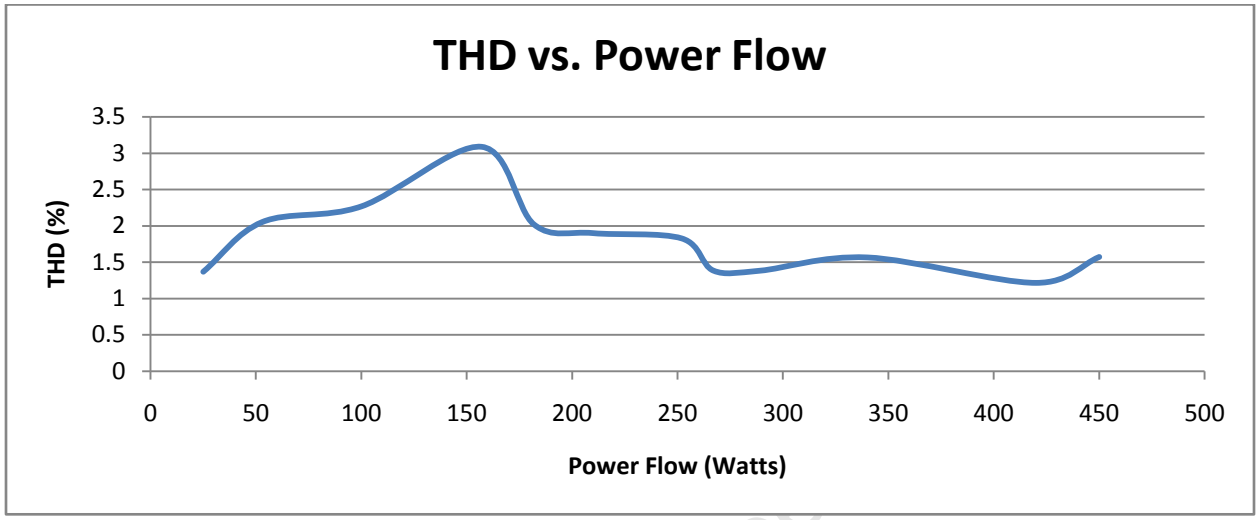

Figure 6-35: Total Harmonic Distortion of Grid tied Inverter Output

The EN61000-3-2 requires that the THD does not exceed 5% of the rated current of the grid tied inverter (30A) and the results of figure 6-35 indicate that the inverter meets these requirements for the power flow range displayed.

6.4.4. Voltage and frequency range

The voltage output of the inverter should not vary between 85% and 110% of the standard 220Vrms output during normal operation according to the EN61000-3-2 standard and the two-stage and three-stage topologies of the interface adhere to this condition.

The frequency of the output waveform of the inverter should not vary between 49Hz and 50Hz during normal operation according to the EN61000-3-2 standard and the two-stage and three-stage topologies of the interface adhere to this condition.

6.5. Power Electronics Interface Efficiency

When determining the efficiency of the system, the efficiencies along points that intersect the polarisation curve of the 1kWe HTPEMFC are of importance because these are the points which the power electronic interface will operate at. The polarisation curve of this fuel cell is

discussed in section 3.3 and from it 7 points along the polarisation curve will be used to characterise the fuel cell, which are outlined in table 6-1.

Table 6-1: Testing Points of the 1kWe HTPEMFC-based Power Electronic Interface

	Voltage	Current
1.	35	2.5
2.	33	5
3.	30.5	7.5
4.	30	10
5.	29.5	15
6.	29	20
7.	28	25

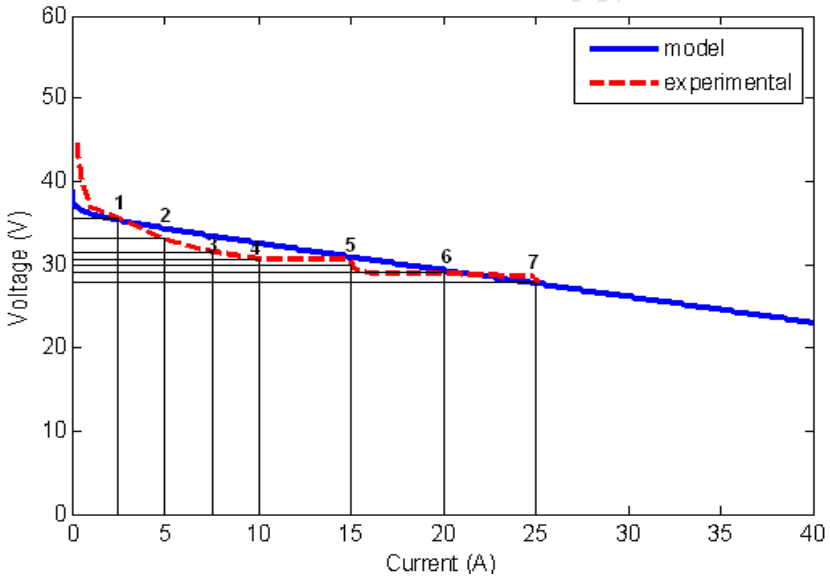

Figure 6-36: Testing Points of the 1kWe HTPEMFC-based Power Electronic Interface

6.5.1. Three-stage Efficiency

The efficiency of each stage of the system was accessed at the operating points indicated in the previous section, after which the overall efficiency was calculated. Figure 6-37 shows the efficiency of the DC/DC converter stage over the entire power range of the system. The efficiency of the boost converter remains fairly constant throughout the power range and slightly above 85%. There are few resistive components within the boost converter so resistive

losses are minimal and the majority of its losses can be attributed to losses across the MOSFET switches.

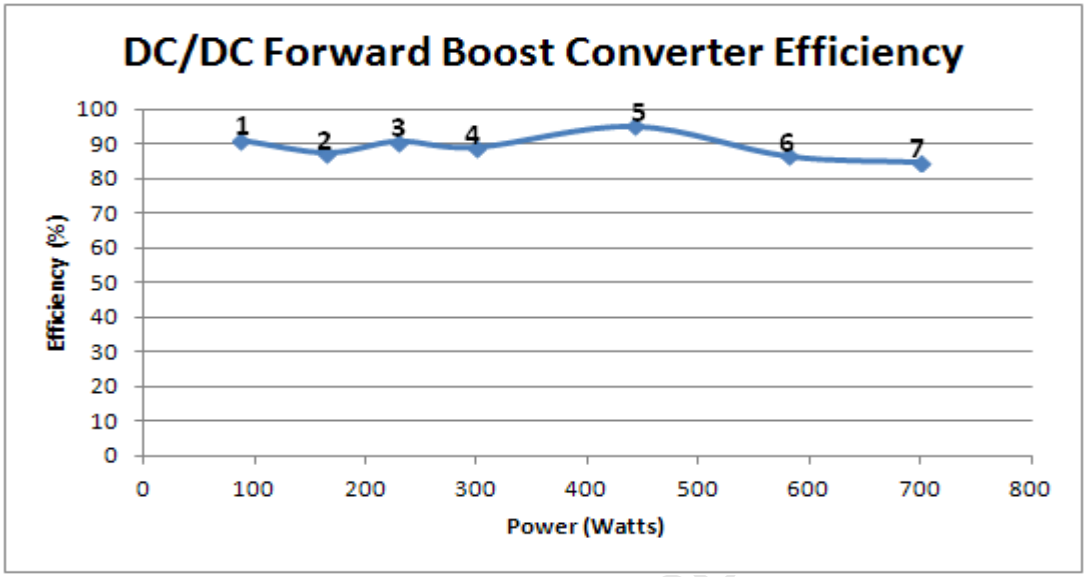

Figure 6-37: Efficiency vs. Power Curve of the DC/DC Forward Boost Converter

The efficiency of the DC/DC Full-bridge Converter was evaluated over the same power range and the results are displayed in figure 6-38. This stage of the interface is operated without control and the fluctuations in efficiency observed can be attributed to dissipative losses across the transformer, diodes and MOSFET switches and switching losses of the MOSFET switches.

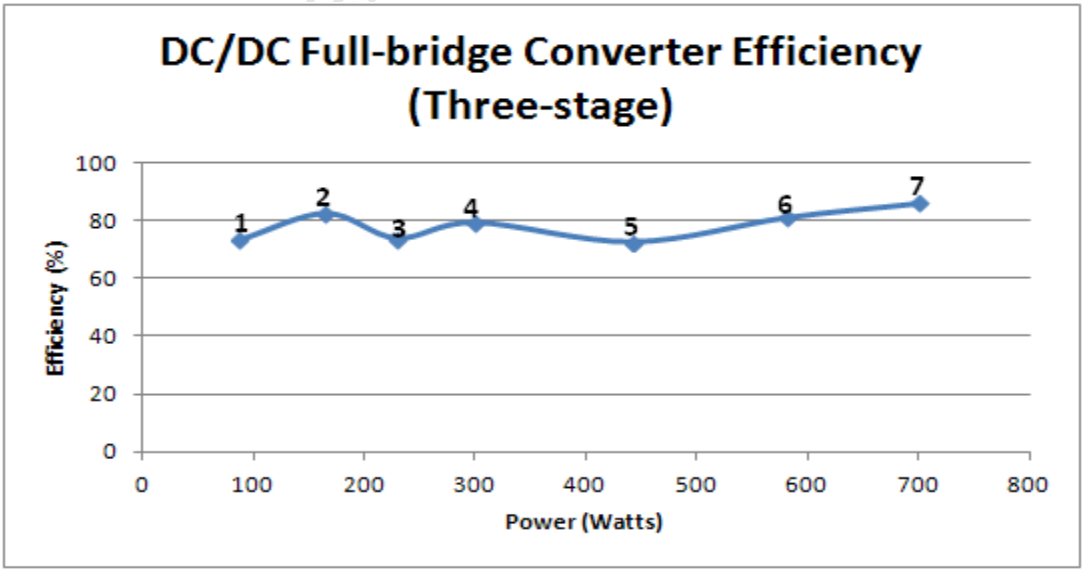

Figure 6-38: Efficiency vs. Power Curve of the DC/AC Rectifier

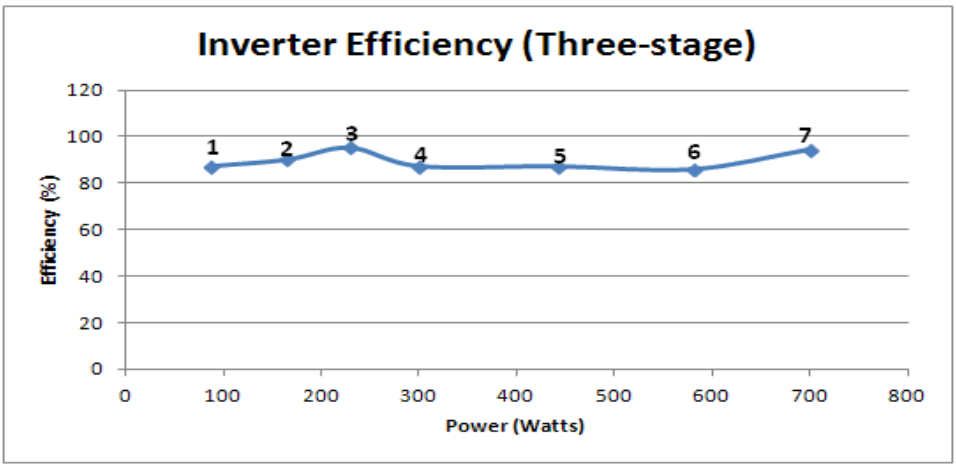

Figure 6-39: Efficiency vs. Power Curve of the Grid-tied Inverter

The inverter stage of the three-stage topology had efficiencies as shown in figure 6-39. The values range from 86% to 95%. Some inverters in literature have been described as having efficiencies of up to 98%, so higher efficiency is possible.

In the case of the three-stage interface, the overall efficiency at the seven fuel cell operating points defined in table 6-1 was measured. The efficiency of this three-stage interface topology was found to lie between 60% and 70%. The non-linearity in the operating points is shown by the non-linear efficiency values. As the fuel cell output current increases the power output increases non-linearly. The power dissipated in the resistances in the two-stage interface increases with increase in current. These two phenomena are the driving factors behind the data measured in figure 6-40.

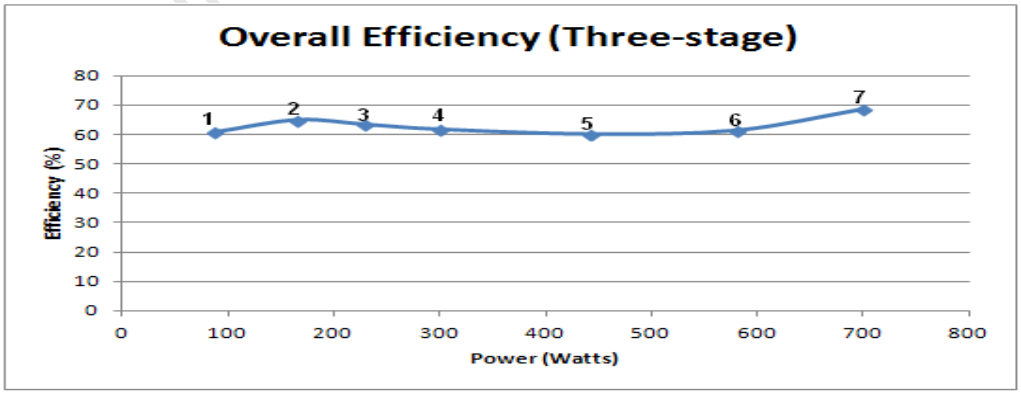

Figure 6-40: Efficiency vs. Power Curve of the Two-stage Power Electronic Interface

6.5.2. Two-stage Efficiency

The efficiency values of the two-stage interface's DC/DC Full-bridge Converter are within the same range as those of the three-stage interface. Less turns are used in the two-stage transformer than in the three stage topology's transformer but the amount of wire removed is not large enough to significantly affect the efficiency of the transformer so no large difference in efficiency is expected or seen in the results of figures 6-38 and 6-41.

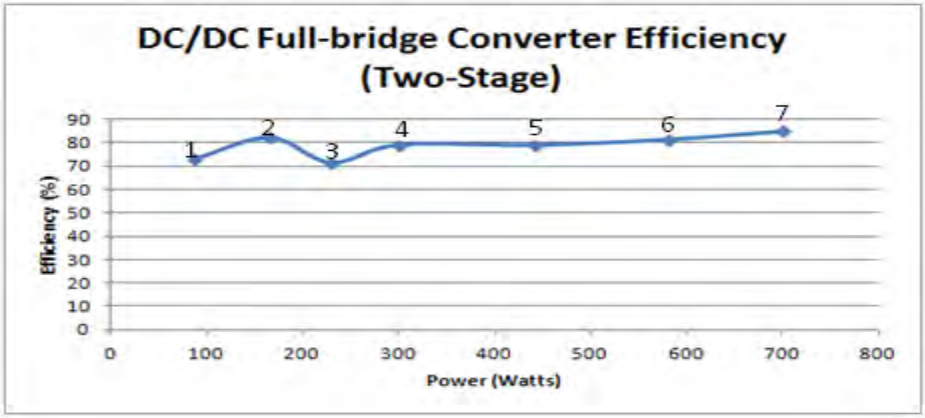

Figure 6-41: Efficiency vs. Power Curve of the Two-stage Power Electronic Interface

The inverter stage of the two-stage topology had efficiencies as shown in figure 6-42. The values are ranging from 86% to 96% which is similar to what was observed with the three-stage inverter. Slight variations in efficiency can be attributed to the control of the modulation index but these are not large since the hardware of the inverter remains unchanged for both interface topologies.

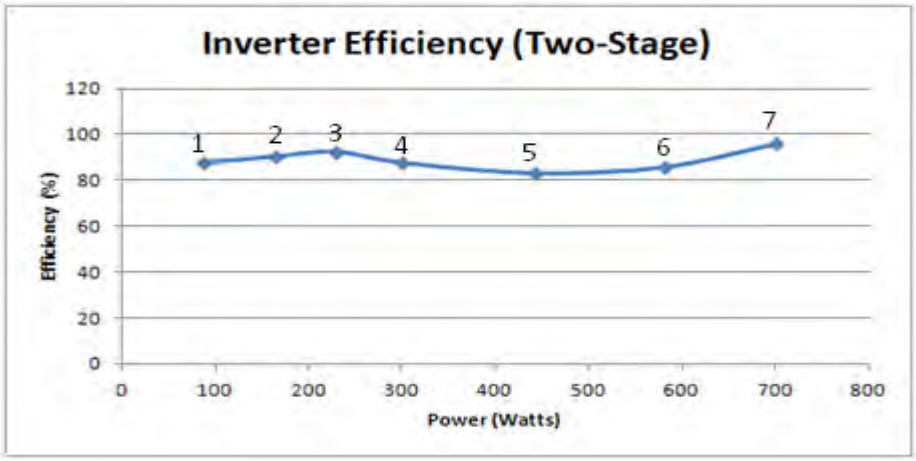

Figure 6-42: Efficiency vs. Power Curve of the Two-stage Power Electronic Interface

Just as in the case of the three-stage interface, the overall efficiency of the two-stage interface efficiencies at the seven fuel cell operating points defined in table 6-1 were measured. The efficiency of this interface topology was found to lie between 63% and 82%, as shown in figure 6-43.

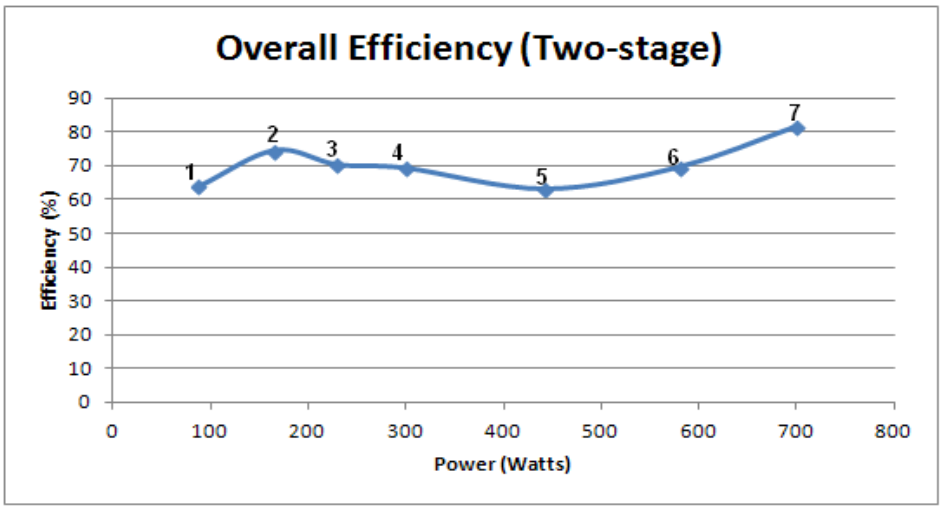

Figure 6-43: Efficiency vs. Power Curve of the Three-stage Power Electronic Interface

6.5.3. Comparison of Interface Efficiencies

Figure 6-44 shows a summary of the efficiency results of the power electronic interface. It is expected that by multiplying of the efficiencies of each individual component of the two-stage and three-stage efficiency should be equivalent to the overall efficiency of the interface.

$$\text{Overall System Efficiency} = (\eta_1 \times \eta_2 \times \ldots \eta_n) \quad (6.2)$$

Where n = number of components in system

η_n = efficiency of component n

It is anticipated that the efficiency of the two-stage system will be greater than that of the three-stage system and this is observed in figure 6-44 and can be attributed to less conducting losses and switching losses of the two-stage interface which has less wiring and switches.

The DC/DC Full bridge boost converter efficiencies of both the two-stage and three-stage efficiencies are similar because the switching losses for this stage are the same in both

topologies. It is expected that the two-stage DC/DC Full bridge boost converter efficiency should be higher because of less conduction losses in the transformer but it is observed that this is not by a significant amount since the copper wire is of a low resistance.

The inverter efficiencies of both topologies are expected to differ since the switching patterns are different because of the control implemented on the inverter of the two-stage system. The difference in efficiencies is not large.

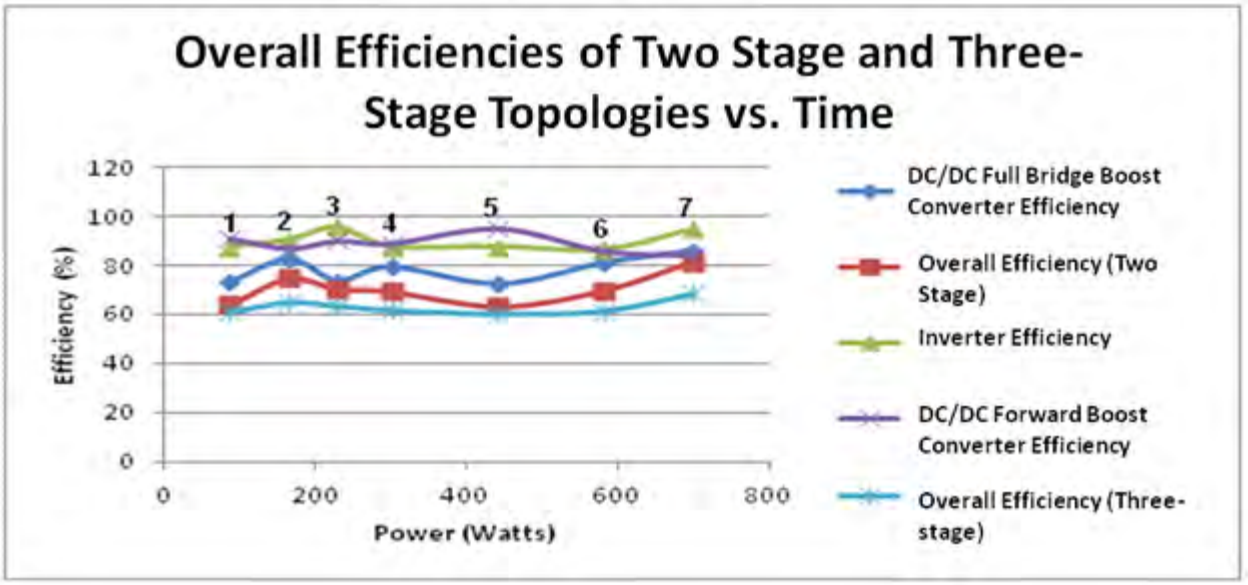

Figure 6-44: Efficiency vs. Power Curve of the two Power Electronic Interfaces

6.6. Conclusion

This chapter describes the experimental implementation of the theory of chapters 2 to 5. Two topologies were designed, built and tested: one with a forward boost converter, DC Full-bridge Converter and grid-tied inverter (three-stage topology) and one with just the DC Full-bridge Converter and grid-tied inverter stages (two-stage topology). The closed-loop control of the forward boost converter of the three-stage topology maintained the voltage at a regulated 48V as anticipated. The closed-loop control of the inverter of the two-stage topology performed better than anticipated. It was expected that the delay in calculation of the root mean square value of the output before comparing this value with the set-point of $220V_{rms}$ would result in

control too slow but this was not the case. The dynamics of the two experimental systems were expected to be slower than those of the simulated system due to stray inductance within the circuit and this was observed for both the three-stage topology and two-stage topology during step-tests. Grid code adherence was anticipated and achieved at steady with adequate THD, DC injection and output frequency and amplitude range being observed at the output of the grid-tied converter. The inverters of the two topologies were expected to be different but did not do so by a significant amount. The two-stage topology was expected to be more energy efficient than the three-stage due to less conduction losses and switching losses and this was observed in experimental results.

Chapter 7

7. CONCLUSION

This thesis investigated the sizing strategy appropriate for application to a fuel cell-based residential µCHP system as well as the hardware interfacing a 1kW HTPEMFC based µCHP system with a residential thermal and electrical load. The electrical interface between the fuel cell and the household is what was investigated without taking into consideration the thermodynamic cycle being implemented.

A literature scan was conducted of the High Temperature Proton exchange Membrane Fuel Cell (HTPEMFC) to gather the necessary theory to improve on a system designed to interface a 1kW HTPEMFC to a household. Energy is generated by the HTPEMFC in two forms: thermal energy and electrical energy. In order for the HTPEMFC to be viable as a source of energy generation both forms of energy must be harnessed from the exothermic reaction of the fuel cell meaning a thermodynamic cycle must be employed. Combined Heat and Power (CHP) systems make use of both the thermal and electrical energy generated by the fuel cell by using the thermal energy generated for heating processes. Fuel cells are one of the technologies that can be used for µCHP systems and can replace engine based µCHP systems. It was found that the fuel cell is more environmentally friendly and has a low heat-to-power ratio which is desirable in residential µCHP operation as this implies less heat dumping.

In order to simulate the system assumptions were made for the fuel cell and balance of plants resulting in a 1kW HTPEMFC fuel cell-based residential µCHP system model. This model was then used to assess three µCHP control strategies used to operate the balance of plant: heat-led control, electricity-led control and cost minimizing control. It was found that the ideal µCHP control strategy to use in a given scenario is dependent on the average load profile of that household amongst other factors.

A methodology for determining the appropriate size for the system in different residential scenarios was developed. A MATLAB µCHP sizing algorithm was developed to be able to determine the size of a range of households. It was observed that the system size depended on the µCHP control strategy being employed, the seasonally varying load profile of the household and the capital costs of manufacturing the system.

A power electronic interface was assessed and system dynamics and efficiency were improved on. The system comprised of a Boost Converter, Voltage Rectifier and Grid-tied Inverter. The PID controller of this three-stage topology to be used as an interface between the HTPEMFC and the household electricity network was tuned for better system dynamics. In an attempt to improve on efficiency a two stage topology was implemented consisting of just the Voltage Rectifier and Grid-tied Inverter. This resulted in an increase in efficiency as a result of reduction in losses and resulted in the need for a different control approach. The control of the voltage amplitude of the two-stage topology was done by varying the modulation index of the output PWM. The dynamics of the system were tested via a voltage step test and the efficiencies of both systems were tested over the rated power range.

The grid-tied inverter of the power electronic interface was connected to the grid via an inductor and tested for compliance with grid codes. Compliance of the grid-tied inverter with the IEC61727, IEEE1547 and EN61000-3-2 standards for DC Current Injection, Voltage Range, Frequency Range and Total Harmonic Distortion is verified. The inverter is connected to the grid and power is made to flow to and from the grid. The amount of active and reactive power flow can be controlled by varying the amplitude and/or phase of the output waveform of the inverter.

Further Research

Integration of the system to an actual fuel cell will enable the theory of this thesis to be further validated. A fuel cell-based µCHP system can be developed and mass produced based on the theory of this thesis provided the HTPEMFC and necessary infrastructure is made available.

The residential μCHP system developed in this thesis is designed for countries in which households have access to a gas supply line which is not the case in many countries including the country of origin of the thesis. A system that uses stored gas containers can be developed which will result in a different operating strategy and sizing approach.

The capital costs of the μCHP systems in this thesis are based on commercially available units. In a country such as South Africa where platinum is readily available the cost of manufacturing will differ from manufacture in the countries investigated in this thesis. A study into fuel cell manufacture within South Africa and similar countries will yield useful information.

As the HTPEMFC increases in age the performance characteristics such as electrical and thermal efficiency of the stack change and a sizing algorithm that incorporates this will be more accurate than that proposed in this thesis.

References

[1] EPCOR. “Distributed Generation”, [Online]. Available: http://www.epcor.com/efficiency-conservation/Documents/Distributed-Generation-Edmonton.pdf, [May 2011].

[2] Consortium on Energy Restructuring, “Benefits of Distributed Generation”, [Online]. Available: http://www.dg.history.vt.edu/ch1/benefits.html

[3] J. Larminie and A. Dicks, “Fuel Cell Systems Explained”, Third Edition West Sussex: John Wiley & Sons Inc., 2001.

[4] J. Clark, “Definitions of Oxidation and Reduction”, [Online]. Available: http://www.chemguide.co.uk/inorganic/redox/definitions.html, [June 2011].

[5] L. J. Bonville, et al., “Development and demonstration of a high temperature PEM fuel cell stack”, Journal of Power Source, 144: pp.107-112, 2005.

[6] C.B. Oland, “Guide to Combined Heat and Power Systems for boiler owners and operators,” Oak Ridge national Laboratory, Oak Ridge, TN, Tech. Rep. ORNL/TM-2004/144, 2004.

[7] M. Nehrir and C. Wang, “Modelling and Control of Fuel Cells: Distributed Generation”, New Jersey: John Wiley and Sons, Inc., 2009, pp. 40-54.

[8] C. Bocaletti et al, “A Reformer Model for Fuel Cell Power Systems”, POWERENG, Setúbal, Portugal, 2007.

[9] G. Maranzana, C. Moyne, J. Dillet, S. Didierjean, O. Lottin, “Internal currents in PEMFC during Start-up or Shut-down”, Journal of Power Sources,18th World Hydrogen Energy conference, 2010.

[10] W. Lehnert. “Lifetime Aspect of PEFC”. Institute of Energy Research, WBZU, 2009.

[11] V. Phlippoteau, C. Turpin, S. Astier. “State of Health of a PEM fuel cell Degraded After ON-OFF Enurance Cycles”, [Online]. Available: http://perso.ensem.inpl-nancy.fr/Olivier.Lottin/FDFC08/CD/Contributions/FCHPHLI10-09_62M.pdf, [April 2012].

[12] The Micropower Council, “Micro-CHP Fact Sheet United Kingdom”, [Online]. Available: http://www.internet-public-library.org/carbon-reduction/combined-heat-and-power-fact-sheet.pdf, [September 2012].

[13] Center For Advanced Energy Systems, “Guidelines to follow when considering Combined Heat & Power (CHP)”, [Online]. Available: http://njchp.rutgers.edu/files/Guidelines_CHP.pdf

[14] Tokyo Gas Co. “ENE FARM Residential Fuel Cells Launched” [Online]. Available: http://www.tokyo-gas.co.jp/tgminutes/64.pdf [Mar. 2, 2011]

[15] Carbon Trust, “MicroCHP Accelerator”, Carbon Trust, London, Tech. Rep. CT726, 2007

[16] D. Kaundinya, P. Balachandra, and N.H. Ravindranath, “Grid-connected versus stand-alone energy systems for decentralized power—A review of literature”, Renewable and Sustainable Energy Reviews, vol. 13, no. 8, Oct. 2009, pp. 2041-2050
[17] G. Simader et al, “Micro CHP systems: state-of-the-art”, Austrian Energy Agency, Deliverable 8 of Green Lodges Energy Project, Vienna, Mar. 2006.
[18] K. Parikh et al, “Planning Commission Report,” Integrated Energy Policy, Tech. Rep. Government of India, 2006.
[19] WADE (World Alliance for Decentralized Energy). “World Survey of Decentralized Energy-2005,” Survey Paper, 2005.
[20] W. Colella, “Design options for achieving a rapidly variable heat-to-power ratio in a combined heat and power (CHP) fuel cell system (FCS)”, Journal of Power Sources, vol. 106, no. 1-2, Apr. 2002, pp. 388-396
[21] J. T. Pukrushpan et al., “Control of fuel cell power systems: Principles, Modeling, Analysis and Feedback Design”, Ed. London: Springer-Verlag, 2004, pp. 1-11.
[22] J. T. Pukrushpan, “Modelling and control of fuel cell systems and fuel processors”, PhD, University of Michigan, 2003.
[23] P. Bajpai and V. Dash, “Hybrid renewable energy systems for power generation in stand-alone applications: A review”, Renewable and Sustainable Energy Reviews, vol. 6, no. 5, pp. 2926-2939, June 2012
[24] RoadsToHyCom, “Introduction to PEFC Operation”, [Online]. Available: http://www.ika.rwth-aachen.de/r2h/index.php/Introduction_to_PEFC_Operation
[25] University of West Indies, “Power Electronic Circuits”, [Online]. Available: http://www.eng.uwi.tt/depts/elec/staff/rdefour/ee33d/s3_fwrc2.html
[26] Coilgun Systems, “Voltage Converter Design”, [Online]. Available: http://www.coilgun.eclipse.co.uk/electromagnetic_pistol_voltage_converter_design.html
[27] Sakshat Virtual Labs, “Single Phase VSI with Sine-Triangular PWM”, [Online]. Available: http://iitd.vlab.co.in/?sub=67&brch=185&sim=469&cnt=1
[28] J. Pontt. “Mitigation of noneliminated harmonics of SHEPWM three-level multipulse three-phase active front end converters with low switching frequency for meeting standard IEEE-519-92.” In IEEE Transactions on Power Electronics, vol. 19. Dept. of Electron., Univ. Tecnica Federico Santa Maria, Valparaiso, Chile, IEEE, November 2004.
[29] G. Sandoval and J. Houdek, “A Review of Harmonic Mitigation Techniques”, [Online]. Available: http://www.artechepq.com/assets/files/AReviewOfHarmMitigTech.pdf
[30] W. Qiao and R. G. Harley, “Grid Connection Requirements and Solutions for DFIG Wind Turbines”, in IEEE Energy 2030 Conference, Atlanta, Georgia, 2008
[31] Associated Power Technologies ®, “Total Harmonic Distortion and Effects in Electrical Power Systems”, [Online]. Available:

http://www.aspowertechnologies.com/resources/pdf/Total%20Harmonic%20Distortion.pdf
[32] V. Salas, et al., “DC Current Injection into the Network from PV Grid Inverters”, in Photovoltaic Solar Energy CIEMAT, Madrid, Spain, 2006
[33] F. Dianbo et al., “Investigation on Transformer Design of High Frequency High Efficiency DC-DC Converters”, APEC, pp. 940-947, 2010
[34] T. Kerekes et al., “A New High-Efficiency Single-Phase Transformerless PV Inverter Topology”, IEEE Transactions On Industrial Electronics, pp. 184-191, Vol. 58, No. 1, Jan. 2011
[35] G. Butti and J. Biela, “Novel High Efficiency Multilevel DC-DC BoostConverter Topologies and Modulation Strategies”, IEEE Power Electronics and Applications, pp. 1-10, Aug. 2011
[36] MicroChap Co., “Internal Combustion Engines.", [Online]. Available: http://www.microchp.nl/internal_combustion_engines.htm [Mar. 2, 2011]
[37] M. Coffey, “Micro-CHP, A Present Day Reality.”, [Online]. Available: http://www.tenalpsevents.com/ContentFiles/1535%20MARTIN%20COFFEY.ppt [Feb. 26, 2011]
[38] C. Lepisto, “Honda and Climate Energy Team Up with Freewatt”, [Online]. Available: http://www.treehugger.com/files/2007/04/honda_and_clima.php [Feb. 25, 2011]
[39] COGEN_Europe. “Micro-CHP needs specific treatment in the European Directive on cogeneration,” presented at COGEN Europe Conference, Brussels, Belgium, 2004.
[40] J. Harrison and S. Redford, “Domestic CHP: What are the potential benefits?,” EA Technology for the Energy Saving Trust, Capenhurst, Chester, Tech. Rep. CH1 6ES, 2001.
[41] Staffell, R. Green, and K. Kendall, "Cost targets for domestic fuel cell CHP," J. Power Sources, vol. 181, no. 2, pp. 339–349, Jul. 2008.
[42] Hawkes andM. Leach, “Solid oxide fuel cell systems for residential micro-combined heat and power in the UK: key economic drivers”. J. Power Source, vol. 149, no. 1, 2005, pp. 72–83.
[43] E. Entchev, “Residential fuel cell energy systems’ performance optimization using ‘soft computing’ techniques”, J. Power Source, vol. 118, no. 1–2, 2003, pp. 212–217.
[44] M. Houwing, R.R. Negenborn and B. de Schutter, “Demand Response with Micro CHP Systems.” Proceedings of the IEEE, vol. 99, 1, pp. 200, Jan. 2011.
[45] J. Lidderdale, T. Day and P Jones, “Fuel cell CHP for buildings.”, [Online]. Available: http://www.cibse.org/pdfs/4b%20John%20Lidderdale.pdf
[46] Delta Energy and Environment Ltd., “Fuel Cell Prospects Within the Global Micro-CHP Industry.”, [Online]. Available: http://www.delta-

ee.com/downloads/Delta_presentation_for_FuelCellSemina_12_Oct10_web_version.pdf
[47] Alfagy ®. “National support policies for CHP/DHC compared: Denmark and Finland lead the way.”, [Online]. Available: http://alfagy.com/chp-news/45-national-support-policies-for-chpdhc-compared-denmark-and-finland-lead-the-way
[48] H.I. Onovwiona and V.I. Ugursal, “Residential Cogeneration Systems: Review of the Current Technology”, Renewable and Sustainable Energy Reviews. vol. 10, 2006, pp. 389-431.
[49] D. Reddy et al. “Development of a High Temperature PEM Fuel Cell Model For Combined Heat and Power (CHP) Systems”, SAUPEC, Cape Town, 2011, pp. 95-100.
[50] J. P. Koetzé, et. al., “A Combined Latent Thermal Energy Storage and Steam Generator Concept Using Metallic Phase Change Materials and Metallic Heat Transfer fluids for Concentrated Solar Power”, [Online]. Available: http://www.crses.sun.ac.za/files/services/conferences/annual-student-symposium-2011/5-18nov_kotze.pdf
[51] Europe’s Energy Portal, “Fuel Prices”, [Online]. Available: http://www.energy.eu/, [August 2011].
[52] Z. Beihong and L. Weiding, “An optimal Sizing Method for Cogeneration Plants”, Energy and Buildings, 2005.
[53] V. Phlippoteau, C. Turpin, S. Astier, “State of Health of a PEM fuel cell Degraded After ON-OFF Enurance Cycles”, [Online]. Available: http://perso.ensem.inpl-nancy.fr/Olivier.Lottin/FDFC08/CD/Contributions/FCHPHLI10-09_62M.pdf, [May 2010].
[54] J. Jensen and A. Olensen, “Solid Oxide Fuel Cell Micro Combined Heat and Powersystem choosing the right reformer”, M.S. thesis, Aalborg University, Aalborg, Jun. 2009
[55] S. Puranik, “Control of Fuel Cell Based Green Energy Systems for Distributed Generation Applications”, PhD, The Ohio State University, 2009.
[56] M. Jang, V. G. Agelidis, “Grid-Interfaced Fuel Cell Energy System Based in a Boost-Inverter with a Bidirectional Back-up Battery Storage”, IEEE, 2010.
[57] S. Jalbrzykowski, T. Citko, “A bidirectional DC-DC converter for renewable energy systems”, Bulletin of the Polish Academy of Sciences, 57:4, 2009.
[58] S. Sumiyoshi, et al, “High-Frequency Transformer Isolated Soft-Switching DC-DC Converter for Fuel Cell Cogeneration System,” presented at the 12th Int. Power Electronics and Motion Control Conference, Portoroz, 2006
[59] V. Arikatla, et al, “DC-DC Power Converter with digital PID controller,” presented at the 26th Applied Power Electronics Conference and Exposition (APEC), Texas, 2011.
[60] J. Zhong, “PID Controller Tuning: A short Tutorial”, [Online]. Available: http://wwwdsa.uqac.ca/~rbeguena/Systemes_Asservis/PID.pdf

[61] P. C. Sehn, “Principles of Electric Machines and Power Electronics”, NY: John Wiley and Sons, 1997.
[62] M. Casanova, “BJT Inverter”, [Online]. Available: https://courseware.ee.calpoly.edu/~dbraun/courses/ee307/F03/2/01_02_ArchanaDatla,MichaelCasanova.html
[63] P. A. Dahono et al., “An LC Filter Design Method for Single-phase PWM Inverters”, Power Electronics and Drive Systems, vol. 2, pp. 571-576, Feb 1995
[64] M. Gole, “Sinusoidal Pulse Width Modulation”, [Online]. Available: http://encon.fke.utm.my/nikd/SEM4413/spwm.pdf [June 2012].
[65] G. He et al, “A Novel Control Strategy to Suppress DC Current Injection of Single-phase PV Inverter to the Grid”, [Online]. Available: http://meetingassistant11.com/extra_files/online/online_41_upload_0206171504.pdf, [August 2012].
[66] A.D Hawkes and M. A. Leach, “Cost-effective operating strategy for residential micro-combined heat and power”, Energy, vol. 32, no. 5, May 2007, pp. 711-723.
[67] EG&G Services, Inc. “Fuel Cell Handbook”, Seventh Edition, U.S. Department of Energy, Office of Fossil Energy, West Virginia, 2004.
[68] Tokyo Gas Co. “ENE FARM Residential Fuel Cells Launched”, [Online]. Available: http://www.tokyogas.co.jp/tgminutes/64.pdf [Mar. 2, 2011]
[69] United States Department of Energy, “Research and Development of Fuel Cells for Stationary and Transportation Applications,” Tech. Rep. DE-FOA-0000360, Dec. 2010.
[70] Rezazadeh et al. ”Proton Exchange Membrane Fuel Cell control using a Predictive control based on Neural Network”, International Journal of Computer and Electrical Engineering, vol. 2, no. 1, pp. 1793-8163, Feb. 2010.
[71] Enotes, “Linear Filter”, [Online]. Available: http://www.enotes.com/topic/Linear_filter
[72] L. Guzzella, “Control oriented modeling of fuel cell based vehicles,” NSF Workshop on the Integration of Modeling and Control for Automotive System, 1999.
[73] C. De Beer et al., “Dynamic Modelling and Emulation of a High Temperature Proton Exchange membrane Fuel Cell (HT PEMFC)”, SAUPEC, Cape Town, 2011, pp. 113-118.
[74] BC Transmission Corporation ®, “Wind Generation Interconnection Requirements”, [Online]. Available: http://transmission.bchydro.com/nr/rdonlyres/34f97eb8-cd04-4861-895f-53d53af2de85/0/november7windinterconnectionworkshop.pdf
[75] N. Mohan, T. Undeland, W. Robbins, “Power Electronics: Converters, Applications and Design”, 3rd edition, 2003, John Wiley and Sons, USA.
[76] Tabtronics, “Transformer basics”, [Online]. Available: http://www.tabtronics.com/TECHNOLOGY/ElectromagneticBasics/TransformerBasics/tabid/110/Default.aspx, [July 2012].

[77] A.C. Olesen, J.R.Jensen, “Solide Oxide Fuel Cell Micro Combined Heat and Power System – choosing the right reformer”, Master Thesis, Aalborg University, Hydrogen and Fuel Cell Technology, 2009.
[78] Energy and Environmental Analysis Inc. and ICF Company, “Technology Characterization: Fuel Cells”, [Online]. Available: http://www.epa.gov/chp/documents/catalog_chptech_fuel_cells.pdf, [August 2011].
[79] S.Pasupathi, “HySA Catalysis: PEM Fuel Cell Catalysis and MEA preparation and characterisation”, 2011.
[80] Europe’s Energy Portal, “Fuel prices, rates for Power and Natural Gas”, [Online]. Available: http://www.energy.eu/, [August 2011].
[81] F.Barbir and T. Gómez, “Efficiency and Economics of Proton Exchange Membrane (PEM) Fuel Cells”, Int. J. Hydrogen Energy, Vol. 22, No. 10-11: pp.1027:1037, 1997.
[82] H.J.Stone, (2005). “Economic Analysis of Stationary PEM Fuel Cell Systems, Battelle Memorial Institue”, [Online]. Available: http://www.hydrogen.energy.gov/pdfs/review05/fc48_stone.pdf, [August 2012].
[83] EPA, “Technology Characterisation: Fuel Cells”, [Online]. Available: http://www.epa.gov/chp/documents/catalog_chptech_fuel_cells.pdf, [August 2012]
[84] H. M. Mzungu, “Impact of Armature Rewinding on Induction Motor Efficiency in South Africa”, MSc, University of Cape Town, 2009.
[85] Federal Energy Regulatory Commission, “Interest Rates”, [Online]. Available: http://www.ferc.gov/legal/acct-matts/interest-rates.asp, [August 2012].
[86] R. Balkin, “Modelling a 500W Polymer Electrolyte Membrane Fuel Cell”, B.Thesis, University of Technology, Sydney, 2002.
[87] R.F. Mann, J.C. Amphlett, B.A. Peppley, C.P. Thurgood, “Application of Butler-Volmer equations in the modeling of activation polarization for PEM fuel cells”. Journal of Power Sources, 161: pp.775-781, 2006.
[88] M. Boaventura and A. Mendes, “Activation procedures characterization of MEA based on phosphoric acid doped PBI membranes”, International Journal of Hydrogen Energy, 35: pp.11649-11660, 2010.
[89] J. Lobato et al, “Study of the influence of the amount of PBI-H3PO4 in the catalytic layer of a high temperature PEMFC”, International Journal of Hydrogen Energy, 35: pp.1347-1355, 2010.
[90] Muthuramalingam and S. Himavathi, “Evaluation of Power Factor Corrected AC-DC Converters and Controllers to meet UPS Performance Index”, International Journal of Electrical and Computer Engineering, 4:9,2009.
[91] H. Fadali, Fuel Cell Distributed Generation: Power Conditioning, Control and Energy Management, MSc, University of Waterloo, Canada, 2008.

[92] N. M. Abdel-Rahim and J. E. Quaicoe, “Analysis and design of a multiple feedback loop control strategy for single-phase voltage-source UPS inverters,” IEEE Transactions on Power Electronics, vol. 11, no. 4, pp. 532-541, July 1996.

APPENDIX A

Dahono's Method MATLAB Program

```
%Program to design LC filter using the method outlined in
[Dahono1995]
Ed = 400; %nominal dc source voltage [v]
Vo = 220; %nominal load voltage [v]
Io = 10; %nominal load current [A]
fr = 50; %fundamental output frequency [Hz]
fs = 20e3; %switching frequency [Hz]
Vo1av = 0.01*Vo; %specified value of the total harmonic of the
load
voltage -> 1% of Vo
%=============================================================
==========
k = (Vo/2)/Ed; %nominal modulation index
K = ((k^2 - (15/4)*k^4 + (64/5*pi)*k^5 -
(5/6)*k^6)/(1440))^(1/2);
Lf = Vo/(Io*fs)*(((K*Ed)/Vo1av)*(1 +
((4*pi^2)*(fr/fs)^2)*K*(Ed/Vo1av)))^(1/2)
%filter inductor
Cf = K*Ed/(Lf*fs^2*Vo1av) %filter capacitor
```

APPENDIX B

Program for plotting a PEMFC Polarisation Curve

```
%%%%%%%%%%%%%%%%%%%%%%%%%%%%%%%%%%
% EXAMPLE 3-3: Calculating the Voltage Losses for a Polarization
Curve
% UnitSystem SI
%%%%%%%%%%%%%%%%%%%%%%%%%%%%%%%%%%
% Inputs
R = 8.314; % Ideal gas constant (J/molK)
F = 96487; % Faraday's constant (Coulombs)

Tc = 120; % Temperature in degrees C
P_H2 = 3; % Hydrogen pressure in atm
P_air = 3; % Air pressure in atm
A_cell=100; % Area of cell
N_cells=48; % Number of Cells
r = 0.19; % Internal Resistance (Ohm-cm^2)
Alpha = 0.5; % Transfer coefficient
Alpha1 = 0.085; % Amplification constant
io = 10^-6.912; % Exchange Current Density (A/cm^2)
il = 1.4; % Limiting current density (A/cm2)
Gf_liq = -228170; % Gibbs function in liquid form (J/mol)
k = 1.1; % Constant k used in mass transport
%%%%%%%%%%%%%%%%%%%%%%%%%%%%%%%%%%
% Convert degrees C to K
Tk = Tc + 273.15;
% Create loop for current
loop = 1;
i = 0;
for N = 0:150
i = i + 0.01;
% Calculation of Partial Pressures
% Calculation of saturation pressure of water
x = -2.1794 + 0.02953 .* Tc-9.1837 .* (10.^-5) .* (Tc.^2) +
1.4454 .* (10.^-7) .* (Tc.^3);
P_H2O = (10.^x);
% Calculation of partial pressure of hydrogen
pp_H2 = 0.5 .* ((P_H2)./(exp(1.653 .* i./(Tk.^1.334)))-P_H2O);
% Calculation of partial pressure of oxygen
pp_O2 = (P_air./exp(4.192 .* i/(Tk.^1.334)))-P_H2O;
% Activation Losses
b = R .* Tk./(2 .* Alpha .* F);
V_act = -b .* log10(i./io); % Tafel equation
% Ohmic Losses
V_ohmic = -(i .* r);

% Mass Transport Losses
term = (1-(i./il));
if term > 0
```

```
V_conc = Alpha1 .* (i.^k) .* log(1-(i./il));
else
V_conc = 0;
end
% Calculation of Nernst voltage
E_nernst = -Gf_liq./(2 .* F) - ((R .* Tk) .* log(P_H2O./(pp_H2 .*
(pp_O2.^0.5)))./(2 .* F);
% Calculation of output voltage
V_out = E_nernst + V_ohmic + V_act + V_conc;
if term < 0
V_conc = 0;
break
end
if V_out < 0
V_out = 0;
break
end

title('Fuel cell polarization curve')
xlabel('Current density (A/cm^2)');
ylabel('Output voltage (Volts)');
subplot(2, 1, 1), plot(i,V_out,'*');
grid on
hold on
disp(V_out)
% Calculation of power
P_out = N_cells .* V_out .* i .* A_cell;

title('Fuel cell power')
xlabel('Current density (A/cm^2)');
ylabel('Power(Watts)');
subplot(2, 1, 2), plot(i,P_out,'*');
grid on
hold on
disp(P_out);
end
```

APPENDIX C

Simulink Model for Power Electronic Interface Control

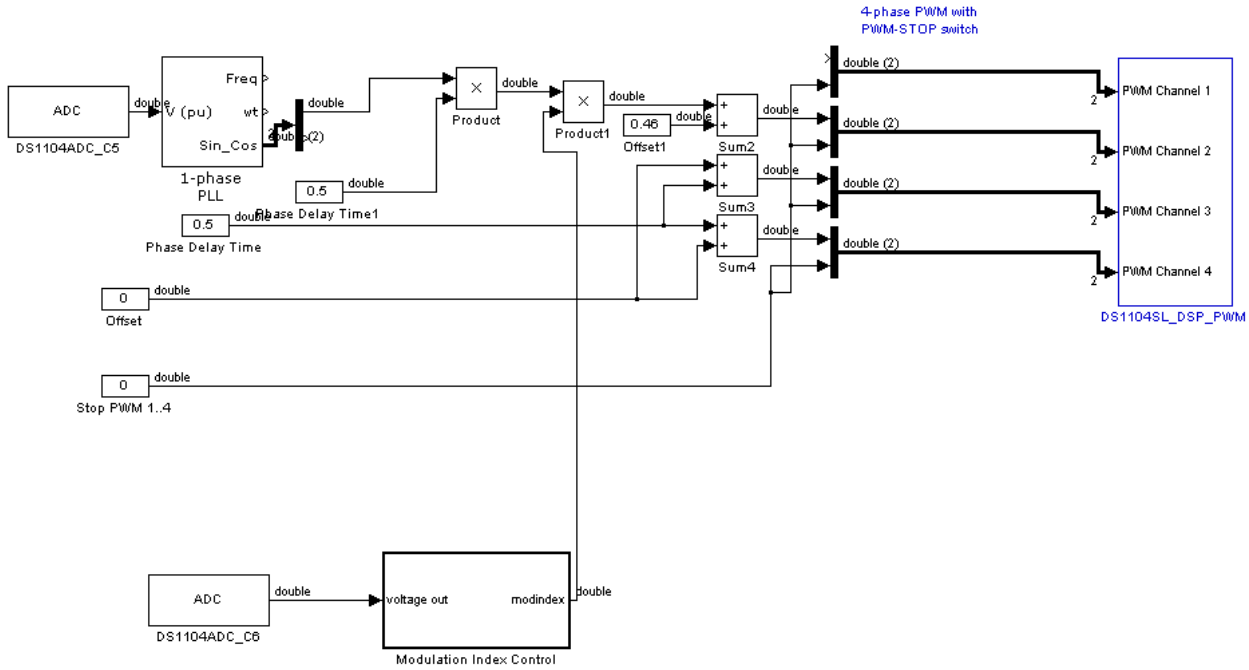

APPENDIX D

MATLAB Code Example for Cost Minimizing Control

```
% The heat to power ratio varies depend on the percentage of
% maximum load the operating point is.
% The total efficiency of the prime mover is constant at 80%

% The electrical efficiency = -0.1x + 0.4

% Where x is the fraction of the maximum output capacity of the
fuel cell that the fuel cell is operating in.

% Electricity price is assumed to be constant

CHPSize = 3; % This is used to calculate chemical and thermal
efficiencies at different fuel cell operating points

% Typical thermal and electrical household demand.
delectrical  = [1.8979 0.5048 1.3209 0.8725 0.9373 0.0804 0.4314
1.8519 1.2210 0.4747 0.2280 0.6277 1.4581 0.8680 1.7791 1.3358
0.4944 1.8169 0.2108 1.2465 0.2426 1.0145 0.4519 1.5018 1.6617
1.7019 0.4387 1.3192 1.3753 0.9493 1.4014 0.9277 1.1950 1.5836
0.0122 1.9664 1.5037 1.9256 0.0697 0.3584 0.8144 0.5821 1.3163
0.2763 1.8804 1.6751 1.3168 1.5291 0.0250 0.4851 0.5124 0.9602
0.9513 1.5507 1.4848 0.7297 1.8546 1.5483 1.2401 1.3437 1.3981
1.7323 0.1049 1.6490 1.8269 1.3459 1.3646 1.3292 0.7488 1.9045
0.4835 1.3753 1.2137 0.2903 1.5275 1.8980 0.9899 1.3465 0.4797
0.9214 0.4513 0.5468 1.3020 1.9291 1.8051 0.6062 0.3629 1.9102
1.4862 1.4261 1.3232 0.8837 1.9720 0.5966 0.5624 0.3652];
dtherm = [0.3629 0.3453 0.4108 0.2714 0.5938 1.0978 0.8832 0.0652
1.1202 1.1356 0.4014 1.0888 0.3561 0.3638 0.7982 1.3941 0.0821
1.1612 0.1025 0.2199 0.7142 1.3698 0.6588 0.5062 0.5983 0.1482
0.5992 1.1846 0.5829 1.4018 0.8982 1.3826 1.1017 1.0429 0.3711
1.3553 0.9531 0.7412 1.1848 1.3626 1.4416 0.6090 1.0468 0.1052
1.2557 1.4264 0.8206 0.9976 0.7362 0.9886 0.5537 1.1811 0.6029
1.1643 0.9767 0.3569 1.4108 1.1692 0.2033 0.5807 0.0491 0.0836
0.6860 1.1935 1.3728 0.1654 0.5650 0.0143 1.1805 0.7316 1.2171
0.8169 0.0166 0.2596 0.2023 0.4593 0.3760 1.1363 1.0773 0.5834
1.3083 1.2481 1.0379 0.2130 0.6997 0.3035 1.3872 0.5540 0.3616
0.5149 1.1345 0.7783 0.2554 1.4652 0.6794 0.8576];

Pimp = 0.41;  % Price of importing electricity from the grid
Pexp = 0.047; % Price paid for electricity sold to grid.
Pg   = 0.16;  % Price paid for natural gas from pipeline

for i = 1:96

     for elecoutput 0.1:0.1:3


     nelec = -(0.1*elecoutput*chpsize + 0.4);
     ntherm = 0.8 - nelec; %prime mover efficiency = 80%
```

```
     thermaloutput = elecoutput * ntherm/nelec;
     Cchp = (elecoutput/nelec + thermaloutput/ntherm)*Cg; % Heat
to power ratio = 1:1

     if thermaloutput < dtherm
        Caux = (dtherm - thermaloutput)*Cg/naux
     else
        Caux = 0;
     end

     if delectrical > elecoutput
        Celec = elecoutput*Pimp;
     else
        Celec = (-1)*(elecoutput - delectrical)*Pexp +
delectrical*Pimp;
     end

     Cr = Cchp + Caux + Celec;
     if Cr < Crmin
        Crmin = Cr
        optimumoutput = elecoutput;
     end


  end
  Cr[i] = Crmin; %array containing moving averages of running
cost at 96 times during the 24Hour day
  Optimumchpoutput = optimumoutput; % Optimal output of fuel
cell at 96 times during the day.
End
```

APPENDIX E

Transfer Function of DC/DC Converter

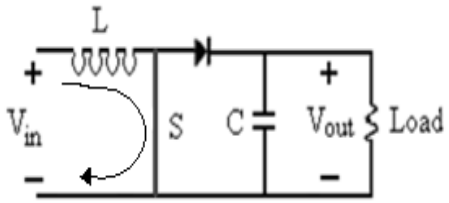

(a) Switch is closed (DT)

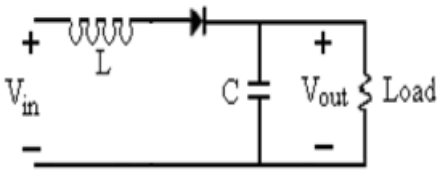

(b) Switch is open ((1-D)T)

A state-space representation of the DC/DC regulator was derived based on the literature of [91]. The left diagram above labelled (a), depicts when the switch is closed (DT), the inductor current and output voltage during this state is:

The differential equations for the

$$\frac{di_L}{dt} = \frac{1}{L}V_{in} \tag{E.1}$$

$$\frac{dV_{out}}{dt} = \frac{1}{C}\frac{V_{out}}{R} \tag{E.2}$$

The diagram to the right above, labelled (b), depicts when the switch is open ((1-D)T), the inductor current and output voltage are now represented as:

$$\frac{di_L}{dt} = \frac{1}{L}(V_{in} - V_{out}) \tag{E.3}$$

$$\frac{dV_{out}}{dt} = \frac{1}{C}(i_L - \frac{V_{out}}{R}) \tag{E.4}$$

Therefore when both stages are incorporated, the state space representation is:

$$\frac{d}{dt}\begin{bmatrix} i_L \\ V_{out} \end{bmatrix} = [A_1(D) + A_2(1-D)]\begin{bmatrix} i_L \\ V_{out} \end{bmatrix} + [B_1(D) + B_2(1-D)] \tag{E.5}$$

$$y = [C_1(D) + C_2(1-D)]\begin{bmatrix} i_L \\ V_{out} \end{bmatrix} \tag{E.6}$$

Therefore becoming:

$$\frac{d}{dt}\begin{bmatrix} i_L \\ V_{out} \end{bmatrix} = \begin{bmatrix} 0 & -\frac{1}{L}(1-D) \\ \frac{1}{C}(1-D) & \frac{1}{RC}D - \frac{1}{RC}(1-D) \end{bmatrix}\begin{bmatrix} i_L \\ V_{out} \end{bmatrix} + \begin{bmatrix} \frac{1}{L}(D+(1-D) \\ 0 \end{bmatrix} \quad \text{(E.7)}$$

$$A = \begin{bmatrix} 0 & -\frac{1}{L}(1-D) \\ \frac{1}{C}(1-D) & \frac{1}{RC}D - \frac{1}{RC}(1-D) \end{bmatrix} \quad \text{(E.8)}$$

$$B = \begin{bmatrix} \frac{1}{L} \\ 0 \end{bmatrix} \quad \text{(E.9)}$$

$$C = [0 \quad 1] \quad \text{(E.10)}$$

Having obtained the state space representation the transfer function can then be reduced to:

$$g(s) = \frac{C^T(adj\ (sI-A))B}{\det(sI-A)} \quad \text{(E.11)}$$

Thus obtaining the following transfer function:

$$g(s) = \frac{\frac{1}{LC}}{s^2 - s\frac{1}{RC}(1-2D) + \frac{1}{LC}(1-D)^2} \quad \text{(E.12)}$$

Transfer Function for Single Phase Inverter

The following is a diagram of a single phase inverter which will be used to obtain an average small signal transfer function for the inverter.

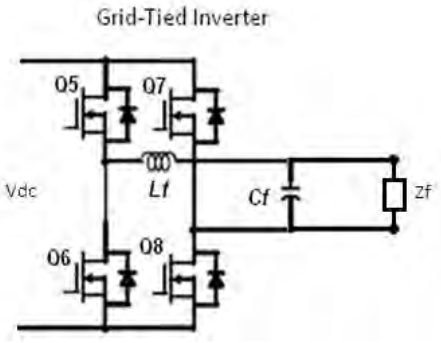

Creating an expression for the transfer function of the single phase inverter is made difficult by the fact that the output is constantly changing. An average small signal model expression will thus be derived to assist in developing a controller.

The switching function of the H-bridge according to [92] can be approximated to

$$d(t) = (\frac{1}{2})(m\sin(\omega t) + 1)) \quad \text{(E.13)}$$

Where d = Normalised H-bridge output between 0 and 1.

m = Modulation index

ω = Line Frequency

t = Time

According to the authors of [92] using this switch function value an average set of differential equations can be formed:

$$\frac{d}{dt}\begin{bmatrix} i_f \\ v_f \\ v_o \end{bmatrix} = \begin{bmatrix} \frac{-R_f}{L_f} & 0 & \frac{-L_f}{L_L} \\ 0 & \frac{R_L}{L_L} & \frac{1}{L_L} \\ \frac{1}{c_o} & \frac{-1}{c_o} & 0 \end{bmatrix} \begin{bmatrix} i_f(t) \\ i_o(t) \\ v_o(t) \end{bmatrix} + \begin{matrix} \frac{m\ v_{dc}\sin(\omega t)}{L_f} \\ 0 \\ 0 \end{matrix} \quad \text{(E.14)}$$

Where:

i_f = current through LC filter
V_f = voltage across LC filter
v_o = output voltage
i_o = output current
R_f = resistance of LC filter
L_f = inductance of LC filter
L_L = inductance of load
C_o = output capacitance
V_{dc} = Voltage of the DC Bus
m = modulation index
ω = angular line frequency

The control (modulation index) to output voltage transfer function derived from [92] is thus:

$$\frac{v_o}{m} = \frac{\frac{v_{dc}}{L_f C_o}(s + \frac{R_L}{L_L})}{s^3 + \left(\frac{R_L}{L_L} + \frac{R_f}{L_f}\right)s^2 + \left(\frac{R_L R_f}{L_L L_f} + \frac{L_L + L_f}{L_L L_f C_o}\right)s + \frac{R_L + R_f}{L_L L_f C_o}} \quad \text{(E.15)}$$